Photoinduced Charge Transfer from Quantum Dots on the Timescale of Chemistry

Micaela Kalmek Homer

A dissertation
submitted in partial fulfillment of the
requirements for the degree of

Doctor of Philosophy

University of Washington

2024

Reading Committee:

Brandi Cossairt, Chair

Bo Zhang

Cody Schlenker

Program Authorized to Offer Degree:
Chemistry

University of Washington

Abstract

Photoinduced Charge Transfer from Quantum Dots on the Timescale of Chemistry

Micaela Kalmek Homer

Chair of the Supervisory Committee:
Brandi Cossairt
Department of Chemistry

Measuring and modulating charge-transfer processes at quantum dot interfaces are crucial steps in developing quantum dots as photocatalysts. In Chapter 1, a viewpoint for conceptualizing photoinduced charge transfer as a bimolecular, multi-step process is presented. The conventionally accepted mechanism that charges directly transfer to an acceptor following exciton dissociation is outlined and challenged. Then, existing methodology for evaluating photoinduced charge transfer is introduced.

In Chapter 2, cyclic voltammetry under illumination is demonstrated to measure the rate of photoinduced charge transfer from CdS quantum dots by directly probing the changing oxidation states of a library of molecular charge acceptors, including both hole and electron acceptors. Observed rates for photoinduced charge transfer on the order of 0.1 s^{-1} are measured, which are distinct from the picosecond dynamics measured by conventional transient optical spectroscopy methods. Surprisingly, we found that charge transfer takes *ca.* 30 min to reach a maximum observed rate and charge transfer lasts for *ca.* 30 minutes after illumination ends, ∼12 orders of magnitude longer than would be expected if charge transfer was directly from exciton dissociation. This timescale challenges the conventionally accepted mechanism of charge transfer.

In Chapter 3, we investigated this new pathway for charge storage and transfer. Altogether, our results confirm that excited electrons are stored at ligated surface Cd, these sites are competent charge donors, and this storage is charge balanced by X-type ligand desorption. We found that

charge storage occurs in every QD system studied, including CdS, CdSe, and InP capped with carboxylate and phosphonate ligands.

TABLE OF CONTENTS

LIST OF FIGURES

LIST OF SCHEMES

LIST OF TABLES

ACKNOWLEDGMENTS

I first have to begin by thanking where I come from: my loving parents and grandparents. I am my parents' favorite (only) child and my paternal grandparents' favorite (only) grandchild, so I am the result of huge amounts of love and care. I often say that my confidence in myself has made graduate school a much easier endeavor, and that confidence comes from them. My mom has been my source of comfort when this whole thing seemed too much, and the more life I live the more I realize how alike we are. My dad's penchant for problem solving and his persistence towards long-term interests are qualities I have tried to emulate during graduate school. I thank my chosen family: Natalie, Eli, Fanrui, Casey, and Caroline. Their love has grounded me when the PhD felt like a marathon (not a sprint!) that wouldn't finish.

I thank my mentors who led me through my undergraduate career. I thank my chemistry professors at Harvey Mudd College, specifically Prof. Kathy Van Heuvelen, Prof. Kerry Karukstis, Prof. Adam Johnson, Prof. Bill Daub, and my thesis advisor Prof. Hal Van Ryswyk. I am endlessly thankful for my education at Mudd; I'm convinced it was the best place in the world for me to fall in love with chemistry. I thank Prof. Darryl Wright who introduced me to philosophy, resulting my greater ability to write and reason. Mudd holds a very special place in my heart, and I am thankful that UW Chemistry flew me back to Claremont to speak and visit old mentors this past fall. I thank my mentors from invaluable summer research experiences, Dr. Rajeev Assary, Dr. Jaya Borgatta, and Prof. Robert Hamers.

I thank my mentors at UW: those who taught me electrochemistry (Ding-Yuan, Ian, David), and those who more generally taught me how to be a graduate student (Max, Ian,

Cecilia, Andrew, Florence, and Nayon). Dr. David Ung has especially guided me through from my first day in the office when he printed me a copy of "A Practical Beginner's Guide to Cyclic Voltammetry" to job searching now. Cossairt Lab, past and present, you have all hugely influenced me. I treasure all of our relationships. I thank my committee: Prof. Bo Zhang, Prof. Cody Schlenker, and Prof. Vincent Holmberg. Your encouragement early on in graduate school gave me drive to continue.

My last acknowledgement is for Brandi. Prof. Brandi Cossairt has been the greatest mentor I could hope for. People often refer to her empathy and humanity, but I think people do not often enough discuss how intensely capable she is. She has directed a research group with many branches that extend far beyond her background which is only possible because her brain somehow isn't full yet. She stays up do date with an absurd number of projects, and has advice to execute them all. But most importantly to me is our mentor-trainee relationship. She has supported me during personally and scientifically difficult times, which I can share with her because I deeply trust her. She is an advocate for me, and I am so thankful to have had her guidance.

DEDICATION

To my parents.

Chapter 1

INTRODUCTION

1.1 Motivation: Photoinduced Charge Transfer Across Quantum Dot Interfaces

Though chemists have been interested in light-induced chemical transformations for a few centuries,[1] the last three decades have seen a renaissance of photochemistry investigation.[2] Photoinduced charge transfer may be among the most basic types of these transformations, where matter that absorbs energy from light becomes a more potent redox agent (Scheme 1.1). Quantum dots (QDs) have been promoted as ideal photosensitizers due to their high extinction coefficients, electronic tunability, and solution processability. However, efficient extraction of charge carriers from QDs remains a design challenge.[3] Efficient extraction requires transport of charge across a complex interface that comprises a high prevalence of defect electronic states in the QD and the covalent and noncovalent interactions between the QD, the ligand shell, the charge acceptor, and other species in the environment (i.e., solvent and electrolyte). This work presents a new approach to measuring photoinduced charge transfer from QDs and in turn uncovers a unique but highly general mechanism for such transfer.

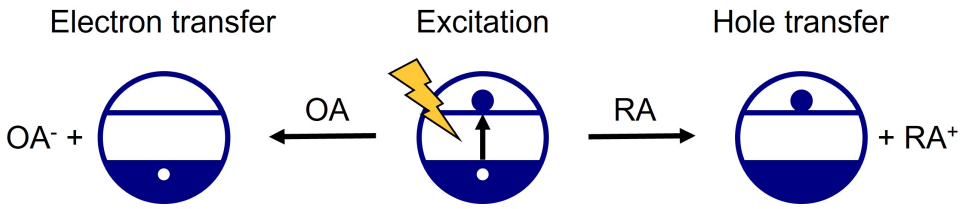

Scheme 1.1: General overview of chemical changes due to photoinduced charge transfer from a semiconductor photosensitizer. Excitation creates an electron-hole pair, where the electron is excited to the conduction band and the hole left behind is in the valence band. After excitation either an oxidizing agent (OA) accepts an electron or a reducing agent (RA) accepts a hole, resulting in either electron or hole transfer from the photosensitizer, respectively.

1.2 Photoinduced Charge Transfer from QDs is a Multi-Step Process

1.2.1 Limitations of the Marcus Formalism

The simplest model for quantum dot charge transfer could view the system as an aggregate: two species, an electron donor and an electron acceptor that are already in close contact, ready to exchange an electron as depicted (D*$\cdots$A) in Scheme 1.2. In this simple case, Marcus theory predicts that the rate of charge transfer (k_3 in Scheme 1.2) depends on the energetic driving force for charge transfer, the electronic coupling between donor and acceptor states, and the reorganization energy.

There has been much investigation of the applicability of the Marcus formalism to nanocrystal charge donors where researchers systematically vary driving force or reorganization energy for photoinduced charge transfer and measuring resulting charge transfer rates.[4–6] In parallel, there has been a large amount of investigation into deviations from Marcus relationships and explanations for these. In QD charge transfer, a particularly highlighted deviation from Marcus relationships comes from the Auger-assisted mechanism, where transfer of a charge carrier is accompanied by intraband excitation of the carrier of opposite sign, effectively decreasing the driving force and

circumventing the Marcus inverted region.[7–9] The Marcus inverted region has only been observed in QD systems that contain a single charge carrier, rather than an electron-hole pair.[10]

It is important to note that Marcus theory, including corrections for Auger-assisted mechanisms, is limited to describing the process of electron transfer illustrated with k_3 in Scheme 1.2 and does not include any of the steps leading up to formation of the (D*···A) aggregate pair. These other steps are depicted in Figure 1.1 and include excitation, exciton dissociation, and favorable collision in the case of diffusive charge transfer. Furthermore, along this pathway excitonic relaxation, recombination of separated charge carriers, nonproductive carrier trapping and backward transfer all lessen the yield of the redox process.

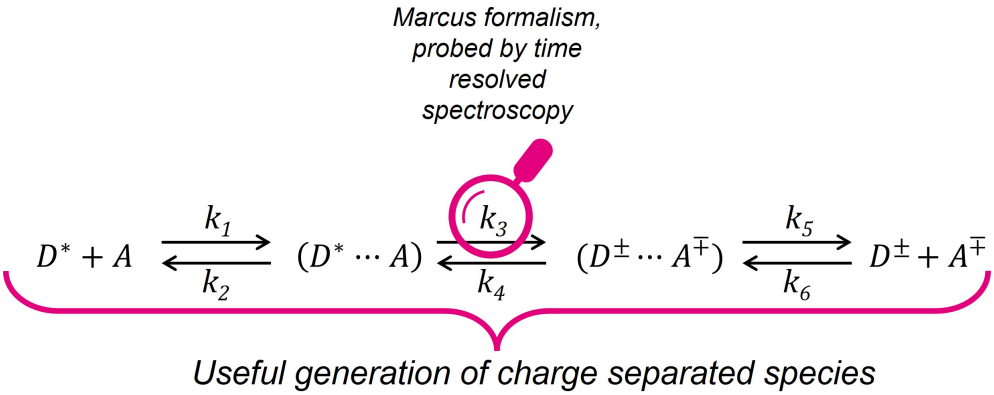

Scheme 1.2: Mechanism for productive charge transfer, which includes formation of the donor-acceptor pair (k_1), transfer of charge (k_3), and dissociation of the pair after charge transfer (k_5), as well as the reverse processes (k_2, k_4, and k_6). Photogeneration of the charge donor is not included.

1.2.2 Bimolecular (diffusive) versus Unimolecular (direct) Charge Transfer

Much research in QD charge transfer is devoted to pseudo-unimolecular processes where charge transfer is between two species that have already formed the charge donor-charge acceptor pair (D*···A) (Figure 1.1, bottom). This preadsorption may be designed through chemically tethering

the charge acceptor to the QD, which conveniently allows for varying the distance between QD surface and charge-accepting moiety, then studying the distance dependent rates.[11,12]

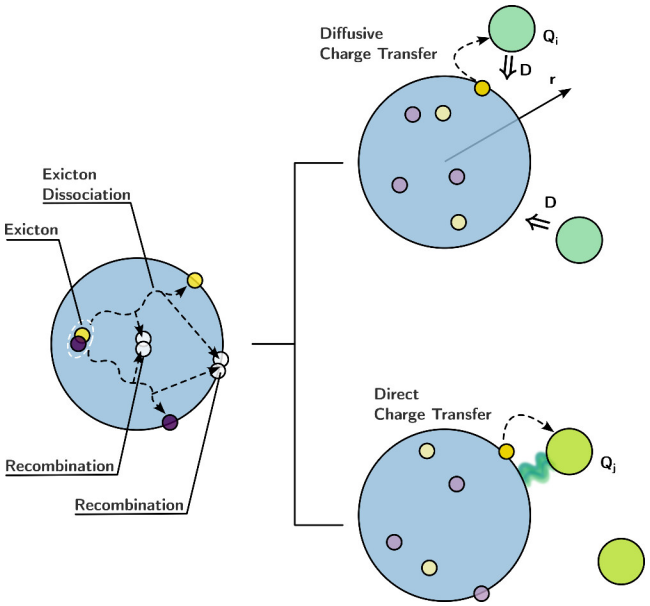

Figure 1.1: Schematic illustration of the charge kinetics of QDs and the photoinduced electron transfer at the QD surface. Reproduced from [13] under CC-By 4.0.

If the charge acceptor is diffusing, the frequency of collisions and the fraction of those collisions that are in a favorable configuration for charge transfer influence the rate of generation of charge separated species. This is described as k_1 in Scheme 1.2. To determine how frequently charge donors and acceptors might collide, both the QD and the charge acceptor are modeled as freely diffusing hard spheres, which neglects the chemical interactions between QD and acceptor. Typical diffusion coefficients for QDs are on the order of $10^{-6}\,\mathrm{cm^2\,s^{-1}}$,[14] and typical diffusion coefficients of acceptors are higher, on the order of $10^{-5}\,\mathrm{cm^2\,s^{-1}}$,[15] which together with estimated hydrodynamic radii make the estimated collision frequency on the order of $10^{10}\,\mathrm{M^{-1}\,s^{-1}}$.[16] However, the QD is generally not a hard sphere, as colloidally stable QDs generally have a semipermeable, insulating ligand shell. In order for good wavefunction overlap between the charge donor (the inorganic core of the nanocrystal) and the acceptor, the acceptor must be able to permeate the ligand shell. Prior work

has shown that more permeable ligand shells increase the rate of charge transfer,[17–19] highlighting the issue with hard-sphere estimations of collisions. Furthermore, even charge accceptors without chemically designed tethers still chemically adsorb to the QD surface,[20,21] so it is unlikely to find truly freely diffusing charge acceptors.

This implies that photocatalysis from QDs generally lies on some continuum between the freely diffusing and the tethered case. Charge acceptors that are preadsorbed to the QD have a higher chance of accepting charge due to better wavefunction overlap. On the other hand, in order for a reaction to be catalytic this adsorption must be temporary to allow for catalyst turnover. One exception to the need for dynamic adsorption of a charge acceptor to the QD surface is the case of a bound cocatalyst[22] or bound reversible charge shuttling ligand.[23,24] In both cases this bound intermediate accepts charge before passing charge over to the diffusing catalytic substrate.

Altogether, the chemical interactions between the QD surface and the charge acceptor control how frequently and for how long donor-acceptor pairs are formed. By only measuring charge transfer after the donor and acceptor are already aggregated, the complexity in the productive generation of charge transfer is neglected.

1.3 Charge Carrier Trapping in Quantum Dots - Friend or Foe?

In many QD applications, surface trapping of charge carriers after excitation must be avoided. In QD solar cells, charge carrier trapping promotes recombination and prevents photocurrent from being transmitted to charge collecting layers.[25,26] In photodetectors, the responsivity depends on long excited state lifetimes, and therefore, minimal trapping.[27–29] For fluorescence technologies like QD light emitting diodes, biocompatible fluorescence imaging, and solar downconverters, surface traps decrease photoluminescence quantum yield by introducing new recombination pathways.[30] In addition to lowering PLQY, trapping causes unwanted blinking in quantum light sources.[31]

In QD photocatalysis, the goal to minimize carrier trapping has been upheld. The existing paradigm is that in order for photoinduced charge transfer to happen with appreciable quantum yield, it must be faster than the excitonic decay, and excitonic decay is sped up by carrier trapping.[3] Of course, this line of thinking presumes that photoinduced charge transfer from QDs is

directly from excitons. There has been some shift in perspective where rather than viewing carrier trapping as depleting excitons, carrier trapping could be engineered to extend the excitonic lifetime (albeit with some energetic cost), perhaps greatly increasing photocatalytic quantum yield.[3] Schemes like adsorbed molecular cocatalysts[22] or charge localizing, catalytic metal islands deposited on nanocrystal surfaces[32,33] reversibly "trap" charge carriers that go on to do redox reactions with high quantum yields. Similarly, it has been demonstrated that charge transfer from QDs may proceed through intermediate states intrinsic to the QD surface.[8,11,34,35] It seems that carriers trapped at QD surfaces could be more effective charge donors than excitonic carriers because their lifetime is several orders of magnitude longer and the surface localized nature may allow better wavefunction overlap with charge acceptors than free carriers which sample the entire QD volume. We present an enhancement of electron transfer in every QD system we tested *via* reversible electron trapping at the QD surface in Chapter 3.

1.4 Conventional Measurement of Charge Transfer

Conventional means of measuring charge transfer rates from QDs use time resolved optical spectroscopies, namely time resolved photoluminescence (TRPL) and transient absorbance (TA). These pseudo unimolecular measurements are able to detect the changing charge carrier occupancy of the QD on rapid timescales. In TRPL measurements, most commonly the photoluminescence being detected is that from the excited QD, and charge transfer from the QD makes it no longer emissive, measurably decreasing photoluminescence lifetimes.[36] One issue with this measurement, as well as other photoluminescence-based experiments such as Stern-Volmer analysis, is that it does not distinguish electron and hole transfer, nor does it cleanly distinguish charge transfer from energy transfer.[37]

Instead, one might consider TA, which is a pump-probe technique. After excitation (pump), the lowest energy excitation transition is bleached (probe) for as long as the electron-hole pair produced by the pump pulse lives due to state filling. In QD systems, it was long accepted that this bleach was sensitive to the population of conduction band electrons and insensitive to the population of valence band holes. This could helpfully inform if the process monitored was hole or electron

transfer, but prohibits measurement of oxidation reactions. Further, recent work has challenged the assertion that TA is completely hole insensitive.[38,39] One advantage of TA measurements is that in addition to the QD's changing absorption profile, sometimes the charge acceptor or its reduced (in the case of electron transfer) or oxidized (hole transfer) form will be optically active, so in addition to tracking the changing occupancy of QD electronic states, the redox state of the acceptor may also be monitored, which lends good assurance that the correct process is being probed.[40]

Beyond the limitations specific to TA or TRPL, an overarching issue is that these spectroscopies both probe only the rate of charge transfer depicted as k_3 in Scheme 1.2. On the rapid timescale of TA or TRPL, we can measure fleeting changes to electronic occupancy between preadsorbed species, but we cannot translate this into a rate of generation of the products $D^{\pm}$ and $A^{\mp}$. Chemists' interest in photocatalysis is, fundamentally, generation of product, so photoinduced charge transfer is a chemical process should be measured on chemically relevant timescales by tracking the formation of products.

1.5 Cyclic Voltammetry to Evaluate Light-Driven Chemistry

Voltammetry has occasionally been used to measure charge transfer when the photoactive species is also the working electrode.[41,42] In these systems, the photoelectrode combines driving force from excitation with driving force from applied potential to promote chemical transformations.[43] Rather than using a sacrificial charge donor, as used in solution-phase QD photocatalysis, the applied potential provides charge balance. From voltammetric measurements, scientists determine the minimum potential needed to drive catalysis[44] and from transient photo current with chopped light, kinetics of electron-hole dynamics may be inferred.[45–47] Though outside the scope of this work, it is worth noting that oftentimes moving to the frequency domain with impedance spectroscopy is a preferred measurement as it allows discrimination of various electrochemical and physical processes in the solid electrode that working in the time domain (voltammetry) does not allow.[48,49]

Photoelectrochemical research where the photoactive species is in the solution phase is much more limited. There are limited instances of cyclic voltammetry (CV) being used during illumination, but these experiments did not obtain kinetic information. Past experiments were used to

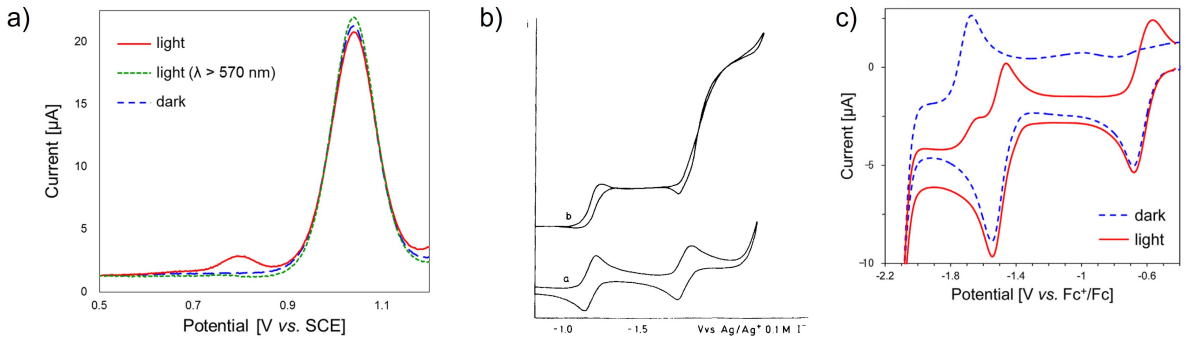

Figure 1.2: Examples of voltammetry of molecular species under illumination to probe light-induced reactivity (a) Square wave voltammogram of $[Ru(bpy)_3]^{2+}$ demonstrating a new oxidative feature at 0.8V when the compound is excited. Reproduced from [50] under CC BY 4.0. (b) Cyclic voltammograms of dimethyl terephthalate and an electron acceptor without (bottom) and with (top) illumination. Reproduced with permission from [51]. (c) Cyclic voltammograms of an iron-porphyrin CO_2 catalyst with and without illumination. Reproduced from with permission from [52].

estimate excited state redox potentials (Figure 1.2a),[50,53,54] to demonstrate the influence of light on electrochemistry of ion radicals (Figure 1.2b),[51,55] or to demonstrate the photoinduced regeneration of a molecular catalyst (Figure 1.2c).[52] While these experiments did investigate photochemical processes electrochemically, they were not generalizable and focused on obtaining mechanistic understanding rather than using CV as a tool for kinetic measurement.

On the other hand, electrochemists have 60 years of experience quantifying ground-state chemical processes using CV.[56] In 1965, Savéant and Vianello developed theory for linear sweep voltammetry in systems where a chemical reaction follows a faradaic reaction (EC mechanism, Scheme 1.3). Furthermore, they showed that this voltammetry could accurately determine the rate constant for the chemical step (k in Scheme 1.3).[57] Of course, useful chemistry is rarely as simple as the EC scheme, and extension of the simple model was even presented in the 1965 work. Since then, the field has moved beyond just determining rates of chemical reactions by applying Savéant's formalism to molecular electrocatalytic schemes. In these schemes, the active catalyst (Q in Scheme 1.3)

is formed through a faradaic process, then the active catalyst performs a reaction in solution to generate product (B in Scheme 1.3). Beyond determining a rate constant for the chemical step, other important parameters for the reaction can be determined with CV, including the relationship between turnover frequency and overpotential, which in turn allows for calculation of the intrinsic turnover frequency, a benchmark for an efficient electrocatalyst.[58]

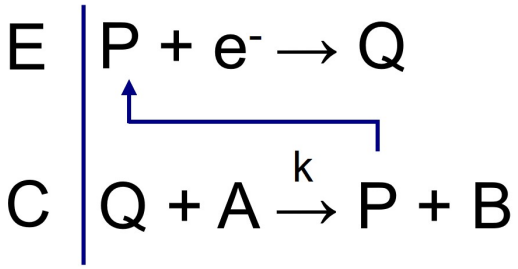

Scheme 1.3: A general scheme for an EC process, where a faradaic reaction (E) is coupled to a chemical redox reaction (C).

In Chapter 2, we aimed to extend this well-established and easily-performed measurement to systems under illumination so that we could obtain kinetic information electrochemically. We treated photoinduced charge transfer as a special case of the chemical redox reaction in the *EC* scheme, and just as had been done 60 years prior, we determined the rate. The major difference was that this time we did it with the lights on. Especially motivating to us was that the rate measures the full chemical process of charge separation (Scheme 1.2) on the same timescale as chemical reactions, not photophysics. In Chapter 3, we used this measurement technique to uncover a novel but highly general surface-mediated mechanism for photoinduced charge transfer. This mechanism was only visible because we were investigating charge transfer on these longer, chemically relevant timescales.

REFERENCES

(1) Roth, H. D. *Angewandte Chemie International Edition in English* **1989**, *28*, 1193–1207.

(2) Mai, S.; González, L. *Angewandte Chemie International Edition* **2020**, *59*, 16832–16846.

(3) Kodaimati, M. S.; McClelland, K. P.; He, C.; Lian, S.; Jiang, Y.; Zhang, Z.; Weiss, E. A. *Inorganic Chemistry* **2018**, *57*, 3659–3670.

(4) Fort, M. J.; Click, S. M.; Robinson, E. H.; He, F. M. C.; Bernhardt, P. V.; Rosenthal, S. J.; Macdonald, J. E. *Angewandte Chemie International Edition* **2022**, *n/a*, e202202322.

(5) Zhao, H.; Sun, C.; Yin, H.; Li, Y.; Gao, J.; Shi, Y.; Sun, M. *Scientific Reports* **2019**, *9*, 7756.

(6) Zhao, H.; Li, Y.; Diao, L.; Sun, C.; Shi, Y. *Spectrochimica Acta Part A: Molecular and Biomolecular Spectroscopy* **2019**, *218*, 237–242.

(7) Olshansky, J. H.; Ding, T. X.; Lee, Y. V.; Leone, S. R.; Alivisatos, A. P. *Journal of the American Chemical Society* **2015**, *137*, 15567–15575.

(8) Olshansky, J. H.; Balan, A. D.; Ding, T. X.; Fu, X.; Lee, Y. V.; Alivisatos, A. P. *ACS Nano* **2017**, *11*, 8346–8355.

(9) Zhu, H.; Yang, Y.; Wu, K.; Lian, T. *Annual Review of Physical Chemistry* **2016**, *67*, 259–281.

(10) Wang, J.; Ding, T.; Gao, K.; Wang, L.; Zhou, P.; Wu, K. *Nature Communications* **2021**, *12*, 6333.

(11) Zeng, S.; Li, Z.; Tan, W.; Si, J.; Huang, Z.; Hou, X. *The Journal of Physical Chemistry C* **2022**, *126*, 9091–9098.

(12) Morris-Cohen, A. J.; Peterson, M. D.; Frederick, M. T.; Kamm, J. M.; Weiss, E. A. *The Journal of Physical Chemistry Letters* **2012**, *3*, 2840–2844.

(13) Ye, C.; Zhang, D.-S.; Chen, B.; Tung, C.-H.; Wu, L.-Z. *ACS Central Science* **2024**, *10*, 529–542.

(14) De Roo, J.; Yazdani, N.; Drijvers, E.; Lauria, A.; Maes, J.; Owen, J. S.; Van Driessche, I.; Niederberger, M.; Wood, V.; Martins, J. C.; Infante, I.; Hens, Z. *Chemistry of Materials* **2018**, *30*, 5485–5492.

(15) Wang, Y.; Rogers, E. I.; Compton, R. G. *Journal of Electroanalytical Chemistry* **2010**, *648*, 15–19.

(16) Homer, M. K.; Kuo, D.-Y.; Dou, F. Y.; Cossairt, B. M. *Journal of the American Chemical Society* **2022**, *144*, 14226–14234.

(17) Zhang, Z.; Edme, K.; Lian, S.; Weiss, E. A. *Journal of the American Chemical Society* **2017**, *139*, 4246–4249.

(18) Knowles, K. E.; Tagliazucchi, M.; Malicki, M.; Swenson, N. K.; Weiss, E. A. *The Journal of Physical Chemistry C* **2013**, *117*, 15849–15857.

(19) Aruda, K. O.; Bohlmann Kunz, M.; Tagliazucchi, M.; Weiss, E. A. *The Journal of Physical Chemistry Letters* **2015**, *6*, 2841–2846.

(20) Peterson, M. D.; Jensen, S. C.; Weinberg, D. J.; Weiss, E. A. *ACS Nano* **2014**, *8*, 2826–2837.

(21) Bagnall, A. J.; Eliasson, N.; Hansson, S.; Chavarot-Kerlidou, M.; Artero, V.; Tian, H.; Hammarström, L. *ACS Catalysis* **2024**, *14*, 4186–4201.

(22) Wolff, C. M.; Frischmann, P. D.; Schulze, M.; Bohn, B. J.; Wein, R.; Livadas, P.; Carlson, M. T.; Jäckel, F.; Feldmann, J.; Würthner, F.; Stolarczyk, J. K. *Nature Energy* **2018**, *3*, 862–869.

(23) Dou, F. Y.; Harvey, S. M.; Mason, K. G.; Homer, M. K.; Gamelin, D. R.; Cossairt, B. M. *The Journal of Chemical Physics* **2023**, *158*, 184705.

(24) Lee, J. R.; Li, W.; Cowan, A. J.; Jäckel, F. *The Journal of Physical Chemistry C* **2017**, *121*, 15160–15168.

(25) Kim, M. R.; Ma, D. *The Journal of Physical Chemistry Letters* **2015**, *6*, 85–99.

(26) Yuan, M.; Liu, M.; Sargent, E. H. *Nature Energy* **2016**, *1*, 1–9.

(27) Konstantatos, G.; Sargent, E. H. *Nature Nanotechnology* **2010**, *5*, 391–400.

(28) Tian, W.; Zhou, H.; Li, L. *Small* **2017**, *13*, 1702107.

(29) Guo, R.; Zhang, M.; Ding, J.; Liu, A.; Huang, F.; Sheng, M. *Journal of Materials Chemistry C* **2022**, *10*, 7404–7422.

(30) Chen, O.; Zhao, J.; Chauhan, V. P.; Cui, J.; Wong, C.; Harris, D. K.; Wei, H.; Han, H.-S.; Fukumura, D.; Jain, R. K.; Bawendi, M. G. *Nature Materials* **2013**, *12*, 445–451.

(31) Galland, C.; Ghosh, Y.; Steinbrück, A.; Sykora, M.; Hollingsworth, J. A.; Klimov, V. I.; Htoon, H. *Nature* **2011**, *479*, 203–207.

(32) Kalisman, P.; Nakibli, Y.; Amirav, L. *Nano Letters* **2016**, *16*, 1776–1781.

(33) Amirav, L.; Alivisatos, A. P. *The Journal of Physical Chemistry Letters* **2010**, *1*, 1051–1054.

(34) Harvie, A. J.; Smith, C. T.; Ahumada-Lazo, R.; Jeuken, L. J. C.; Califano, M.; Bon, R. S.; Hardman, S. J. O.; Binks, D. J.; Critchley, K. *The Journal of Physical Chemistry C* **2018**, *122*, 10173–10180.

(35) La Croix, A. D.; O'Hara, A.; Reid, K. R.; Orfield, N. J.; Pantelides, S. T.; Rosenthal, S. J.; Macdonald, J. E. *Nano Letters* **2017**, *17*, 909–914.

(36) Jones, M.; D. Scholes, G. *Journal of Materials Chemistry* **2010**, *20*, 3533–3538.

(37) DuBose, J. T.; Kamat, P. V. *Chemical Reviews* **2022**, *122*, 12475–12494.

(38) Grimaldi, G.; Geuchies, J. J.; van der Stam, W.; du Fossé, I.; Brynjarsson, B.; Kirkwood, N.; Kinge, S.; Siebbeles, L. D.; Houtepen, A. J. *Nano Letters* **2019**, *19*, 3002–3010.

(39) Taheri, M. M.; Elbert, K. C.; Yang, S.; Diroll, B. T.; Park, J.; Murray, C. B.; Baxter, J. B. *The Journal of Physical Chemistry C* **2021**, *125*, 31–41.

(40) Morris-Cohen, A. J.; Frederick, M. T.; Cass, L. C.; Weiss, E. A. *Journal of the American Chemical Society* **2011**, *133*, 10146–10154.

(41) Santangelo, P. G.; Miskelly, G. M.; Lewis, N. S. *The Journal of Physical Chemistry* **1989**, *93*, 6128–6136.

(42) Santangelo, P. G.; Lieberman, M.; Lewis, N. S. *The Journal of Physical Chemistry B* **1998**, *102*, 4731–4738.

(43) Fujishima, A.; Honda, K. *Nature* **1972**, *238*, 37–38.

(44) R. Harris-Lee, T.; Marken, F.; L. Bentley, C.; Zhang, J.; L. Johnson, A. *EES Catalysis* **2023**, *1*, 832–873.

(45) Spadavecchia, F.; Ardizzone, S.; Cappelletti, G.; Falciola, L.; Ceotto, M.; Lotti, D. *Journal of Applied Electrochemistry* **2013**, *43*, 217–225.

(46) Peter, L. M.; Walker, A. B.; Bein, T.; Hufnagel, A. G.; Kondofersky, I. *Journal of Electroanalytical Chemistry* **2020**, *872*, 114234.

(47) Schwarzburg, K.; Willig, F. *Applied Physics Letters* **1991**, *58*, 2520–2522.

(48) Peter, L. M.; Li, J.; Peat, R.; Lewerenz, H. J.; Stumper, J. *Electrochimica Acta* **1990**, *35*, 1657–1664.

(49) Lazanas, A. C.; Prodromidis, M. I. *ACS Measurement Science Au* **2023**, *3*, 162–193.

(50) Fukatsu, A.; Kondo, M.; Okamura, M.; Yoshida, M.; Masaoka, S. *Scientific Reports* **2014**, *4*, 5327.

(51) Carlsson, H. S.; Lund, H.; Heby, O.; von Bahr, C.; Glaumann, H. *Acta Chemica Scandinavica* **1980**, *34b*, 409–412.

(52) Fukatsu, A.; Kondo, M.; Okabe, Y.; Masaoka, S. *Journal of Photochemistry and Photobiology A: Chemistry* **2015**, *313*, 143–148.

(53) Oda, N.; Tsuji, K.; Ichimura, A. *Analytical Sciences* **2001**, *17*, i375–i378.

(54) Ballardini, R.; Varani, G.; Indelli, M. T.; Scandola, F.; Balzani, V. *Journal of the American Chemical Society* **1978**, *100*, 7219–7223.

(55) Lund, H.; Carlsson, H. S.; Nishida, T.; Enzell, C. R.; Matsuno, T. *Acta Chemica Scandinavica* **1978**, *32b*, 505–509.

(56) Saveant, J. M. *Electrochimica Acta* **1967**, *12*, 999–1030.

(57) Saveant, J. M.; Vianello, E. *Electrochimica Acta* **1965**, *10*, 905–920.

(58) Costentin, C.; Drouet, S.; Robert, M.; Savéant, J.-M. *Journal of the American Chemical Society* **2012**, *134*, 11235–11242.

Chapter 2

PHOTOINDUCED CHARGE TRANSFER FROM QUANTUM DOTS MEASURED BY CYCLIC VOLTAMMETRY

2.1 Introduction

Photoinduced charge separation is a key step in artificial photosynthesis for the conversion of solar energy to high-value chemical compounds.[1] Quantum dots (QDs) have long been promoted as ideal photosensitizers for photocatalysis due to their high extinction coefficients, electronic tunability, and solution processability,[2] but efficient extraction of high-energy charge carriers from QDs remains a design challenge.[3] Photoinduced charge transfer from QD donors requires transfer of charges across a complex interface between the inorganic QD core and a molecular cocatalyst or substrate in solution.[4,5] This complicated interface comprises a high prevalence of defect electronic states in the QD,[6,7] and the covalent and noncovalent interactions between the QD, the insulating ligand shell, and the charge acceptor.[8] Conventional models of charge transfer in molecular systems (*e.g.*, the two-state system described by the Marcus formalism) are therefore insufficient to predict the rate of useful charge extraction from QDs, prompting experimental exploration.[9]

Photoluminescence spectroscopy[10–12] and transient absorbance spectroscopy[13,14] are frequently employed to determine rates of photoinduced charge transfer in QD systems. In these experiments, the charge-transfer process measured is pseudo-unimolecular with a first-order rate constant. This rate presumes preadsorption of the charge acceptor to the QD and does not consider freely diffusing charge acceptors nor the dynamic noncovalent chemical interactions between the QD and acceptor.[10,13,15,16] While determination of the first-order rate has utility, especially when compared with other unimolecular photophysical processes such as electron/hole recombination, there is a

large disconnect in the literature between the time scale for this fundamental process (picoseconds) and the time scale of photocatalytic reactions (minutes).[17,18] It may then be counterintuitive that several reports have found that the rate-limiting step of photocatalysis is charge transfer from nanocrystal photosensitizers to substrate or cocatalyst.[18–21] This disconnect begs us to consider that the spectroscopic first-order rate of charge transfer does not accurately report on the rate of production of charge-separated states, and instead a new method is needed to understand processes taking place on the same time scales as chemical reactions.[3]

Alternatively, charge transfer can be rationalized as a bimolecular reaction that is first order with respect to both the charge donor (excited QD) and acceptor (substrate).[22] The two species must first collide before charge can be extracted from the QD, and the rate of observed charge extraction will depend on the frequency of collisions, the rate of the fundamental photophysical process observed by time-resolved spectroscopies, and the fraction of collisions that allow strong electronic coupling between the QD and charge acceptor.

To this end, we turned to cyclic voltammetry (CV), a measurement tool that directly probes the changing oxidation state of a redox-active small molecule. CV has been employed in homogeneous electrocatalysis literature as a probe for the changing oxidation states of a molecular electrocatalyst[23] and has been theorized to be a tool for evaluating molecular photoelectrocatalysis.[24] We hypothesized that CV could be extended to systems involving photoinduced charge transfer from QDs. In the electrocatalysis literature, one of the simplest and most well-understood systems is described by two reactions: the oxidation and reduction of the electrocatalyst at the electrode, and the catalytic reaction in which the electrocatalyst transfers charge to the substrate. This mechanism is termed E_rC_i'. In such a system, the CV is modulated as compared to CVs in the absence of substrate, and this modulation can be quantified to obtain the rate constant for the catalytic reaction. For a thorough review of this technique, see Rountree et al.[23] In this work we aim to analogously measure the rate of productive charge extraction from QDs using CV (Scheme 2.1). We believe that the rates obtained through this measurement will accurately reflect the extraction of charge from QDs and will bridge the gap in time scales between photophysics and chemical transformations.

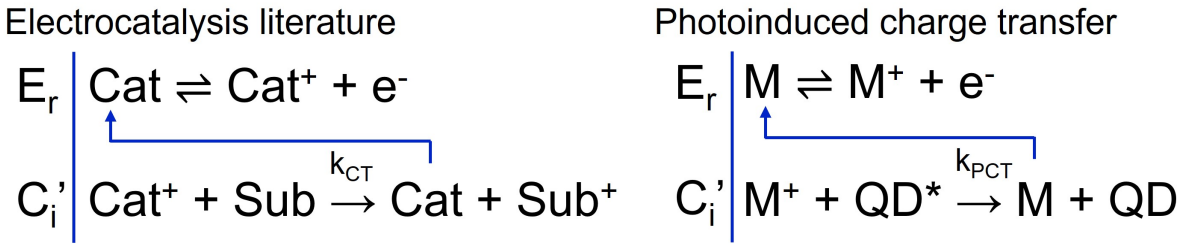

Scheme 2.1: E_rC_i' Mechanism and Extension to Photoinduced Charge Transfer. The mechanism used in electrocatalysis (left) is extended to photoinduced charge transfer (right) from an excited QD (QD*) to a molecular acceptor (M^+). In this work, k_{PCT} represents the intrinsic rate constant of photoinduced charge transfer.

2.2 Materials and Methods

2.2.1 Photoelectrochemistry Cell Design

A traditional three-electrode electrochemical cell was modified for *in situ* illumination. A 448 nm LED (Luxeon Star, equipped with a 12° beam optic, FWHM 20 nm) was positioned under a quartz cuvette with a polished bottom and open top (Figure 2.1). The LED was powered by a DC power supply (Nice-Power). The driving current was 0.2–0.8 A, corresponding to approximately 0.3–1.1 W of illumination.

Holes were drilled in a cuvette cap for the three electrodes, and the glassy carbon disc working electrode (BASi) was epoxied to the cap, ensuring the light had a constant and known path length (0.67 mm) through the solution to the active area of the working electrode. The path length is small to minimize undesired convection effects on the voltammogram from photoirradiation,[25] as well as to decrease the amount of light that is attenuated by the highly absorbent QDs in solution before reaching species near the working electrode surface. The counter electrode was a platinum wire, and the pseudoreference electrode was a silver wire in a ceramic-fritted glass tube (Pine) filled with 0.1 M [TBA][$B(C_6F_5)_4$].

In the photoelectrochemical setup, the cuvette was placed on top of the LED optic before each measurement, leading to slight variances in their relative positions, and thus slight differences in the amount of light reaching the electrode, causing some variance in the measurement. Variance could be minimized by designing a sample holder to fix the cuvette and LED's relative positions. We expect that this is our largest source of data variance, and this effect should be of a similar magnitude for all measured redox probes.

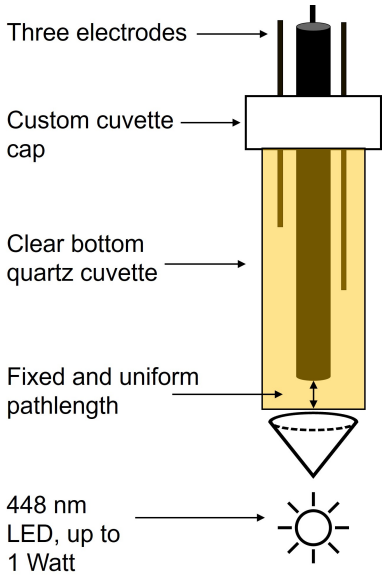

Figure 2.1: Drawing of the electrochemical cell for voltammetry under illumination.

2.2.2 Solvent and Electrolyte Design for Photoelectrochemistry

The selection of solvent and supporting electrolyte is critical to obtaining electrochemical measurements suitable for quantitatively monitoring photoinduced charge transfer. The solvent reorganizes to facilitate charge transfer, both from the working electrode to the redox probe and between the QD and the redox probe, so it must be polar to minimize internal resistance. The solvent must also allow high electrolyte concentration and have a wide electrochemical window to screen a wide range of redox probes. These electrochemical considerations are general, but for photoelectrochemistry,

the solvent must additionally not undergo any photodecomposition nor reactivity with excited QDs. Previously, our group found that a mixture of 9:1 tetrahydrofuran (THF)/acetonitrile was able to suspend oleic acid capped QDs with low internal resistance.[26] However, when THF was used in this work, the CV exhibited current crossover (Figure 2.2a), an unusual observation that indicates that the product of Faradaic oxidation on the forward scan of the CV has been chemically converted to another species that is more easily oxidized and observed on the backward segment.[27] Given prior observations that THF degrades under illumination to form reactive radicals,[28] THF is not a suitable solvent for this study.

Dichloromethane was another attractive solvent due to its modest polarity and ability to disperse as-synthesized QDs. Unfortunately, CVs under illumination displayed oscillations in the current, especially in the diffusion-limited regime (Figure 2.2b). These oscillations were the result of gas bubbles evolving and reaching the surface of the working electrode, which was observed visually during illumination of the sample. Headspace analysis detected production of methane after illumination (Figure 2.2c). With these observations, as well as prior observation of dehalogenation of CH_2Cl_2 with QD photocatalysts,[29] we conclude that the system photocatalytically dehalogenates CH_2Cl_2 to methane, so CH_2Cl_2 is not a suitable choice for photoelectrochemical measurement.

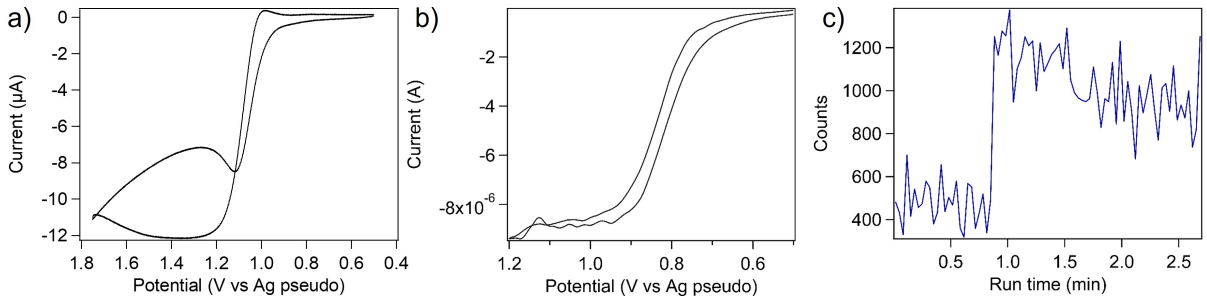

Figure 2.2: (a) CV of FcCOOH and oleate-capped CdS QDs in 9:1 THF:MeCN (50mV/s, 0.15M [TBA][PF_6]). under illumination (b) CV of FcCOOH and oleate-capped CdS QDs in CH_2Cl_2 (10 mV/s, 0.1M [TBA][$B(C_6F_5)_4$]) under illumination. (c) Headspace analysis using a real-time gas analyzer to detect methane in a vial prepared with 10 mmol FcCOOH, 0.077 μmol CdS QDs in 10 mL DCM

Another limitation in solvent choice is the solubility of the QDs, as QDs are often natively capped with aliphatic ligands that prevent dispersion in polar solvent at high electrolyte concentration. Ligand exchange was performed on QDs to replace the native oleic acid ligand shell with 2-[2-(2-methoxyethoxy)ethoxy]acetic acid (MEEAA), which is known to be an amphiphilic ligand that has dissolved nanocrystals in solvents ranging from toluene to water.[30,31] In our hands, 3.8 nm CdS QDs capped with this ligand are readily soluble in a variety of polar solvents, including water, acetone, and ethanol, but cannot be dispersed in some polar, aprotic solvents suitable for electrochemistry such as acetonitrile and propylene carbonate. Ultimately, benzonitrile (PhCN) was selected for this study because of the good colloidal stability of QDs in electrolyte solutions prepared using this solvent. MEEAA-capped QDs in benzonitrile solution remain suspended for at least several months even in the presence of electrolyte.

Finally, the solvent and electrolyte should allow reversible CVs for all the redox probes in the absence of QDs and illumination. Using the more common tetrabutylammonium salt of the $[PF_6]^-$ anion prevented reversible redox behavior of ferrocenecarboxylic acid (FcCOOH), presumably due to the high electrophilicity of the $[FcCOOH]^+$ cation. Instead, the tetrabutylammonium salt of the weakly coordinating anion $[B(C_6F_5)_4]^-$ was used. This completely fluorinated phenyl borate is known to stabilize organometallic cations, such that the only allowed processes in the CVs were oxidation and reduction of the metal center.[32] When this anion was used in the supporting electrolyte, FcCOOH displayed nearly ideal electrochemical reversibility.[33]

2.3 Results and Discussion

2.3.1 Charge Storage During Illumination and Slow Discharging after Illumination Observed Electrochemically

By illuminating the sample, the chemical reaction in the E_rC_i' mechanism is turned on, and we observe distortion of the CV shape. Classically, the shape of the CV in this mechanism can be described by a zone diagram (Figure 2.3a), where the zone observed will depend on the concentrations of charge donor and acceptor as well as the scan rate and the intrinsic rate of charge transfer. Generally, the solution in the electrochemical cell was 1.1×10^{-5} M QDs and approxi-

mately 130 equivalents of the redox probe. After beginning illumination of a solution of CdS QDs with ferrocene, a representative redox probe, successive CV scans continue to distort as compared to the dark trace for several minutes (Figure 2.3b). The CVs move to the right across the E_rC_i' zone diagram, from zone D to zone KD to zone KS, which by analogy to electrocatalysis literature[23] demonstrates an increase in the concentration of charge donor states (herein represented as [QD*]) (Figure 2.3a,b). This distortion occurs over *ca.* 20 min of illumination and then stabilizes, corresponding to a stabilization of [QD*]. We also monitored the solution with successive CV scans after illumination was stopped. Over the course of *ca.* 20 min, the CV recovers back to its original dark trace as [QD*] is slowly depleted to zero, thus tracking to the left along the E_rC_i' zone diagram (Figure 2.3c). This extremely long time scale until equilibration of [QD*] and long-lasting charge transfer after illumination ended was surprising, especially as compared to the speed of photoexcitation (femtoseconds) and exciton recombination (picoseconds-nanoseconds).[34] This implies that the charge donor state is not simply an exciton, but rather a long-lived product of a slow chemical process following excitation. Some excitons may directly act as charge donors, but exciton dissociation directly to the molecular probe is not the only process observed.

The photoelectrochemical technique demonstrated in this chapter is agnostic to the specific nature of the electron donor state. The changing oxidation state of the redox probe is being measured rather than changing photophysics of the QD, so the measurement is general regardless of the identity of the charge donor state. This generality is advantagous as it allows extension to a variety of chemical systems, but we cannot use this technique to probe why charges are stored after minutes of illumination. Investigation of the chemical identity of the charge donor state is the subject of Chapter 3.

While [QD*] stabilizes for a given light intensity after many minutes, the stable CVs of a representative redox probe, FcCOOH, are not the same when the light intensity is varied. As the power of illumination is increased from 0.33 W to 1.14 W, the stable CV is distorted further from the dark CV, again well matched to traversing to the right across the zone diagram (Figure 2.3d). This observation indicates that although at any given light intensity [QD*] reaches an equilibrium, a maximum concentration of charge donors has not been reached. It is expected that as light

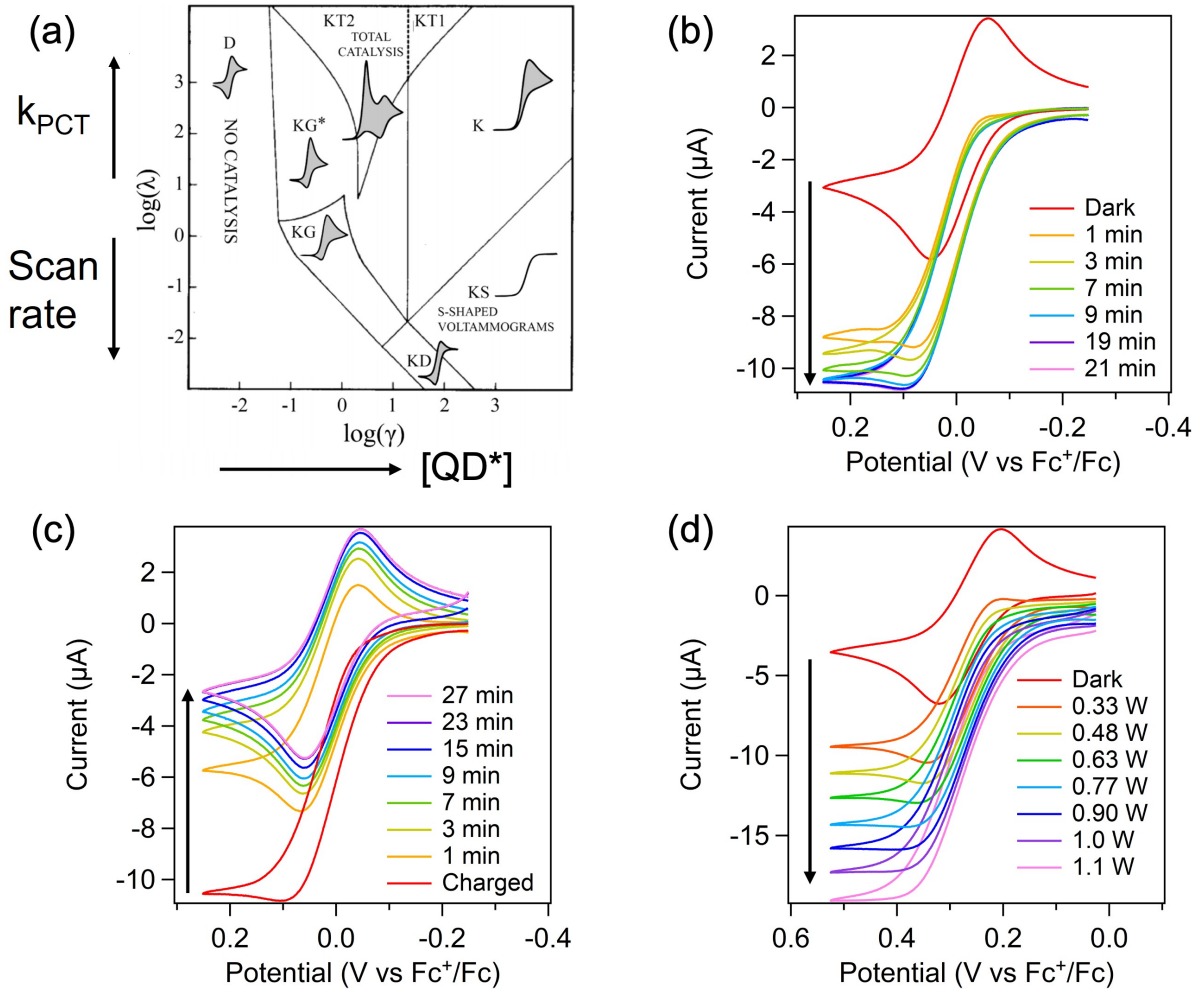

Figure 2.3: (a) Zone diagram for the E_rC_i' mechanism, adapted from Rountree et al. *Inorg. Chem.* **2014**, 53, 19, 9983–10002. Copyright 2014 American Chemical Society. (b) Increase in [QD*] monitored by successive CV scans of Fc after illumination begins. (c) Depletion of charge donor states by slow electron trapping monitored by CVs of Fc after illumination ends. (d) Light intensity dependence on equilibrated CVs of FcCOOH. 0.1 M [TBA][$B(C_6F_5)_4$], benzonitrile, glassy carbon working, Pt counter, Ag wire pseudoreference electrodes, 10 mV/s.

intensity is further increased, the CV would eventually stop distorting, but this light-saturated regime is not observed due to the limited power output of the LED light source.

2.3.2 Electron Acceptors: Co(Cp)(dppe), $FcNH_2$, Fc, FcCOOH, and $FcCOCH_3$

When QDs are added to solutions of Co(Cp)(dppe) (Cp = cyclopentadienyl, dppe = 1,2-bis(diphenylphosphino)ethane), aminoferrocene ($FcNH_2$), ferrocene (Fc), FcCOOH, or acetylferrocene ($FcCOCH_3$), the CV remains unchanged for traces without illumination. This observation, alongside no observed change in the dark open-circuit potential, demonstrates that none of these probes exhibit charge-transfer reactions with the QDs in the dark. Furthermore, the magnitude of the current does not change upon addition of QDs to the probes in the dark, indicating no adsorption to the QDs. If indeed there was adsorption, the effective diffusion coefficient of the redox probes would decrease due to the much larger QD, decreasing the current measured in CV. Previously, FcCOOH was observed to bind to oleate-capped CdSe QDs using CV through carboxylate–carboxylate exchange with the native ligand shell.[26] In contrast, FcCOOH does not undergo similar exchange with MEEAA-capped CdS QDs. The lack of exchange is rationalized by the lower pK_a of MEEAA ($pK_a = 3.61$)[35] compared to oleic acid ($pK_a = 9.85$).[36]

The CVs of solutions containing Co(Cp)(dppe), $FcNH_2$, Fc, FcCOOH, and $FcCOCH_3$ together with QDs all distort under illumination and stabilize after several minutes as described in the charge storage discussion above. For all probes at all light intensities and scan rates, there is an increase in oxidative current and a decrease of reductive current as compared to dark traces (Figure 2.4a). This implies that under illumination the oxidized probe, M^+, is reduced to M through photoinduced electron transfer from the QD. To elaborate, during the oxidative segment of the CV, as the potential is increased, M is oxidized to M^+ at the working electrode (E_r in Scheme 2.1). Then, some of this M^+ is reduced back to M by QD* (C_i in Scheme 2.1). This additional M can be oxidized at the electrode and so on, increasing the measured oxidative current as compared to the dark scan. On the reductive segment, M^+ formed at the electrode has been depleted by photoinduced charge transfer, so the magnitude of the reductive current is decreased. At high relative rates of electron

transfer, M^+ near the electrode is rapidly reduced to M, making $[M^+] = 0$ at the electrode surface, so there is no reductive current.

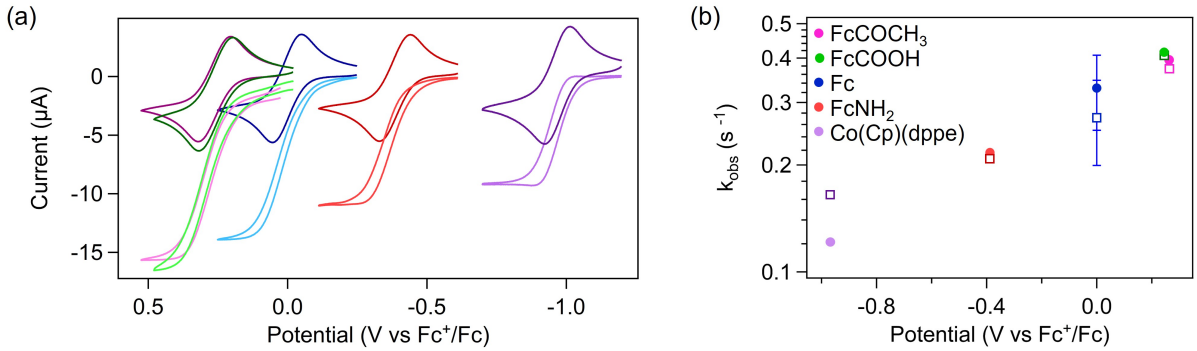

Figure 2.4: (a) CVs of the series of electron acceptors without illumination (dark colors) and with 1.1 W illumination (light colors). From left to right, the redox probes are $FcCOCH_3$ (fuchsia), FcCOOH (green), Fc (blue), $FcNH_2$ (red), and Co(Cp)(dppe) (purple). (b) Observed rate for photoinduced charge transfer under 0.77 W illumination determined mathematically (open squares) and by electrochemical modeling assuming a large value of γ (closed circles), plotted against the redox potential of each probe. Error bars on the Fc data point were obtained from quadruplicate experiments.

2.3.3 Mathematical Determination of E_rC_i' Rate Constant for Co(Cp)(dppe), $FcNH_2$, Fc, FcCOOH, and $FcCOCH_3$

The rate for the photoinduced charge transfer reaction (C_i' in the E_rC_i' mechanism) can be determined mathematically from voltammograms when in zone KD or KS, which are the zones observed in this work. In these experiments, the observed rate in the experiment (k_{obs}) is related to the scan-rate-independent plateau current (i_c) observed in zone KS and zone KD by 2.1, where n is the number of electrons transferred at the electrode, and i_p and ν are the peak current and scan rate for a reversible, dark experiment. Notably, this equation does not require any knowledge of the diffusion coefficient or concentration of the redox probe because the currents are taken as a ratio.

$$\frac{i_c}{i_p} = \frac{1}{0.446}\sqrt{\frac{RT}{nF\nu}k_{obs}} \tag{2.1}$$

The forward rate, k_{obs}, is a direct reporter on the rate of effective charge extraction and is distinct from values obtained spectroscopically. k_{obs} is plotted against the redox potential of the charge-accepting probes in Figure 2.4b. For a plot against the estimated driving force for electron transfer, see Figure 2.10.

2.3.4 Uncertainty in [QD] Results in Uncertain Intrinsic Rate*

The intrinsic rate constant, k_{PCT}, is related to the number of charge donors, [QD*], and k_{obs} by 2.2.

$$k_{obs} = k_{PCT}[QD^*] \tag{2.2}$$

It is experimentally challenging to determine [QD*] especially given that these charge donors may be electrons from excitons as well as stored charges, whose chemical identity and therefore means of quantification were not investigated in this chapter. The simplest starting hypothesis is that [QD*] is approximately equal to the analytical concentration of QDs, $[QD]_0$. In this assumption, each QD has one conduction band electron that is available for charge transfer. If we estimate that each QD has exactly one conduction band electron ready for electron transfer, then $[QD^*] = [QD]_0 = 1.1 \times 10^{-5}\,\text{M}$ and k_{PCT} is on the order of $10^4\,\text{M}^{-1}\,\text{s}^{-1}$.

Though estimating $[QD^*] = [QD]_0$ has solid conceptual backing, this value cannot explain the data with a simple E_rC_i' mechanism. The CVs taken during illumination pass from zone D to KD to KS (Figure 2.3a,b). In electrocatalysis, zones KS and KD are observed when operating under conditions of no substrate consumption due to large excess of substrate compared to the concentration of catalyst. In our scheme, (Scheme 2.1) the "substrate" in the C_i' reaction of the E_rC_i' mechanism is QD*. By analogy, this implies that zones KS and KD should only be observed when QD* is not consumed by the charge-transfer reaction. This could occur either when QD* is in excess compared to the molecular probe M or when QD* is regenerated once an electron is transferred from QD* to M^+, effectively making [QD*] constant despite being small. The amount

of excess QD* compared to M is quantified by the dimensionless parameter γ, defined in 2.3. With only the two reactions in the E_rC_i' mechanism, zone KS should only be observed when $log(\gamma) > 1$.

$$\gamma = \frac{[QD*]}{[M]} \tag{2.3}$$

If [QD*] = $[QD]_0$, then $log(\gamma) \approx -2$ and M is in excess, not QD*. So, if we assume [QD*] = $[QD]_0$, then QD* must be regenerated to explain the experimental data. This conclusion is exemplified by electrochemical modeling of CVs in DigiElch. When [QD*] = $[QD]_0$ without an explicit regeneration step, the modeled CVs show very little deviation from the ground state dark CVs, regardless of the rate of charge transfer, because there is so little QD* compared to the redox probe and it is quickly depleted at the electrode (Figure 2.5a,c). When a third reaction allowing for the fast regeneration of QD* was added to the model, we can capture the observed data even with small values of γ (Figure 2.5a,b). The modeled values of k_{PCT} when fast regeneration is added to the model are on the order of $10^4\,\text{M}^{-1}\,\text{s}^{-1}$, and inputting [QD*] = $[QD]_0$ into 2.2 gives observed rates on the order of 0.1 s^{-1}. Modeling parameters can be found in the Appendix.

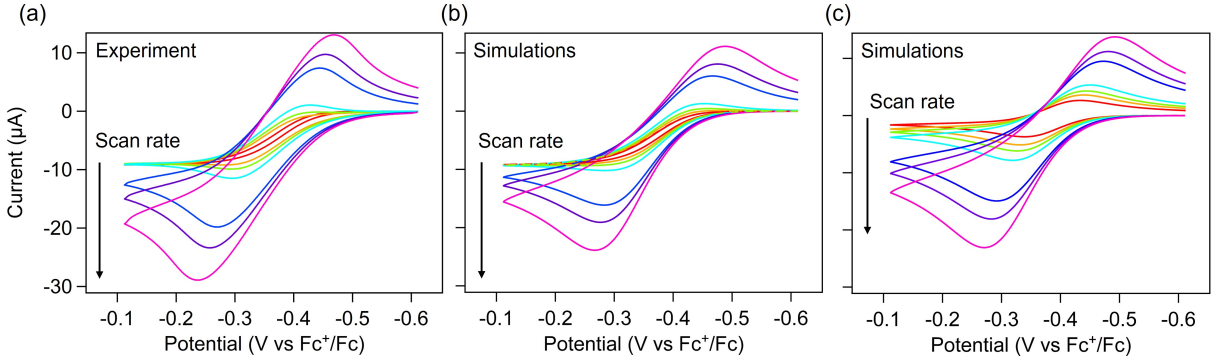

Figure 2.5: Comparison of the experimental data (a) to the simulated data (b,c). In (b), the simulations with [QD*] = 10^4 × [QD]0 are plotted in dashed lines and the simulations with [QD*] = $[QD]_0$ and regeneration of QD* are plotted in solid lines; these nearly perfectly overlay. In (c), [QD*] = $[QD]_0 = 1.1 \times 10^{-5}$ M without any regeneration of QD*. 0.1M [TBA][$B(C_6F_5)_4$], benzonitrile, glassy carbon working, Pt counter, Ag wire pseudo reference electrodes, scan rate was varied from 5 mV/s (red) to 250 mV/s (fuchsia).

During illuminated studies, regeneration of QD* makes good sense; after electron transfer the QD can be re-excited. However, when illumination is stopped, there cannot be any photoinduced regeneration of QD* at the electrode, which is inconsistent with our observation of CVs in zone KD (Figure 2.3c) even after illumination ends. This implies [QD*] at the electrode cannot be approximately equal to $[QD]_0$ because the CVs still show deviation from the dark ground state CVs even without the possibility of regeneration. To explain the experimental data then, [QD*] could be several orders of magnitude larger than $[QD]_0$, so that [QD*] is not greatly changed after charge is transferred to M^+. Furthermore, this concentration is not immediately depleted in the absence of photoexcitation, allowing observation of zone KD after illumination is stopped. For example, if we let $log(\gamma) = 2$ under illumination, [QD*] near the working electrode increases to $10^4 \times [QD]_0$. The local [QD*] at the electrode might be higher than the bulk $[QD]_0$ if the QDs adsorb to the working electrode. Alternatively, during illumination many electrons per QD may accumulate as reduced surface Cd^0 that act as charge donors, making the concentration of donor states higher than the local concentration of QDs. If we set $[QD^*] = 10^4 \times [QD]_0 = 0.11\,\text{M}$, the experimental CVs with different scan rates can be modeled with only the two reactions corresponding to those in the $E_r C_i'$ mechanism (Figure 4). In this method, the modeled intrinsic rate constants are on the order of $1\,\text{M}^{-1}\,\text{s}^{-1}$, and multiplying by [QD*] again gives observed rates on the order of $0.1\ \text{s}^{-1}$. These observed rates are comparable to those quantified by the direct mathematical calculation from the plateau and peak currents (Figure 2.4b). The two methods of modeling the data give nearly the same simulated CVs in addition to well-matching the experiment (Figure 4). We are pleased to report that electrochemical modeling was an effective method of determination of the observed rate because it adds generality to our method. In these experiments, only zones D, KD, and KS were observed, but in other systems reaching these zones may be experimentally constrained, precluding the use of the direct mathematical determination of the rate.

2.3.5 Discussion of Photoinduced Charge Transfer to Co(Cp)(dppe), $FcNH_2$, Fc, FcCOOH, and $FcCOCH_3$

Using both mathematical determination of charge transfer and electrochemical modeling, k_{obs} was determined for the range of electron-accepting probes. When comparing the mathematical determination and the modeling results (Figure 2.4b), k_{obs} from the two methods was commensurate. Unsurprisingly, with larger driving force, k_{obs} monotonically increases in both methods of determination. This observation is well supported by existing QD literature, wherein the Marcus inverted region is never observed and photoinduced charge transfer from quantum dots is better explained by other rationalizations.[9,11,37,38] While others have demonstrated a similar relationship between driving force and rate of charge transfer,[9,11,39,40] we were uniquely able to measure this through CV.

We have demonstrated that the driving force for photoinduced charge transfer is the critical factor controlling k_{obs} rather than chemical identity. FcCOOH and $FcCOCH_3$ have nearly the same E^0 but have different chemical interactions with solvent, electrolyte, and the QD ligand shell. Despite these differences, the k_{obs} values for these two redox probes are nearly identical. Therefore, the differences between these redox probes are due to different rates of the pseudo-unimolecular photoinduced charge-transfer elementary step (which is directly controlled by the driving force) rather than chemical interactions with the QD. This observation contrasts with studies where the charge acceptor was bound to the quantum dot through a headgroup, and the identity of this headgroup controlled the rate of photoinduced charge transfer by controlling the binding equilibrium to the QD surface. (15)

The estimated k_{PCT} values are on the order of $1\,\mathrm{M}^{-1}\,\mathrm{s}^{-1}$ for the model with high [QD*] and without regeneration and are on the order of $10^4\,\mathrm{M}^{-1}\,\mathrm{s}^{-1}$ for the model with low [QD*] and regeneration. As a benchmark, the diffusion-controlled rate constant (k_{diff}, the rate assuming every collision results in a charge transferred) is estimated by the Smoluchowski equation (2.4), where R_{QD} and R_M are the radii of the QD and molecular charge acceptor, respectively, and D_{QD} and D_M are the diffusion coefficients (see the SI for details).[41] Importantly, k_{diff} can be directly compared to the result from this work, as both describe bimolecular processes with the same units. Then,

$k_{diff} \approx 10^{10}\,\mathrm{M}^{-1}\,\mathrm{s}^{-1}$ is at least 6 orders of magnitude larger than k_{PCT} determined in this work. This implies that productive photoinduced charge transfer is a rare event in these experiments: for one million collisions, less than one charge is effectively transferred to the charge acceptor. We believe the low k_{PCT} helps explain common observations that photocatalytic reactions suffer from extremely poor quantum yield.[18] We attribute the small k_{PCT} to the extremely weak electronic coupling between the inorganic QD core and M in solution. Either charges must tunnel through the ligand shell to reach M in solution or M must bury itself in the ligand shell to get better electronic overlap.[42]

$$k_{diff} = \frac{4\pi N}{1000}\left(R_{QD} + R_M\right)\left(D_{QD} + D_M\right) = 2 \times 10^{10} M^{-1} s^{-1} \tag{2.4}$$

Further, we can compare the observed rate constant (k_{obs}) to reported turnover frequencies (TOF) for homogeneous catalysts.[23] In this context,k_{obs}describes the moles of electrons transferred from QD to redox probe, per unit time per mole of the oxidized redox probe in the diffusion layer. Then, the maximum TOF for the electron acceptors in this work is just the observed rate and is on the order of $0.1\,\mathrm{s}^{-1}$. In comparison, the well-known nitrogenase enzyme, which reduces N_2 to NH_3, was measured electrochemically to have an electron transfer TOF of $14\,\mathrm{s}^{-1}$.[43] Similarly, we can compare to photocatalytic systems. In an iridium photocatalytic system tuned for CO2 reduction, the highest observed TOF was $0.006\,\mathrm{s}^{-1}$.[44] In a CdSe QD photocatalytic system tuned for C–O bond cleavage, the TOF was $1.7\,\mathrm{s}^{-1}$.[17] These benchmarks place observed photoinduced electron transfer from QDs faster than reductive photocatalysis in a molecular system, slower than an enzymatic reduction, and about on par with a QD photocatalysis system.

2.3.6 Net Hole Transfer to $CoCp_2$

To expand the utility of this method, we considered a probe with lower E^0: cobaltocenium ($CoCp_2^+$). In illuminated CV experiments with this redox probe, the oxidative current decreases and the reductive current increases in a manner consistent with the E_rC_i' mechanism, indicating that there is effective photoinduced hole extraction from the QD to the reduced form of the probe (Figure 2.6). We are particularly excited by this result because it demonstrates that our method

for measuring charge transfer can be generalized to hole transfer as well as electron transfer. This is in contrast with spectroscopic characterization, where electron and hole dynamics are difficult to isolate.[45]

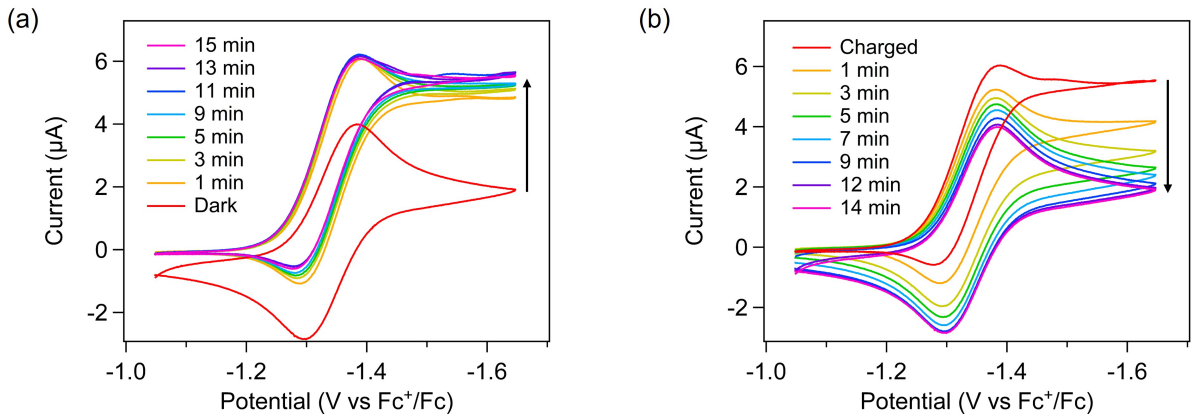

Figure 2.6: (a) CVs of $CoCp_2^+$ taken after illumination is begun. (b) CVs of $CoCp_2^+$ monitored after illumination ends, demonstrating slow depletion of hole donor states. 0.1 M [TBA][PF_6], benzonitrile, glassy carbon working, Pt counter, Ag wire pseudoreference electrodes, 10 mV/s.

In the $CoCp_2^+$ solution with QDs, after illumination is begun the CV distorts over several minutes as described above; then the CVs stop changing (Figure 2.6a). Similarly, when illumination is stopped, the CVs take several minutes before overlaying with the trace before illumination (Figure 2.6b). This indicates that, as in the case of electron transfer, the hole-donating species forms over several minutes under illumination before equilibration, and some of these hole-donating species are long-lived. We propose that this long-lived hole-donating species is formed in a complimentary process to formation of the electron-donating species. Trap-mediated hole transfer to molecules has previously been demonstrated in similar QD systems, though on different timescales.[11,39] In the same manner as the electron acceptor series, the rate of photoinduced hole transfer to $CoCp_2$ was determined mathematically and through electrochemical modeling. The mathematical method gives a k_{obs} of 0.15 s^{-1}, and the modeling method with [QD*] = 0.11 M gives 0.12 s^{-1}. This is in good agreement with prior observations that in reductive photocatalysis hole quenching rather

than electron transfer to cocatalyst is rate limiting.[20,46] Uniquely, we are able to easily disentangle hole-transfer dynamics from electron transfer by directly monitoring either oxidation or reduction of the molecular probe.

2.4 Conclusion

In this work, cyclic voltammetry has been used for the first time to quantify the rate of photoinduced charge transfer in solution. By carefully designing the photoelectrochemical cell and solvent/electrolyte combination, we were able to simultaneously irradiate and take CV data, generating dynamics that could be readily described by a two-reaction E_rC_i' mechanism. This technique is a powerful tool for screening photocatalytic systems by directly measuring the effective rate of charge extraction from a photosensitizer. By varying the redox potential of molecular charge acceptors, both net electron and hole transfer from colloidal quantum dots were observed. Using this technique, we were able to reproduce spectroscopic observation that the rate of photoinduced electron transfer from QDs increases monotonically with driving force. This method is especially compelling because it directly probes the changing oxidation state of the charge acceptor, in contrast with many other techniques that focus on the photophysics of the photosensitizer. The resulting observed rates of charge transfer, on the order of 0.1 s^{-1}, are distinct from the spectroscopically measured picosecond dynamics and report on the rate of generation of charge-separated states relevant to photocatalysis. Long-lived and slow to generate electron and hole donors were formed during illumination, and this process was uniquely observed with photoelectrochemistry.

2.5 Outlook

This work demonstrated a new way to measure charge transfer in a relatively simple system: one kind of QD (CdS), and the comparison between different rates was controlled by the redox potential of the molecular redox probe. Furthermore, the only reactivity being studied was the simple one-electron oxidation or reduction of the probe. However, the nature of this measurement is that it is agnostic to the identity of the photoactive charge donor so long is it does not engage in redox chemistry directly with the working electrode. This allows for vast variation of the photoactive

charge donor including other QDs, other colloidal nanomaterial, or even molecular photocatalysts with no modification to experimental setup.

One extension of this work would be to apply the technique to a real photocatalytic system. That is, it would be interesting to investigate charge transfer from QD to a cocatalyst, and then subsequent charge transfer from the cocatalyst to substrate of a useful reaction. An additional reaction would be added to the E_rC_i' mechanism, as shown in Scheme 2.2. This mechanism is is more complicated than E_rC_i' because Cat and Cat^+ are both part of all three reactions. However, one could imagine breaking the reaction up into to experiments as shown in Scheme 2.2 and measuring k_{PCT} and k_{CAT} separately. Then, the overall rate of photocatalysis is dependent on both, and perhaps even the slow step of photocatalysis will be easily revealed. By extension, this might allow more rapid screening of photocatalytic systems.

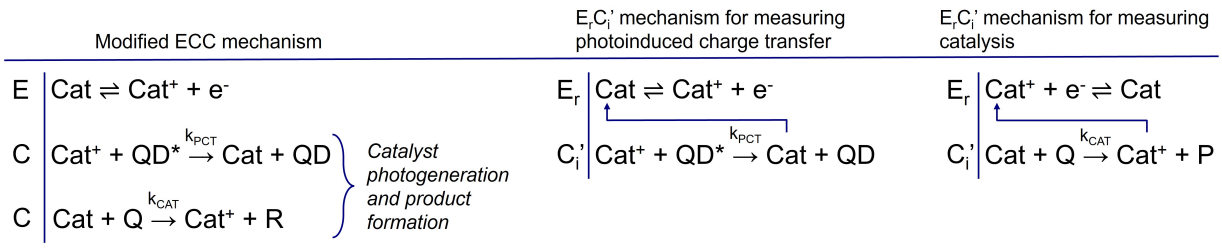

Scheme 2.2: An example of how the E_rC_i' mechanism might be amended if the redox probe is instead a redox cocatalyst. The left set of reactions may be disentangled by separately measuring charge transfer from QD to catalyst (middle) and from catalyst to substrate (right).

One promising variation of this experiment is to vary the dipole moment of the QD surface ligands. It is known that the dipole moment of the surface ligands can tune the band edge positions of QD films by up to 2 eV.[47,48] Despite application of this phenomenon in QD photovoltaic literature, has yet to be shown that by varying the ligand shell the effective driving force for charge transfer in the solution phase is modified. One recent work has compared ligands with positively or negatively charged tails, which should greatly influence their dipole, and there were large differences between

the two.[49] This effect could be probed simply with the photoelectrochemistry technique presented here.

One challenge with this measurement is that it required that the QD charge donor be colloidally stable in polar solvent. We could consider experiments where the QD does not need to be colloidally stable, that is, setups where QDs are deposited on the electrode surface. Our research group has had some success with this method already and have preliminary results that show the same modulation of CV from reversible to S-shaped during illumination, encouraging us that charge transfer from immobilized QDs can be measured and modeled similarly to freely diffusing. Of course, this measurement requires that the working electrode still be conductive and that the applied potential does not induce electrochemical changes directly to the QD. In other words, the applied current should not have to pass through the QD so the QD should be fairly distantly dispersed. Depending on the targeted use of charge transfer, immobilization of the QD might make the experiment more or less close to application.

2.6 Experimental Details

2.6.1 Chemicals and General Considerations

Anhydrous hexadecane (≥99%), anhydrous chloroform (99%), anhydrous methanol (99.8%), cadmium oxide (99.95% trace metals basis), oleic acid (90%), trifluoroacetic anhydride (≥99%), trifluoroacetic acid (99%), acetylferrocene (95%), aminoferrocene (98%), dicarbonylcyclopentadienyl cobalt(I) ($CoCp(CO)_2$, technical grade), ethylenebis(diphenylphosphine) (99%), ethynyltrimethylsilane (98%), cobaltocenium hexafluorophosphate (98%), n-butyllithium solution (1.6M in hexanes), tritylium hexafluorophosphate, sodium fluoride (≥99%), potassium permanganate (≥99%), hexafluorophosphoric acid (∼55 wt% in H_2O), magnesium sulfate (anhydrous, ≥97%), acetonitrile (≥99.9%), methanol (MeOH, 99%) diethyl ether (99%), biphenyl (99.5%), and diphenyl oxide (98%) were purchased from MilliporeSigma and used as received. Ferrocene (95%) was purchased from MilliporeSigma and purified by sublimation. Ferrocenecarboxylic acid (97%) was purchased from MilliporeSigma and purified by recrystallization from acetonitrile and toluene. Benzonitrile (anhydrous, ≥99%) was purchased from MilliporeSigma and dried and distilled twice over phosphorus

pentoxide (99%), then stored over 3Å sieves in a nitrogen-filled glovebox. Triethylamine (99%), tetrabutylammonium bromide ([TBA][Br], ≥99%), methylene chloride (≥99.9%) we purchased from Fischer and used as received. Lithium tetrakis(pentafluorophenyl)borate etherate was purchased from Boulder Scientific Company and used as received. [2-(2- Methoxyethoxy)ethoxy]acetic Acid (>95%) was purchased from Tokyo Chemical Industry and dried over 3Å sieves, then distilled before storing over sieves in a nitrogen-filled glovebox. Tetrabutylammonium hexafluorophosphate ([TBA][PF6], 98%) was purchased from VWR Scientific and recrystallized twice from ethanol.

2.6.2 Photoelectrochemistry Details

All electrochemical experiments were performed in a nitrogen-filled glove box. This is an especially important detail, as even trace oxygen may be capable of reacting with stored electrons. The potentiostat used was an EC Epsilon from BASi. Glassy carbon disk electrodes with a diameter of 3.0 mm were polished using 5, 1, and 0.1 micron polishing powder with sonication in ultrapure water between steps. All experiments were referenced to an internal ferrocene standard added after experiment. Typical measurements used a 0.001 42 M solution of the redox probe. The concentration of QDs was equal to 11 µM, determined by optical absorption spectroscopy.[2] This concentration corresponds to about 130 redox probes/QD. The LED power was determined from the datasheet provided by the manufacturer (Luxeon) that correlated driving current to power.

2.6.3 Synthesis of Cadmium Oleate

Cadmium oleate was prepared following a procedure by Hamachi et al[50] in air. Cadmium oxide (5.14 g, 40 mmol) was stirred with 55 mL acetonitrile. Trifluoroacetic acid (0.86mL, 11.2 mmol) then trifluoroacetic anhydride (6.12 mL, 44 mmol) were added dropwise. This mixture was stirred for an hour and turned from heterogeneous with red CdO to clear. In a separate flask, oleic acid (22.6g, 80 mmol), dichloromethane (400 mL) and triethylamine (13.9 mL, 100 mmol) were combined. The cadmium solution was added dropwise with stirring and then heated to 60 °C. The now clear solution was allowed to slowly cool to room temperature, then put in a freezer. The white powder precipitate was isolated with vacuum filtration and washed with acetonitrile.

2.6.4 Synthesis of CdS QDs

CdS QDs were prepared under nitrogen using standard Schlenk procedures. following a procedure by Hamachi et al.[50] Briefly, cadmium oleate (2.43 g, 3.6 mmol) and oleic acid (2.04 g, 7.2 mmol) were added to 140 mL of hexadecane. This mixture was heated to 120 °C and held under vacuum for 1 hour. The flask was refilled with N_2 and then further heated to 230 °C. In a nitrogen-filled glovebox, tetramethyl thiourea (0.396 g, 3 mmol) was dissolved in biphenyl/diphenyl ether eutectic (6 mL). This solution was swiftly injected into the cadmium oleate mixture. The reaction occurred over 90 minutes and the solution changed from clear to yellow. Then the reaction mixture was cooled to room temperature. The solvent was removed with vacuum distillation. The nanocrystals are then isolated with repeated suspension and precipitation with pentane and methanol.

2.6.5 Ligand Exchange of Oleic Acid for MEEAA

The ligand exchange procedure was adapted from De Roo et al.[30] Oleic acid-capped QDs (9.35×10^{-7} mol) were dried then 7.2 mL chloroform and MEEAA (2.43 g, 6.82 mmol) were added to the pellet. The mixture was stirred overnight, then sonicated for 30 minutes to yield a clear, yellow QD suspension. Three suspension and precipitation washes using chloroform and pentane were performed, each time yielding a yellow pellet and clear, colorless supernatant. After the third washing cycle, 1.2 g additional MEEAA was added to encourage a more complete exchange. This solution was sonicated for 30 minutes, followed by four additional purification washes. The sample was stored as a dry powder, and complete exchange was verified by ^{1}H NMR (Figure 2.7). The final QDs show a first excitonic transition at 460 nm (Figure 2.8). The particles have an average diameter of 3.76 ± 0.42 nm by TEM analysis (Figure 2.9). The photoluminescent quantum yield of these particles is 0.52% when excited at 420 nm.

2.6.6 Preparation of [TBA][B(C_6F_5)$_4$]

Tetrabutylammonium tetrakis(pentafluorophenyl)borate ([TBA][B(C_6F_5)$_4$]) was prepared from salt metathesis of lithium tetrakis(pentafluorophenyl)borate etherate and [TBA][Br] according to LeSuer et al.[51] Briefly, lithium tetrakis(pentafluorophenyl)borate etherate (25g) was dissolved in

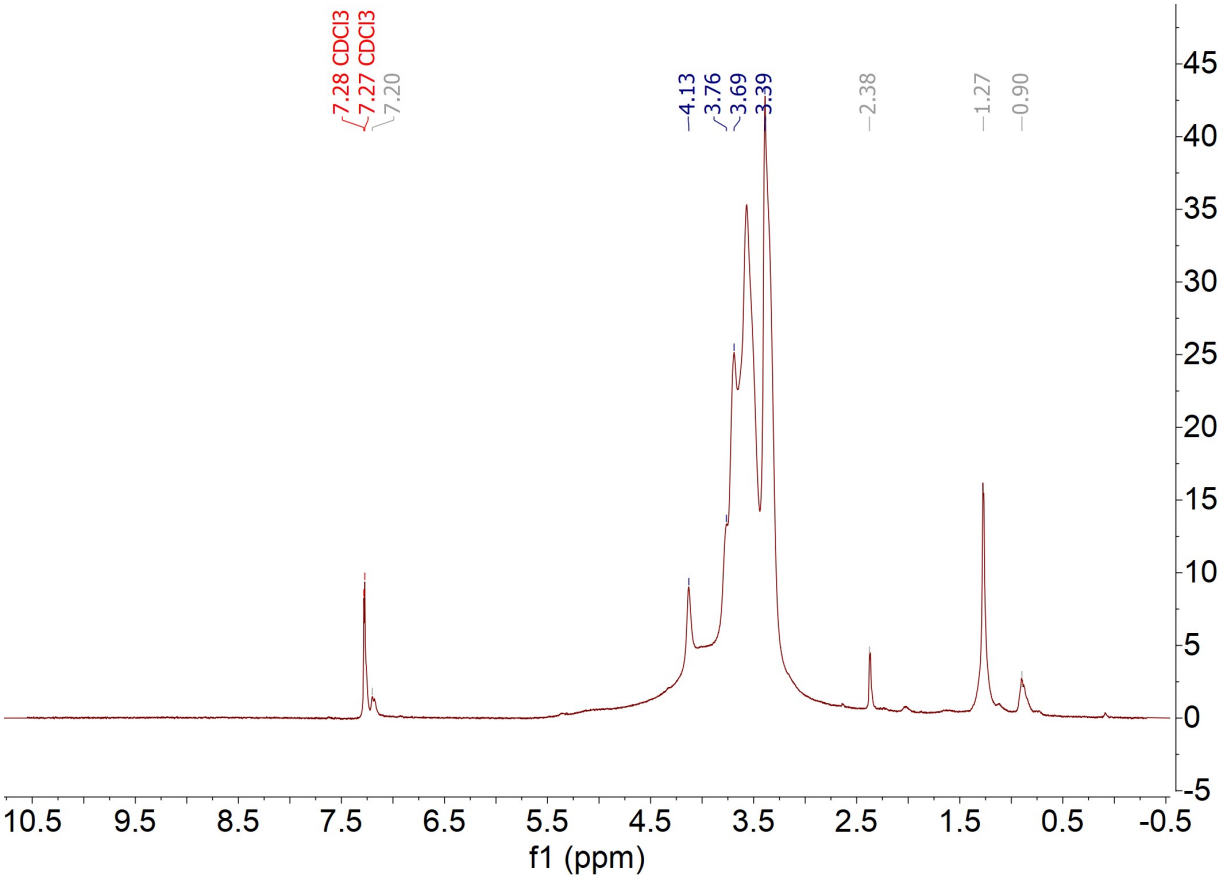

Figure 2.7: ^{1}H NMR ($CDCl_3$, 300 MHz) of CdS QDs after exchange for MEEAA ligands.

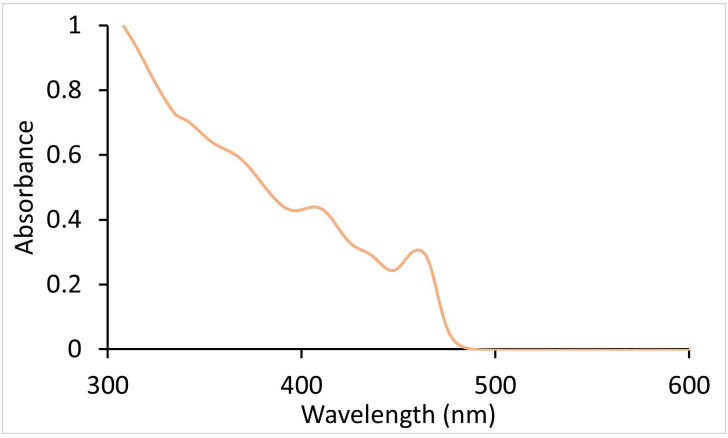

Figure 2.8: UV-vis absorption spectrum of MEEAA-capped CdS QDs.

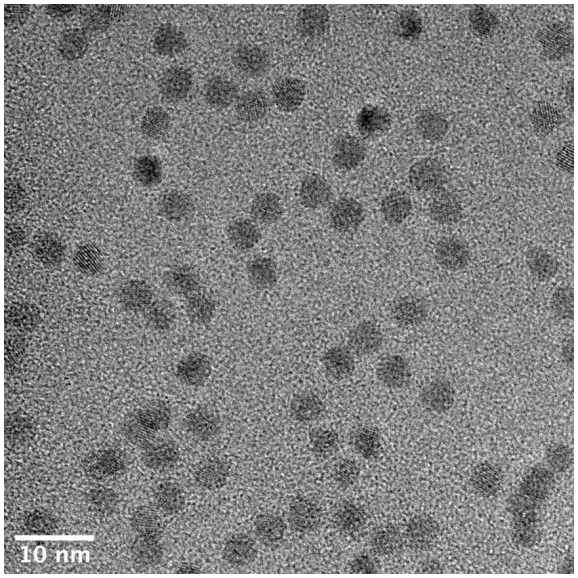

Figure 2.9: Representative transmission electron microscopy image of MEEAA-capped CdS QDs.

MeOH (50 mL). [TBA][Br] (12.75 g) was dissolved in MeOH (25 mL). The [TBA][Br] solution was added dropwise to the first solution with stirring. Ultrapure water (18 MΩ, 7.5 mL) was added dropwise to precipitate the product. The product was recrystallized twice from methylene chloride and diethyl ether.

2.6.7 Synthesis of Co(Cp)(dppe) (Cp = cyclopentadienyl, dppe = 1,2-Bis(diphenyl phosphino)ethane)

Co(Cp)(dppe) was prepared from the decarbonylation of CoCp(CO)2 according to literature procedure[52] and used without further purification.

2.6.8 Synthesis of [$CoCp_2COOH$][PF_6]

Cobaltocenium carboxylic acid hexafluorophosphate ([$CoCp_2COOH$][PF_6]) was prepared from [$CoCp_2$][PF_6] according to a three-step literature procedure.[53] The product was purified by recrystallization from anhydrous acetonitrile and anhydrous chloroform.

2.6.9 Preparation of Biphenyl and Diphenyl Ether Eutectic Mixture

A eutectic mixture of biphenyl (26.5 wt%) and diphenyl oxide (73.5 wt%) was prepared by heating both components to 70 °C. This liquid was dried over sieves and distilled before storing in a nitrogen-filled glove box.

2.7 Data Processing Details

2.7.1 Estimation of the Diffusion-Controlled Rate Constant, k_{diff}

The diffusion-controlled rate constant was roughly estimated with the Smoluchowski equation (2.5). R_{QD} , or the radius of the quantum dot, was estimated as $\frac{1}{2}$of the diameter measured by TEM plus the estimated length of one ligand (1.5 nm)[31] to make a total radius of 3.38 nm. The radius of the molecular probe, R_M was the hydrodynamic radius of ferrocene, which others have estimated as 0.32 nm.[54] The diffusion coefficients were the same as those used in the electrochemical modeling ($4.67 \times 10^{-6}\,cm^2\,s^{-1}$ for Fc and $3.12 \times 10^{-6}\,cm^2\,s^{-1}$ for QD).

$$k_{diff} = \frac{4\pi N}{1000}\left(R_{QD} + R_M\right)\left(D_{QD} + D_M\right) = 2 \times 10^{10}\,M^{-1}\,s^{-1} \tag{2.5}$$

2.7.2 Estimation of Driving Force for Electron Transfer

This section estimates that the energy of the electron before transfer to be the same as the energy of the conduction band edge. Measurement of the band edge potentials of solution phase QDs is notoriously difficult. Instead, we estimate the band edge potentials by expanding the band gap as compared to the bulk bandgap. For CdS, the bulk band gap is 2.42 eV with bulk conduction band edge at -4.05 eV vs vacuum.[55] In the QD system, the band gap estimated to be 2.70 eV from the energy of the first excitonic transition at 460 nm in the UV-vis spectrum. Then, we estimate that the difference between QD band gap and bulk band gap (0.28 eV) is split evenly between raising the conduction band edge and lowering the valence band edge. Then, the conduction band edge (ECB) is about -3.91 eV vs vacuum.

The redox potential of each redox probe ($E_{M+/M}$) was measured vs the Fc^+/Fc couple. The Fc^+/Fc couple is approximated to be –5.06 V vs vacuum[56] and $E_{M+/M}$ is then referenced vs

vacuum. Then, the driving force for electron transfer from the conduction band edge is estimated as

$$-\Delta G^0_{ET} = E_{CB} - E_{M^+/M} \tag{2.6}$$

For example, for electron transfer to unsubstituted Fc+, the driving force $-\Delta G^0_{ET}$ is

$$-\Delta G^0_{ET} \ = -3.91eV - (-5.06eV) = 1.14eV \tag{2.7}$$

Then, the observed rate of charge transfer can be plotted against the estimated driving force in Figure 2.10

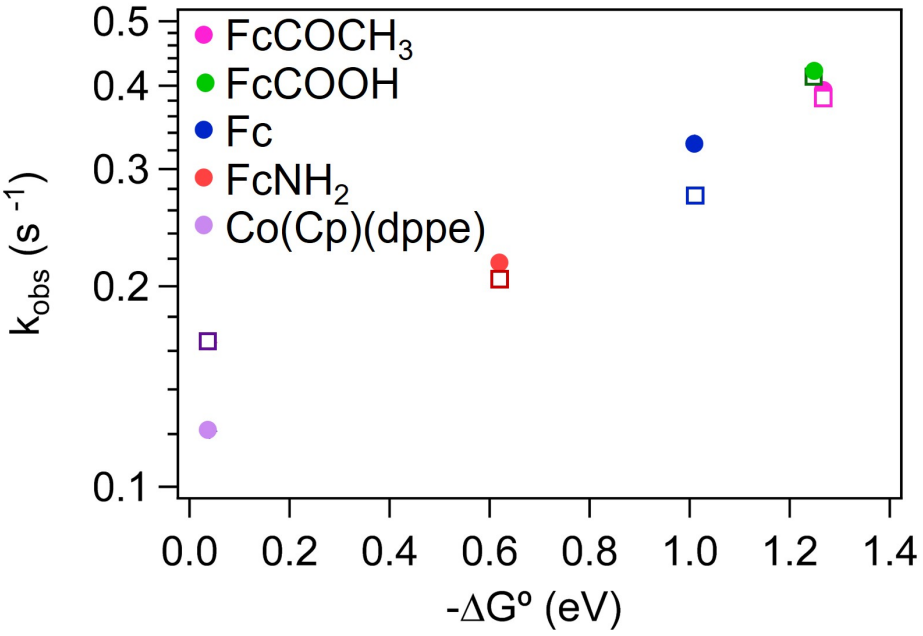

Figure 2.10: A plot of the observed rate against the estimated driving force for electron transfer. The open squares were calculated with the direct mathematical method and the closed circles were calculated with electrochemical modeling assuming $[\mathrm{QD}^*] = [\mathrm{QD}]_0 = 1.1 \times 10^{-5}$ M.

REFERENCES

(1) Qiu, F.; Han, Z.; Peterson, J. J.; Odoi, M. Y.; Sowers, K. L.; Krauss, T. D. *Nano Letters* **2016**, *16*, 5347–5352.

(2) Yu, W. W.; Qu, L.; Guo, W.; Peng, X. *Chemistry of Materials* **2003**, *15*, 2854–2860.

(3) Rabouw, F. T.; de Mello Donega, C. *Topics in Current Chemistry* **2016**, *374*, 58.

(4) Graetzel, M.; Frank, A. J. *The Journal of Physical Chemistry* **1982**, *86*, 2964–2967.

(5) Wang, X.; Li, C. *Journal of Photochemistry and Photobiology C: Photochemistry Reviews* **2017**, *33*, 165–179.

(6) Cho, E.; Kim, T.; Choi, S.-m.; Jang, H.; Min, K.; Jang, E. *ACS Applied Nano Materials* **2018**, *1*, 7106–7114.

(7) Guyot-Sionnest, P.; Shim, M.; Matranga, C.; Hines, M. *Physical Review B* **1999**, *60*, R2181–R2184.

(8) Morris-Cohen, A. J.; Peterson, M. D.; Frederick, M. T.; Kamm, J. M.; Weiss, E. A. *The Journal of Physical Chemistry Letters* **2012**, *3*, 2840–2844.

(9) Zhu, H.; Yang, Y.; Wu, K.; Lian, T. *Annual Review of Physical Chemistry* **2016**, *67*, 259–281.

(10) Song, N.; Zhu, H.; Jin, S.; Zhan, W.; Lian, T. *ACS Nano* **2011**, *5*, 613–621.

(11) Olshansky, J. H.; Balan, A. D.; Ding, T. X.; Fu, X.; Lee, Y. V.; Alivisatos, A. P. *ACS Nano* **2017**, *11*, 8346–8355.

(12) Buckley, J. J.; Couderc, E.; Greaney, M. J.; Munteanu, J.; Riche, C. T.; Bradforth, S. E.; Brutchey, R. L. *ACS Nano* **2014**, *8*, 2512–2521.

(13) Morris-Cohen, A. J.; Frederick, M. T.; Cass, L. C.; Weiss, E. A. *Journal of the American Chemical Society* **2011**, *133*, 10146–10154.

(14) Rawalekar, S.; Kaniyankandy, S.; Verma, S.; Ghosh, H. N. *The Journal of Physical Chemistry C* **2010**, *114*, 1460–1466.

(15) Morris-Cohen, A. J.; Aruda, K. O.; Rasmussen, A. M.; Canzi, G.; Seideman, T.; Kubiak, C. P.; Weiss, E. A. *Physical Chemistry Chemical Physics* **2012**, *14*, 13794–13801.

(16) Knowles, K. E.; Peterson, M. D.; McPhail, M. R.; Weiss, E. A. *The Journal of Physical Chemistry C* **2013**, *117*, 10229–10243.

(17) Enright, M. J.; Gilbert-Bass, K.; Sarsito, H.; Cossairt, B. M. *Chemistry of Materials* **2019**, *31*, 2677–2682.

(18) Zhang, Z.; Edme, K.; Lian, S.; Weiss, E. A. *Journal of the American Chemical Society* **2017**, *139*, 4246–4249.

(19) Lu, H.; Zhu, X.; Miller, C.; San Martin, J.; Chen, X.; Miller, E. M.; Yan, Y.; Beard, M. C. *The Journal of Chemical Physics* **2019**, *151*, 204305.

(20) Wu, K.; Chen, Z.; Lv, H.; Zhu, H.; Hill, C. L.; Lian, T. *Journal of the American Chemical Society* **2014**, *136*, 7708–7716.

(21) Lian, S.; Weinberg, D. J.; Harris, R. D.; Kodaimati, M. S.; Weiss, E. A. *ACS Nano* **2016**, *10*, 6372–6382.

(22) Woodward, J. R. *Progress in Reaction Kinetics and Mechanism* **2002**, *27*, 165–207.

(23) Rountree, E. S.; McCarthy, B. D.; Eisenhart, T. T.; Dempsey, J. L. *Inorganic Chemistry* **2014**, *53*, 9983–10002.

(24) Costentin, C.; Fortage, J.; Collomb, M.-N. *The Journal of Physical Chemistry Letters* **2020**, *11*, 6097–6104.

(25) Fukatsu, A.; Kondo, M.; Okabe, Y.; Masaoka, S. *Journal of Photochemistry and Photobiology A: Chemistry* **2015**, *313*, 143–148.

(26) Henckel, D. A.; Enright, M. J.; Panahpour Eslami, N.; Kroupa, D. M.; Gamelin, D. R.; Cossairt, B. M. *Nano Letters* **2020**, *20*, 2620–2624.

(27) Fox, M. A.; Akaba, R. *Journal of the American Chemical Society* **1983**, *105*, 3460–3463.

(28) Araujo, J. J.; Brozek, C. K.; Kroupa, D. M.; Gamelin, D. R. *Nano Letters* **2018**, *18*, 3893–3900.

(29) Wu Lizhu; Huan Maoyong; Li Xubing; Zhou Shuai; Zhang Liping; Tong Zhenhe Method for photocatalytic halogenation conversion of halogenated hydrocarbon using quantum dot/rod photocatalyst, CN109438156A, 2019.

(30) De Roo, J.; Yazdani, N.; Drijvers, E.; Lauria, A.; Maes, J.; Owen, J. S.; Van Driessche, I.; Niederberger, M.; Wood, V.; Martins, J. C.; Infante, I.; Hens, Z. *Chemistry of Materials* **2018**, *30*, 5485–5492.

(31) Monahan, M.; Homer, M.; Zhang, S.; Zheng, R.; Chen, C.-L.; De Yoreo, J.; Cossairt, B. M. *ACS Nano* **2022**, DOI: 10.1021/acsnano.2c01203.

(32) Geiger, W. E.; Barrière, F. *Accounts of Chemical Research* **2010**, *43*, 1030–1039.

(33) Swarts, P. J.; Conradie, J. *Journal of Electroanalytical Chemistry* **2020**, *866*, 114164.

(34) Ye, C.; Zhang, D.-S.; Chen, B.; Tung, C.-H.; Wu, L.-Z. *ACS Central Science* **2024**, *10*, 529–542.

(35) Deblock, L.; Goossens, E.; Pokratath, R.; De Buysser, K.; De Roo, J. *JACS Au* **2022**, *2*, 711–722.

(36) Kanicky, J. R.; Shah, D. O. *Journal of Colloid and Interface Science* **2002**, *256*, 201–207.

(37) Wang, L.-W.; Califano, M.; Zunger, A.; Franceschetti, A. *Physical Review Letters* **2003**, *91*, 056404.

(38) Harvie, A. J.; Smith, C. T.; Ahumada-Lazo, R.; Jeuken, L. J. C.; Califano, M.; Bon, R. S.; Hardman, S. J. O.; Binks, D. J.; Critchley, K. *The Journal of Physical Chemistry C* **2018**, *122*, 10173–10180.

(39) Olshansky, J. H.; Ding, T. X.; Lee, Y. V.; Leone, S. R.; Alivisatos, A. P. *Journal of the American Chemical Society* **2015**, *137*, 15567–15575.

(40) Nagelj, N.; Brumberg, A.; Peifer, S.; Schaller, R. D.; Olshansky, J. H. *The Journal of Physical Chemistry Letters* **2022**, 3209–3216.

(41) Joseph Lakowicz, *Principles of Fluorescence Spectroscopy*, 3rd ed.; Springer: Baltimore, 2006.

(42) Huang, Y.; Cohen, T. A.; Sperry, B. M.; Larson, H.; Nguyen, H. A.; Homer, M. K.; Dou, F. Y.; Jacoby, L. M.; Cossairt, B. M.; Gamelin, D. R.; Luscombe, C. K. *Materials Horizons* **2022**, *9*, 61–87.

(43) Gu, W.; Milton, R. D. *Chemistry* **2020**, *2*, 322–346.

(44) Genoni, A.; Chirdon, D. N.; Boniolo, M.; Sartorel, A.; Bernhard, S.; Bonchio, M. *ACS Catalysis* **2017**, *7*, 154–160.

(45) Morgan, D. P.; Kelley, D. F. *The Journal of Physical Chemistry C* **2020**, *124*, 8448–8455.

(46) Berr, M. J.; Wagner, P.; Fischbach, S.; Vaneski, A.; Schneider, J.; Susha, A. S.; Rogach, A. L.; Jäckel, F.; Feldmann, J. *Applied Physics Letters* **2012**, *100*, 223903.

(47) Kroupa, D. M.; Vörös, M.; Brawand, N. P.; McNichols, B. W.; Miller, E. M.; Gu, J.; Nozik, A. J.; Sellinger, A.; Galli, G.; Beard, M. C. *Nature Communications* **2017**, *8*, 15257.

(48) Brown, P. R.; Kim, D.; Lunt, R. R.; Zhao, N.; Bawendi, M. G.; Grossman, J. C.; Bulović, V. *ACS Nano* **2014**, *8*, 5863–5872.

(49) Hernandez, F.; Yang, M.; Nagelj, N.; Y. Lee, A.; Noh, H.; P. Hur, K.; Fu, X.; J. Savoie, C.; M. Schwartzberg, A.; H. Olshansky, J. *Nanoscale* **2024**, *16*, 5624–5633.

(50) Hamachi, L. S.; Yang, H.; Plante, I. J.-L.; Saenz, N.; Qian, K.; Campos, M. P.; Cleveland, G. T.; Rreza, I.; Oza, A.; Walravens, W.; Chan, E. M.; Hens, Z.; Crowther, A. C.; Owen, J. S. *Chemical Science* **2019**, *10*, 6539–6552.

(51) LeSuer, R. J.; Buttolph, C.; Geiger, W. E. *Analytical Chemistry* **2004**, *76*, 6395–6401.

(52) Elgrishi, N.; Kurtz, D. A.; Dempsey, J. L. *Journal of the American Chemical Society* **2017**, *139*, 239–244.

(53) Vanicek, S.; Kopacka, H.; Wurst, K.; Müller, T.; Schottenberger, H.; Bildstein, B. *Organometallics* **2014**, *33*, 1152–1156.

(54) Bond, A. M.; Colton, R.; Harvey, J.; Hutton, R. S. *Journal of Electroanalytical Chemistry* **1997**, *426*, 145–155.

(55) Grätzel, M. *Nature* **2001**, *414*, 338–344.

(56) Pavlishchuk, V. V.; Addison, A. W. *Inorganica Chimica Acta* **2000**, *298*, 97–102.

Chapter 3

EXTREMELY LONG-LIVED CHARGE DONOR STATES FORMED BY VISIBLE IRRADIATION OF QUANTUM DOTS

3.1 Introduction

Interfacial charge transfer from quantum dots (QDs) has garnered attention in the last several decades because it is a key process in many applications such as photovoltaics,[1] photodetectors,[2] light-emitting technologies,[3] and photoredox catalysis.[4] Chemists often idealize photoinduced charge transfer through a two-state, Marcus-type event in which an excited electron (or hole) moves from the conduction band (valence band) edge to an external acceptor. The expansion of this model recently culminated in a review by Wu et al., where the many complications of this simple picture are presented.[5] However, we note that much of the research in this field still focuses on using optical spectroscopy to track the charge carriers' migration from the QD on relatively short timescales (ps-µs). Insights from these studies are unable to capture longer timescale processes, which become relevant in any practical use of these materials in the applications listed above.

Previously, we reported a method to measure photoinduced charge transfer from CdS QDs to redox-active molecules using cyclic voltammetry (CV) under illumination.[6] This measurement allowed us to quantify effective, bimolecular charge transfer on the same timescale as chemical reactions by observing distortion of the CV of the redox-active molecule during illumination. The measurement is performed as follows: an electrolyte solution containing QDs and a one-electron molecular redox probe (*e.g.*, ferrocene, Fc) is loaded into a three-electrode cell equipped with an LED that allows for simultaneous illumination and electrochemical measurement. CVs are taken before, during, and after illumination, and the shape of the CV distorts from the reversible shape

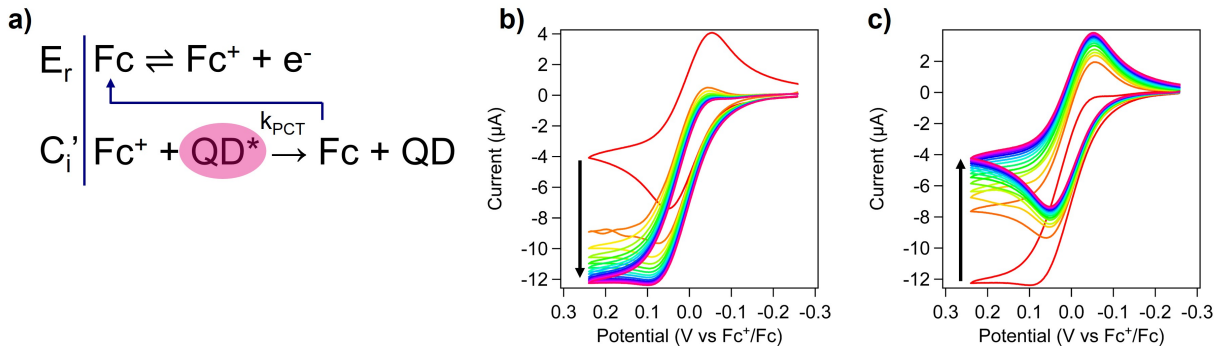

Figure 3.1: (a) The ErCi' mechanism we used to explain changes to the voltammogram upon illumination, where QD* refers to the charge donor species investigated in this work. (b) CVs of ferrocene distort to an S-shaped CV after illumination is turned on over *ca.* 30 minutes. There were 130 seconds between the start of one scan and the start of the next. (c) Slow recovery from S-shaped CV to reversible shape over *ca.* 30 minutes after illumination ends. CV data shown are original to this work.

in a manner consistent with adding a chemical reaction (charge transfer) to the reversible faradaic process (Figure 3.1a). Ferrocene is faradaically oxidized to form ferrocenium (Fc^+), which can be reduced by a photogenerated charge donor, QD*. The extent of the CV distortion corresponds to the observed rate of charge transfer from QD to molecular redox probe.

An unexpected finding from this measurement was the gradual distortion of CV during illumination, occurring over timescales much longer than exciton formation, *ca.* 30 minutes. Moreover, this distortion persisted for *ca.* 30 minutes after illumination stopped (Figure 3.1b,c). These slow changes to CV were consistent with the amount of charge donating species (QD*) in solution increasing during illumination for much longer than excitation and the charge donating species persisted for much longer than excitonic decay. This was true for both electron- and hole-transfer. These observations challenge conventionally held beliefs that charge transfer must proceed directly after excitation and be faster than carrier trapping. The following work aims to understand the chemical processes undergone by the QD during illumination that allow for charge transfer to occur long after illumination stops.

Others have observed similar long-lived reactivity after illumination in other materials, which has been termed "dark photocatalysis" or "photocatalytic memory."[7] The most common system consists of a semiconductor that acts as the light sensitizer and an energy-storing substance that can store photo-generated charge carriers during illumination and slowly release those carriers in the dark.[7,8] There are many examples of nanocrystals acting as semiconductors in dark photocatalytic systems.[9–18] However, systems where the light absorber is the same as the energy storage material are rarely reported, and in these, the identity of the charge-storing species was not explored.[19,20] Our observations fall into the category of dark photocatalysis, but we have uniquely observed this behavior intrinsically on QDs.

Photoinduced changes to QDs on long timescales have been well-investigated in relation to their photoluminescence behavior. Photobrightening[21–27] is the process in which the photoluminescence quantum yield increases over minutes to hours of QD illumination. There is more than one mechanism behind this phenomenon, though the general description of photobrightening is that irradiation smooths the QD core's surface and removes or passivates surface defects. This decrease in surface trapping may be thermal (photoannealing), or the charge carriers generated during illumination may remove surface states through trap filling or other surface redox reactions.[28] Related processes include photodarkening[29] and photoluminescence blinking,[30,31] where similar photoinduced surface redox activity causes PL changes over timescales longer than exciton generation and decay. It seems reasonable that the photoinduced surface redox processes that affect PL may be chemically related to the processes that slowly generate long-lived charge donors. Altogether, we hypothesized the redox-active surface of the QDs may act as the intermediate between exciton dissociation and charge transfer.

Considering our prior observations of these long-lived charge donor states, we sought to understand the ubiquity of this effect and gain a chemical understanding of this new mechanism for photoinduced charge storage and transfer. We considered the mechanisms presented in Scheme 3.1 as well as several more rejected mechanisms presented in Scheme 3.3. We considered photodoping (Scheme 3.3a) as a mechanism because the timescale of the long-lived donors is appropriate,[32] and n-doped QDs should be excellent electron donors. This mechanism was ultimately rejected because,

as we will discuss below, there is no evidence for the presence of free carriers in the present work. We also considered that charge could be stored at ligated surface Cd (Scheme 3.1a,b), which best agrees with all our findings. Ligated surface metal ions can be reduced by external reductants,[33–35] so they may be susceptible to reduction by conduction band electrons.

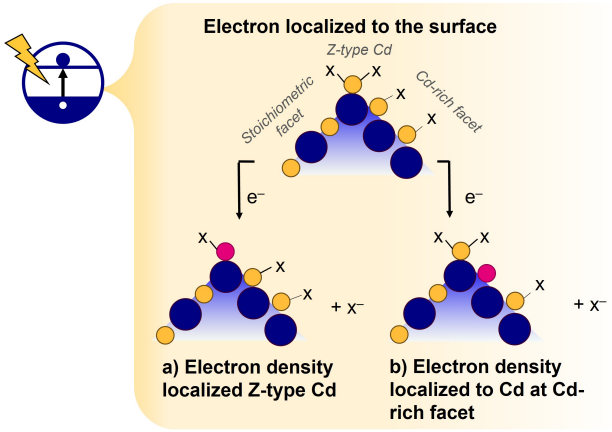

Scheme 3.1: Proposed mechanisms for electron storage. (a) Electron density localized to Z-type Cd, causing displacement of one ligand per electron stored. (b) Electron density localized to Cd on Cd-rich facets. (b,c) detail the localization of a photogenerated electron. Rapid localization of the corresponding hole[36–38] is not shown.

3.2 Results and Discussion

3.2.1 Charges Are Stored Locally Rather Than as Free Carriers

Previous work has demonstrated long-lived excited states or long-lived charge donors after illumination of QDs via photodoping. Chemical photodoping of QDs is a well-explored phenomenon wherein, after exciton generation, the hole is quenched by a reducing agent,[39–42] leaving behind the electron as a free carrier in the conduction band, otherwise known as an n-type doped semiconductor (Scheme 3.3a). Generally, excess strong reducing agent, R, must be added to the system to generate electronically doped particles. However, we observed charge storage without any such chemical reductant being added. In one report, Shulenberger and coworkers demonstrated native

photo-n-doping of CdS QDs.[43] During minutes of illumination, they observed an absorbance bleach at the excitonic transition, which was attributed to n-type photodoping, even without adding a reducing agent, which more closely mimics our observations. Especially relevant to our photoelectrochemical observation, the excess charges in photodoped QDs live for many minutes,[32] so we hypothesized that the long-lived charge donors we observed could be natively photodoped particles.

However, the observation of long-lived hole donors in our system, in addition to electron donors, conflicts with the photodoping hypothesis. To the best of our knowledge, stable p-type photodoped CdS QDs have not been experimentally prepared due to rapid hole localization at the QD surface. The same is true of related materials, including CdSe and PbS. If there was photodoping, we expect it to be n-type, so there should not be free holes. Initially, we postulated that in a natively photo-n-doped system, after excitation, the hole could be localized elsewhere (on the surface or the ligands as postulated by Shulenberger et al.), and this localized hole could act as a long-lived oxidizing agent we observe electrochemically.

To rule out the possibility of photodoping, we used optical spectroscopy after illumination to probe the presence of free conduction band electrons. Photodoping should cause bleaching of the first excitonic transition and quenching of band-edge photoluminescence.[44] Instead, during 30 minutes of illumination, we saw only very small (<1 nm) shifts in the lowest energy excitonic transition rather than a bleach (Figure 3.2a). These slight shifts resemble those others have observed upon surface charging and restructuring, causing an internal electric field known as the Stark effect.[45–48] We did not observe NIR absorption attributed to intraband excitation of conduction band electrons, which others have reported in photodoped QDs (Figure 3.3).[44]

Of the CdS QDs investigated in this work, only those capped with (2-[2-(2-methoxyethoxy) -ethoxy]ethyl)phosphonic acid (MEEEPA) had appreciable band-edge photoluminescence (Other surface can be found in Figure 3.4). After 30 minutes of illuminating phosphonate-capped CdS QDs, the band-edge photoluminescence modestly increases in intensity, which is inconsistent with photodoping and is more consistent with photobrightening due to surface reconstruction[28] (Figure 3.2b). This reinforces that under our experimental conditions, the CdS QDs do not photodope, and therefore the long-lived stored charges are localized and not free carriers.

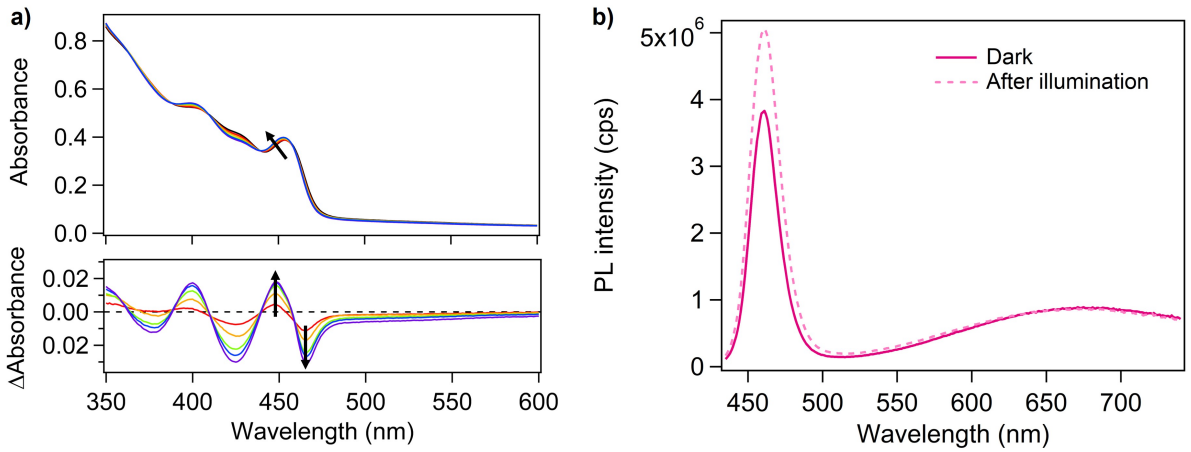

Figure 3.2: (a) UV-vis absorbance changes over 30 minutes of illumination of MEEEPA-capped CdS. (b) Photoluminescence brightening in MEEEPA-capped CdS after 30 minutes of illumination.

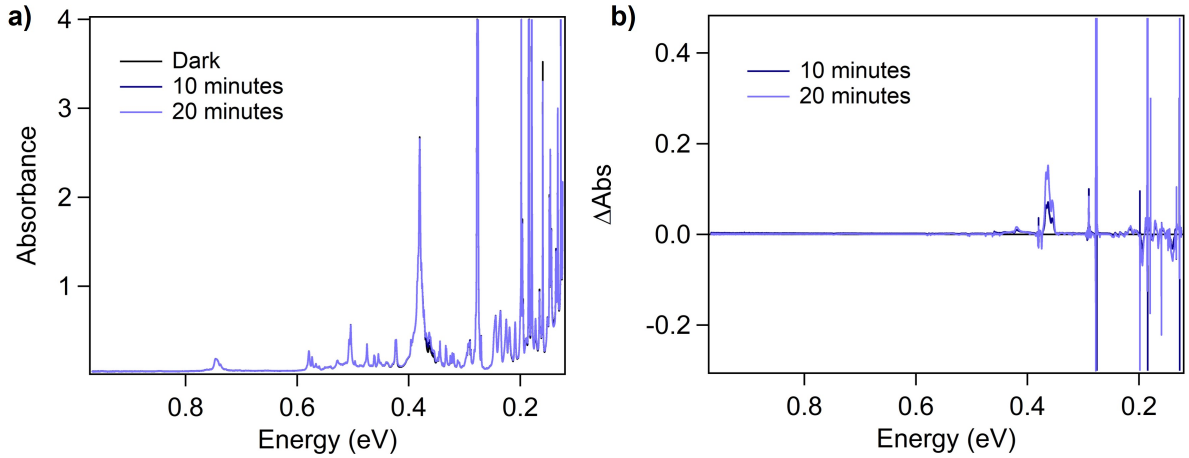

Figure 3.3: (a) FTIR before and after 10 and 20 minutes of irradiating MEEAA-capped CdS QDs in PhCN. (b) Difference from dark to 10 and 20 minutes in panel (c). FTIR Measurements taken in a liquid cell equipped with CaF_2 windows. The pathlength was 200 µm.

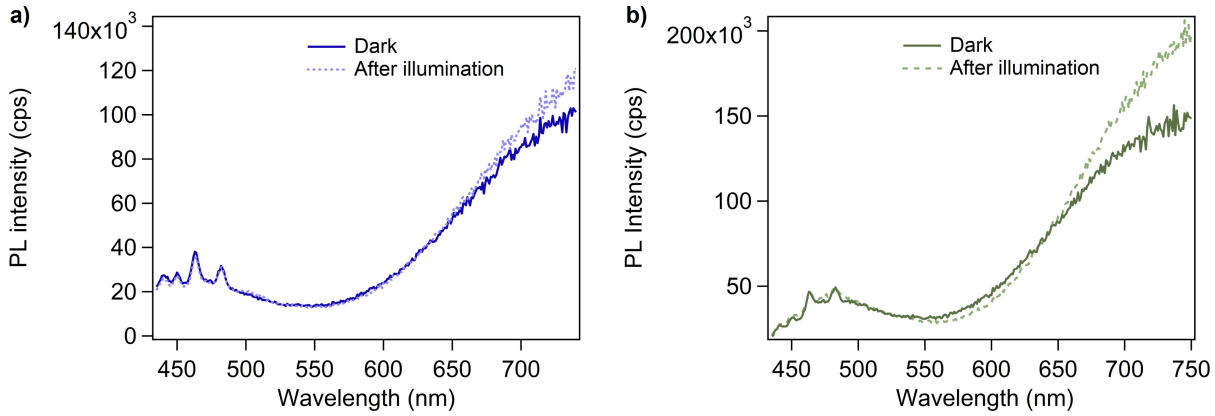

Figure 3.4: Photoluminescence before (dark colors) and after (light colors) illumination in (a) MEEAA and (b) etched MEEAA CdS QDs. The sharp features below 500 nm are Raman features from the organics.

3.2.2 Three Surface Chemistries to Assess the Role of the QD Surface in Charge Storage

It is well documented that there are generally many types of surface sites on a Cd chalcogenide QD surface.[49–52] We have evidence from XPS that ours are no different as the Cd 3d lines are best fit to two Cd environments at the surface (see SI for details). Because of the distinct chemistries associated with Cd in different chemical environments, these surface sites should not necessarily be expected to have equivalent redox chemistry. For example, Hartley and Dempsey suggested that in PbS QDs, the Pb on the edges between facets were more likely to be reduced by cobaltocene than Pb on (111) or (100) facets.[53]

We were interested in probing which types of surface atoms are most likely to store electrons after illumination. To this end, we prepared QDs with three different surface chemistries and investigated their differences. We assessed the role of the head group of the ligands by comparing MEEEPA and 2-(2-methoxyethoxy)ethoxy acetic acid (MEEAA) capped CdS QDs. We assessed the role of surface stoichiometry by comparing MEEAA capped particles to MEEAA capped CdS QDs with lower Cd (and ligand) coverage prepared through surface etching. TEM and optical characterization of these different QDs can be found in Figure 3.13 and Figure 3.12.

We characterized the surfaces of these three kinds of QDs by quantifying their ligand coverage with ^{1}H DOSY NMR (Figure 3.5a). We wanted to accurately quantify the ligand coverage, but needed to ensure that we were only counting ligands adsorbed to the QD surface and not including free ligands in solution. Quantitative DOSY NMR offers a technique where bound and free ligands are differentiated by their diffusion coefficient and can be used in cases where there is no simple spectroscopic handle to differentiate bound and freely diffusing species.[54] We used DOSY to quantify the ratio of bound and free ligands (Figure 3.5b) and then used an internal standard (mesitylene) to calculate the number of bound ligands per particle. These are plotted in Figure 3.5c. We first found that the as-synthesized oleate capped QDs have 250 ligands per QD, which corresponds to 5 ligands/nm^2 (calculated using diameter from TEM and assuming spherical particles) and is consistent with literature reports and calculations of carboxylate ligand density.[52,55,56]

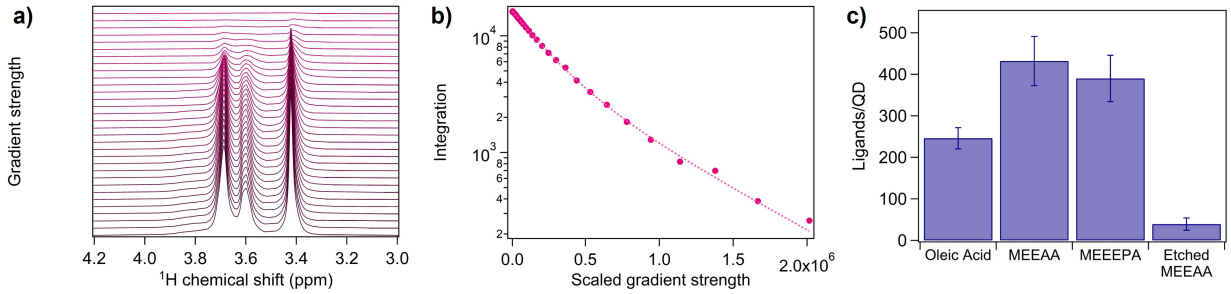

Figure 3.5: (a) ^{1}H DOSY NMR of MEEEPA capped CdS at 32 different gradient strengths. At higher gradient strengths, only signals from ligands bound to the QD surface are observed. (b) Integration of the peaks in (a) plotted against the squared and scaled gradient strength. Data (circles) and fit to a biexponential decay (dotted line). (c) Results after using DOSY to determine the fraction of ligands in solution that are bound to CdS QDs with different ligands and surface stoichiometries. Error bars are from the propagation of uncertainty; see 3.5.4 for details.

The short chain polyethylene glycol-terminated carboxylate and phosphonate ligands, MEEAA and MEEEPA, have 430 and 390 ligands per QD, which is approximately twice the number found in the oleate case. This gives ligand densities of 11 ligands/nm^2 and 7 ligands/nm^2, respectively.

The higher density for MEEAA is consistent with previous observations of higher carboxylate than phosphonate density due to the diacidic nature of alkyl phosphonic acids.[57] These densities are far higher than any reported experimental or calculated ligand densities we have seen on CdS QDs. Furthermore, these are higher than the ligand density of a perfectly passivated cadmium-rich 100 surface of zinc blende CdS (5.76 ligand/nm^2, one ligand per surface Cd).[58] This implies that the MEEAA and MEEEPA ligands cannot all have their head groups bound to the QD surface; some ligands are associated with the QD but not bound to the surface. We propose that the ligands form an interdigitated bilayer in these materials, where some head groups point out from the QD surface. Ligand bilayers have previously been constructed on nanocrystal surfaces with other ligands.[59–61]

We also made the QD surface less cation-rich by employing an established protocol wherein Z-type surface cadmium carboxylates were etched from the surface using diamines.[49] After etching, we exchanged the remaining ligands for MEEAA. After etching and then MEEAA ligand exchange, there were 39 MEEAA ligands per QD, or 0.9 ligands/nm^2. This extremely low ligand density, despite the large excess of MEEAA present in solution during ligand exchange, reinforces that we have effectively stripped the surface of Z-type Cd, decreasing the density of binding sites available to carboxylate.

3.2.3 Chemical Changes After Illumination

We considered that redox chemistry may promote charge storage on the surface ligands rather than the inorganic core, especially considering our non-conventional surface ligands bearing relatively weak C—O bonds. The report of native photodoping of CdS showed a ligand dependence on photodoping and invoked the double bond of oleic acid as a hole acceptor.[43] Similarly, a recent report found that when oleic acid capped CdSe QDs were irradiated with a 400 nm laser, the ligands desorbed from the QDs and fragmented to aldehydes, terminal alkenes, H_2, and water.[62] When we irradiated our MEEAA or MEEEPA capped CdS QDs for one hour, which is longer than the time to complete charge storage, we did not observe fragmentation of the ligand shell in the ^{1}H NMR spectrum. This confirms that charges are not stored by redox chemistry on the ligand backbone.

Analysis using DOSY did not show a significant difference in the fraction of ligands bound to the QD surface, though the estimated variance in this measurement was 60 ligands per QD. The only change in the ^{1}H NMR spectrum we noted was that the signal assigned to the protons alpha to the carboxylic acid in MEEAA had a small shift (0.01 ppm) further downfield after illumination. Between different QD samples, we noticed that the chemical shift of this peak varied and was linearly correlated to the fraction of ligands in solution that were bound, as determined by DOSY (Figure 3.6). This differs from archetypal NMR experiments using oleic acid capped QDs in nonpolar solvent, where bound and free ligands are observed as distinct resonances.[57,63–65] We assert that because the QD surface is in dynamic equilibrium, the observed chemical shift of this proton is a weighted average of protons on ligands bound to the QD surface and those on ligands freely diffusing in solution, as shown in 3.1.

$$\delta_{obs} = \chi_{bound}\delta_{bound} + \chi_{free}\delta_{free} \tag{3.1}$$

Then, we can determine that a change in chemical shift from 3.8723 to 3.8881 ppm represents an 11% decrease in the bound fraction of ligands, or 48 fewer ligands bound per particle (see SI for calculations). Ligand dissociation after illumination is consistent with the reduction of ligated surface Cd (Scheme 3.1), where surface reduction is locally charge compensated by X-type ligand dissociation.[35] The analogous protons alpha to the phosphonic acid in MEEEPA are not observed as a distinct resonance in the NMR spectra of the QDs, so an analogous interpretation was not possible.[66]

The hypothesis that stored charge is compensated by ligand dissociation is supported by a parallel set of electrochemical measurements where we irradiated MEEAA capped CdS solutions with and without electrolyte. As measured using cyclic voltammetry, the charge transfer rate after illumination ended was not significantly different between the two experiments, suggesting the presence of electrolyte did not impact charge storage (Figure 3.7). The lack of dependence on electrolyte further supports that charge storage is compensated intrinsically, *i.e.*, by ligand loss. This contrasts with work studying QD films, wherein electrolyte is necessary to stabilize surface charges,[67–70] presumably because ligand desorption is not a viable mechanism in the solid state.

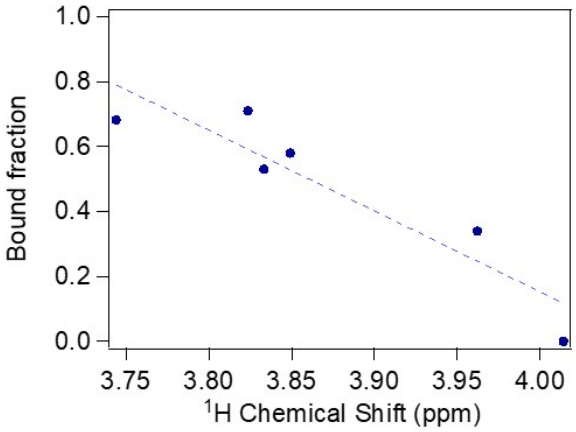

Figure 3.6: The fraction of ligands in solution bound to QDs, as determined by DOSY NMR plotted against the chemical shift of the signal assigned with the protons alpha to the carboxylic acid in MEEAA. Line between points is a linear fit.

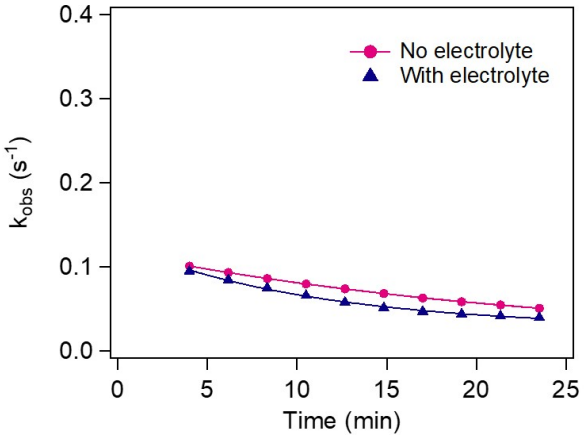

Figure 3.7: Comparison of the observed rate of charge transfer over time after illumination ends, comparing QDs that had been illuminated with and without electrolyte present. During measurement, the electrolyte concentration was 0.1M [TBA][PF_6] in both.

When the MEEAA capped CdS QDs were irradiated overnight, they degrade. An insoluble grey powder formed and was identified as Cd^0 metal with large crystallite size by XRD (Figure 3.8a). Our coworkers recently also reported Cd^0 deposits formed during photocatalysis with CdS QDs.[71] Interestingly, UV-vis absorbance of the soluble fraction does not show that the QD size decreases even when insoluble Cd metal forms, suggesting degradation of the material does not evenly etch all particles (Figure 3.9a). DOSY NMR analysis of the soluble fraction showed that half as many of the ligands were bound. The signal assigned to the protons alpha to the carboxylic acid in MEEAA shifted further downfield (0.14 ppm) after overnight illumination (Figure 3.8). We did see a few new minor peaks assigned to alcohol or ether degradation products (Figure 3.9b). In contrast, MEEEPA capped CdS QDs do not form Cd^0 deposits, and there are no changes to ligand binding observable by 1D or DOSY NMR.

Altogether, redox chemistry on the ligand backbone cannot be the primary site of charge storage, considering we don't observe these changes after one hour of illumination. In contrast, charge storage appears saturated by our electrochemical measurements after *ca.* 30 min. X-type ligand desorption is a mechanism for charge compensation of reduced surface sites in this system, at least in the case of the carboxylate capped QDs (Scheme 3.1). Even under more extreme conditions like overnight irradiation of a QD solution, carboxylic acid capped QDs show Cd reduction and material degradation while phosphonate capped QDs do not measurably change. The ligand-dependent formation of Cd^0 and subsequent ligand desorption supports charge localization to ligated surface Cd atoms and suggests that these ligated surface Cd have different propensities for electron storage depending on the binding strength of the ligand.

3.2.4 Long-Lived Charge Donors Observed Electrochemically with All Surfaces

The observed rate of charge transfer from QDs was determined using photoelectrochemistry using cyclic voltammetry.[6] This measurement allows us to determine the observed rate of charge transfer (k_{obs}) from the magnitude of the CV distortion. Furthermore, we can track how this rate changes over time during extended illumination and after illumination ends. The changing k_{obs} over time gives insight into how charge donors form and are depleted over time as k_{obs} is related to the

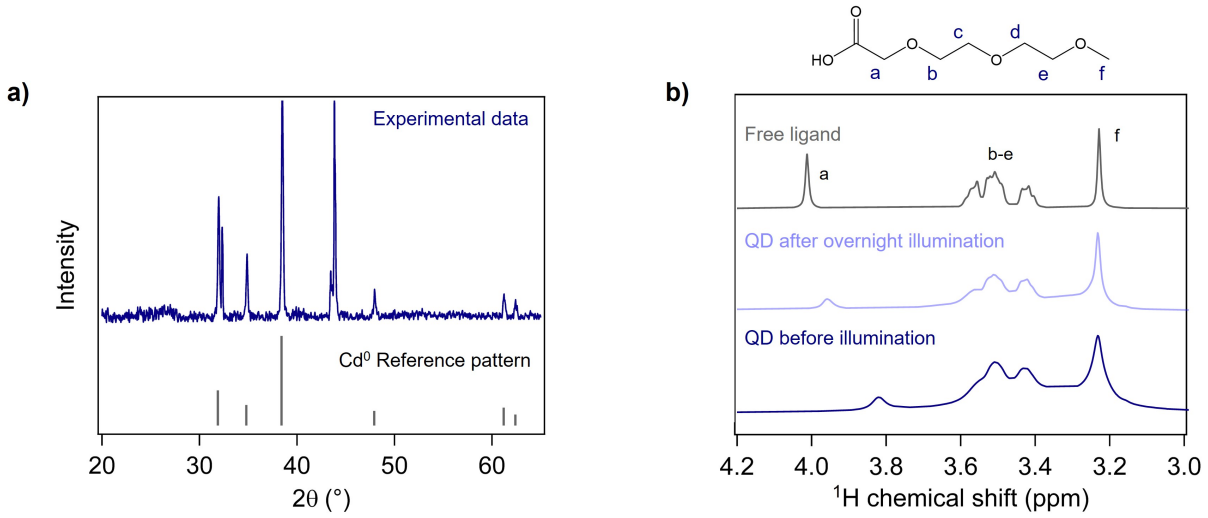

Figure 3.8: (a) XRD of the grey precipitate formed after illumination of MEEAA capped QDs overnight (top) compared to the reference pattern for hexagonal Cd^0. (b) The ^{1}H NMR spectrum of MEEAA (top) and MEEAA capped CdS QDs before (bottom) and after (middle) overnight illumination in DMSO-d_6, 300 MHz, d1=15s.

concentration of charge donors [QD*] and the intrinsic rate of charge transfer (k_{PCT}) by 3.2. Assuming there is no change in the intrinsic rate over time, the variation of k_{obs} is linearly related to the number of charges stored. It is worth noting that k_{PCT} cannot be separately determined and varies between samples.

$$k_{obs} = [QD^*] \times k_{PCT} \tag{3.2}$$

In all samples, there is a rapid initial increase in k_{obs} after illumination starts but before the first scan is finished (50 s), which we hypothesize largely represents charge transfer that is not from stored charges, *i.e.*, from direct exciton dissociation (Scheme 3.2a). This is followed by a slow increase caused by the slow process of storing charges that are competent charge donors (Scheme 3.2b). When fitting this data to exponential curves, good fits were only obtained when the point at (0,0) was excluded, presumably because the fast initial rise in k_{obs} before the first scan is a distinct process

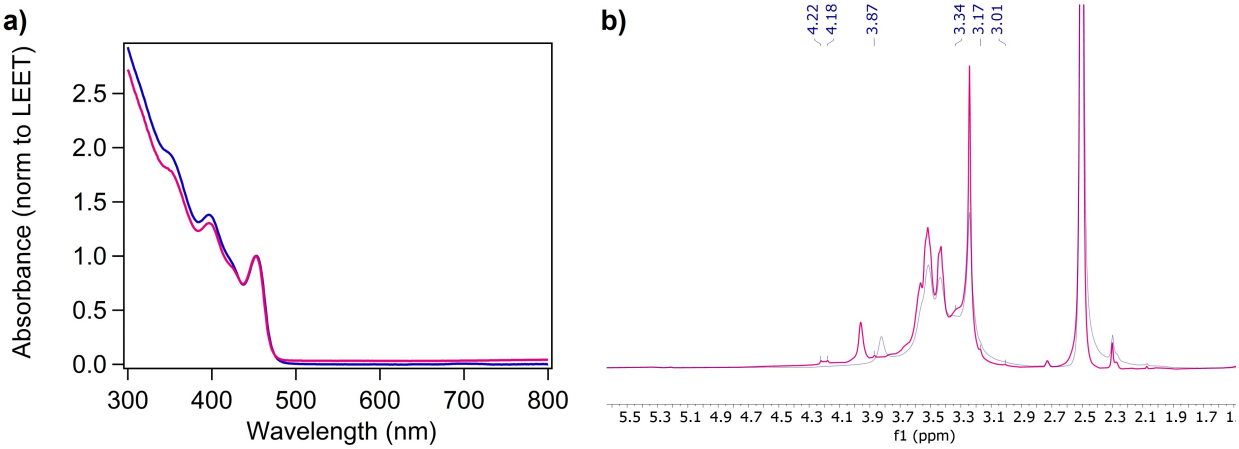

Figure 3.9: Characterization of MEEAA capped CdS QD solutions after overnight illumination. (a) UV-Vis absorption before illumination (blue) and after overnight illumination (pink). (b) ^{1}H NMR of QD solutions before (blue) and after (pink) overnight illumination. The solution was centrifuged to remove insoluble Cd^{0} prior to NMR acquisition. DMSO-d_6, 300 MHz, d1=15s. New minor peaks after illumination are noted.

from the slow charge storage. Analogously, k_{obs} quickly drops after illumination ends before the first scan is finished (50 s), then slowly decreases. As with the data during illumination, the decay results reinforce our hypothesis of two processes on different timescales: a rapid process completed before the first scan is taken and the slow decay of charge storage over many minutes, which is well-fit to an exponential curve.

We observe that MEEAA, MEEEPA, and etched MEEAA capped particles all have k_{obs} that slowly increase over *ca.* 30 min. Furthermore, charge transfer does not stop as soon as illumination ends but instead takes at least 15 min to stop (Figure 3.10). Therefore, QDs with all three surface chemistries store charge. The raw CV data is available in B.2.

The magnitude of k_{obs} does vary between the QDs with different surfaces: MEEAA and MEEEPA capped QDs have the same k_{obs} within experimental variance, while the etched MEEAA sample has k_{obs} that is approximately twice as large as the others. The measured k_{obs} is inherently linked to the number of stored charges, as well as k_{PCT}, which depends on the permeability of

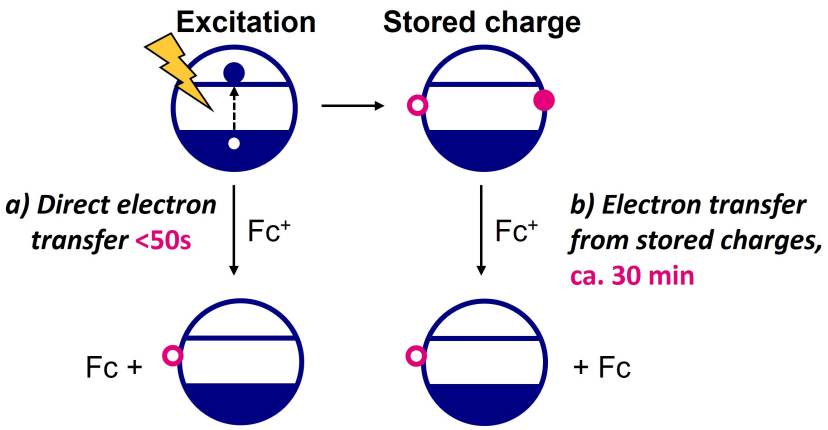

Scheme 3.2: Two pathways for charge transfer from QDs after excitation during the CV experiment. (a) Direct electron transfer that does not go through storage, *i.e.*, from exciton dissociation. Hole trapping in CdS QDs is very rapid,[36–38] so holes are likely trapped rather than left behind in the valence band after charge transfer. This mechanism reaches a maximum rate and ends within 50s of lights on/off. (b) Electron transfer from stored charges. This pathway lasts many minutes after illumination ends because of the long lifetime of stored charges.

the ligand shell and the driving force for charge transfer, among other factors. This means that comparing k_{obs} between samples does not directly inform on the relative number of charges that are stored, so while this measurement affirms charge storage in all samples, we needed a direct measurement of the number of stored charges to understand the dependence of charge storage on surface ligation.

3.2.5 Number of Charges Stored Varies with QD Surface

Others interested in quantifying stored charges have used direct spectroscopic measurements of free carriers, including shifting plasmonic absorbance[9,72] or bleaching of excitonic features.[44,73] Because of the localized nature of the stored charges observed here, we are unable to use those methods. Others have observed long-lived stored charges in dark photocatalytic systems using XPS, wherein they can quantify the charges stored by observing reduced metal.[17] We were unable to observe redox changes to Cd or S in XPS after illumination of QD films, perhaps in part due to the low concentration of reduced species or similarity between the Cd^0 and Cd^{2+} binding energy (Figure 3.11).[74] Occasionally, EPR has been used to observe stored charge,[75,76] though we have not pursued this avenue. Still others have quantified free carriers in doped nanocrystals using potentiometric titration, where an oxidizing agent is titrated, causing the solution's open circuit potential to shift.[40,41] This measurement requires many minutes for each point on the titration curve to stabilize open circuit potential, which sums to many hours to determine an equivalence point. Our electrochemistry data informs us that the stored charges live for less than *ca.* 30 minutes, so any measurement technique must take less time.

To quantify the number of charges stored, we aimed to titrate all stored charges with an excess of molecular acceptor (Figure 6a). This measurement does not rely on any spectroscopic changes to the QDs and is inherently only sensitive to charges stored that are competent charge donors. We first considered the use of dicationic methyl viologen, which, upon reduction by one electron, forms an intensely colored radical easily quantified with absorption spectroscopy. This substrate has been extensively studied as an electron acceptor from QDs.[77–81] It has even been used to quantify the formation of reduced metal species in colloidal suspensions of CdS and ZnS.[82–84] However, it is

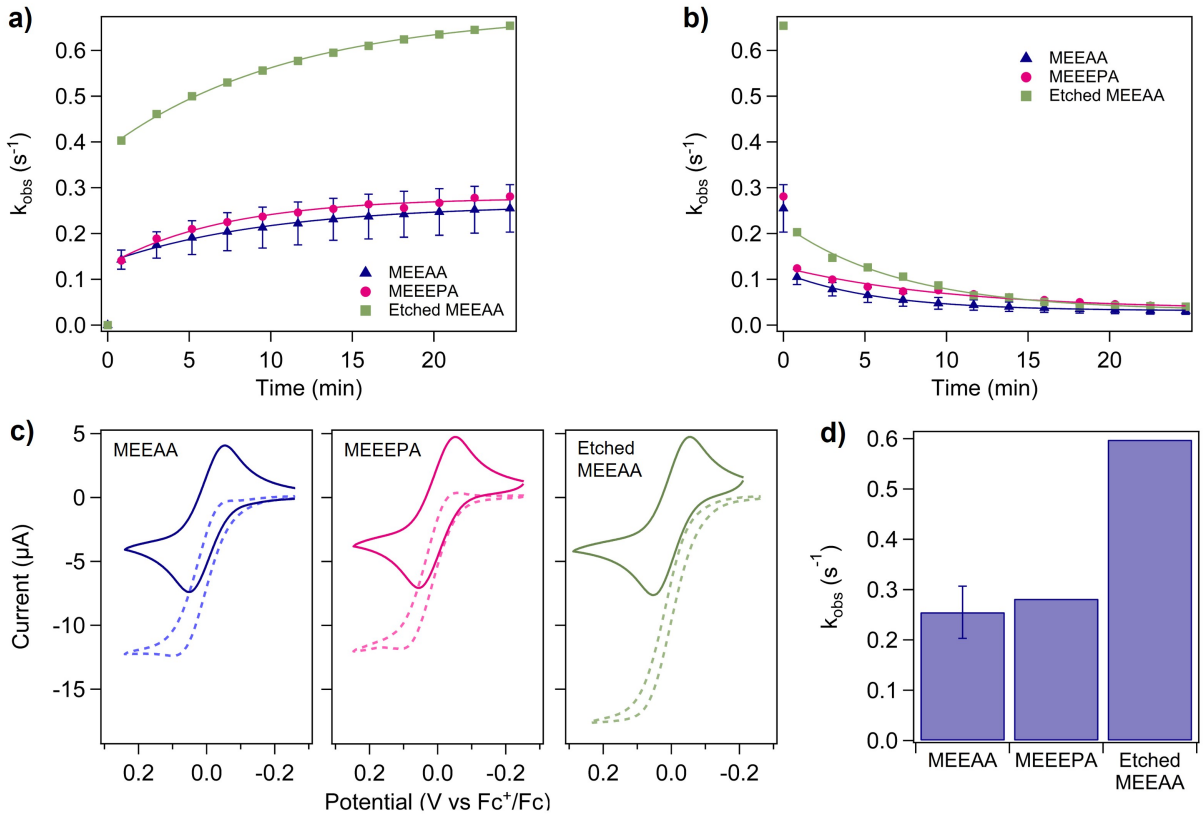

Figure 3.10: Comparison of the rate of electron transfer from CdS QDs with different surfaces. (a,b) The observed rate of electron transfer (kobs) from CdS QDs to Fc+ measured by cyclic voltammetry shows the slow increase in rate during minutes of illumination (a) and decay of electron transfer rate after illumination ends (b). The CdS QDs tested were MEEAA (blue triangles), MEEEPA (pink circles), and etched MEEAA (green squares). Lines between points are from fitting to an exponential function (details in B.3). (c) Comparison of CVs before illumination (solid) compared to after 25 minutes of illumination (dashed) (d) The rate of electron transfer after 25 minutes of illumination for all three surface chemistries, obtained comparing the before and after CVs in (c). Error bars were obtained from triplicate measurements of the MEEAA sample.

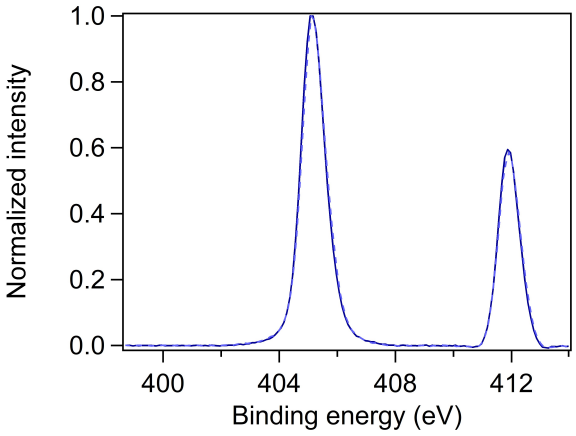

Figure 3.11: XPS of the Cd 3d spectral envelope before (solid) and after (dashed) 60 min. illumination. There traces nearly perfectly overlay. Experimental details can be found in 3.5.5

also well-documented that the reduced methyl viologen radical is a reasonably good Brønsted base, reacting with protons to yield non-colored products.[85–88] We did not observe the reduced radical in solutions containing MEEEPA capped QDs and we attribute this to degradation by the strongly acidic ligand. Because of this degradation pathway, it was not possible to use methyl viologen reduction to quantify the stored charges across the library of different QD surfaces.

Instead, we reacted the stored electrons with excess ferrocenium (Fc^+) to form ferrocene (Fc), which we selected due to its simple 1 e^- chemistry and the stability of the reduced form of the molecule. Furthermore, this is the same substrate used in our electrochemical experiments, which allows for clear comparison between k_{obs} and the number of stored charges. Because of the poor molar absorptivity of Fc, we monitored the formation of Fc using ^{1}H NMR spectroscopy, where the chemical shift of the peak corresponding to Fc and Fc^+ (observed as one peak due to rapid self-exchange, Figure 6b) can be related to the fraction of Fc^+ that was reduced (see Methods). We subtracted the number of Fc^+ reduced by QDs that had not been previously irradiated to control for different background reactivity. We note that the number of Fc formed is a lower bound of the number of electrons stored because some stored electrons may decay before they can react

with Fc^+, and some Fc formed by stored electrons may be re-oxidized by stored holes (backward transfer).

All three surface chemistries studied did store charge, that is, previously irradiated QD samples formed more Fc than particles that had not been irradiated. We found that MEEAA capped particles stored the most charges (54 ± 7 per QD), while the etched particles stored fewer (31 ± 5 per QD) and the MEEEPA capped particles stored the fewest (9 ± 6 per QD) (Figure 6c). We note the similarity between the number of charges stored on the MEEAA capped QDs and the number of ligands we measured to desorb (48 per QD, discussed earlier). This suggests that for every stored electron, approximately one ligand is desorbed, which reinforces our proposed mechanism that electron donors are formed by the reduction of ligated surface Cd, charge-balanced by ligand desorption (Scheme 3.1).

The quantification of stored charges does not mirror k_{obs} and reinforces the importance of measuring the number of stored charges in addition to their rate of transfer. The etched particles had twice the rate of charge transfer, but about half as many stored charges as regular MEEAA capped QDs. This is explained by the much higher permeability of the ligand shell (1/10 as many ligands), which is known to increase the rate of charge transfer due to the higher probability of collisions between QD inorganic surface and substrate.[89,90] Fewer charges stored on the etched particles confirms that some charge storage is at Z-type Cd (Scheme 3.1a), considering these are the species removed by the etching procedure. Notably, this does not rule out charge storage at Cd on Cd-rich surfaces (Scheme 3.1b); it may be that both kinds of ligated Cd may store charge.

We note that the MEEEPA capped QDs store far fewer charges than MEEAA, which further suggests the importance of surface ligands controlling the reactivity of surface Cd. MEEEPA binds more strongly to the QD surface, so presumably, it is a better Lewis base, making the Cd bound to it less Lewis acidic, decreasing the likelihood of electron localization. Surprisingly, despite the lower number of charges stored, MEEEPA and MEEAA capped QDs have the same k_{obs}. Because both ligand shells are very dense, ligand shell permeability cannot explain this discrepancy. We hypothesize that the lower number of stored charges (QD* in 3.2) is balanced by the higher driving force for charge transfer (increasing k_{PCT} in 3.2), leading to similar k_{obs}. Because of the indirect

measurement of these stored charges, the relative energy of these states cannot be directly measured, though future work could use charge acceptors with different redox potentials to estimate this, analogously to Hartley and Dempsey.[53] Again, the dependence of the number of charges stored on the chemistry at ligated Cd supports the model presented in Scheme 3.1. The much higher number of charges stored in MEEAA is consistent with our overnight illumination experiments where MEEAA but not MEEEPA capped CdS QDs form Cd^0 deposits and desorb ligands.

3.2.6 Generality of Charge Storage

We considered whether charge storage was unique to CdS QDs, so we synthesized InP and CdSe QDs that were also capped with MEEAA. InP is a III-V semiconductor that is more covalent than CdS or CdSe, which was especially interesting to us because the reactivity of ions in the lattice should be very different, though electron trapping at Z-type In is still a viable mechanism.[91] We performed identical cyclic voltammetry experiments under illumination and found that, as before, the CV distorted over slow timescales (See SI Figure 10 for CV data). When CV data was interpreted to extract observed rates of charge transfer, we saw that charge transfer took many minutes to reach a maximum rate (Figure 7a), and charge transfer lasted for many minutes after illumination (Figure 7b). This was true for both electron transfer to ferrocenium (Fc^+) and hole transfer to cobaltocene (SI Figure 11). These results show the generality of the observation of charge storage.

The magnitudes of k_{obs} are difficult to directly compare between materials because of different band edge potentials, solution absorbance at the LED wavelength (solutions were normalized by concentration), QD size and diffusivity, ligand density, and other factors. However, the time constants from fitting the decay of k_{obs} are independent of those differences and can be interpreted as the relative lifetimes of stored charges. InP has the longest-lived charges by far (τ = 25.5 ± 0.4 min), CdSe is intermediate (τ = 11.1 ± 0.5 min), and CdS has the shortest lifetime (τ = 7.2 ± 0.4 min). The difference between the different materials highlights the importance of the reactivity at the inorganic surface for charge storage. Furthermore, we posit that the high covalency in the InP lattice[92] might render redox changes to the QD surface less reversible, leading to the long lifetime of stored electrons.

We have determined that illumination causes storage of charge carriers for many minutes in all QD systems studied, spanning a variety of QD compositions, surface chemistries, and experimental conditions. Furthermore, while charge storage is sensitive to surface chemistry, charge storage is not directly based on localization to surface ligands, further generalizing this surprising phenomenon.

3.3 Conclusion

Photoinduced charge transfer from QDs is a critical process but cannot be explained by Marcus formalism and free carriers alone. We have shown that photoinduced charge transfer persists for many minutes after illumination ends, conflicting with the conventional viewpoint that charge transfer must compete with excitonic lifetimes. Furthermore, charges were stored in all QD systems we tested, including with or without electrolyte, using CdSe, InP, or CdS; using QDs capped with carboxylates or phosphonates, and using QDs with different surface stoichiometries. We devised a measurement for the number of charges stored via their reactivity with the electron acceptor, Fc^+. We emphasize the importance of measuring both the rate of stored charge transfer using our electrochemical measurement and the number of stored charges when comparing different materials, as the observed rate depends on more than just the number of charge donors.

We found that charges are not stored as free carriers (e.g., as photodoped particles); similarly, charges are not stored via reactivity on the ligand backbone. We found that charge storage depended on the surface stoichiometry and the identity of the ligand head group, implying that charge is stored at the organic/inorganic interface on the QD surface. Furthermore, charge storage is intrinsically compensated by X-type ligand desorption. Because of this observation, as well as the dependence of the ligand on the number of charges stored, we propose that electrons are stored at ligated surface Cd. This paper did not investigate hole trapping, though we expect it to be trapped elsewhere on the surface. The electron and hole are trapped at separate sites, which is the origin of the extremely long-lived charge donors. There is likely a high kinetic barrier to the recombination of separately localized carriers.

We believe that others may have missed these intermediate states in QD charge transfer investigations because of the extremely long timescale of storage and depletion of stored charge and the

subtle spectroscopic changes upon illumination. Despite the uniqueness of our observation, we do not view it as contradictory to other measurements of QD photophysics but rather as an extension of their behavior on longer timescales. QD luminescence blinking is a less understood photophysical phenomenon that also happens on longer timescales than other photophysical processes, and considering blinking is known to be turned off when the QD surface is electrochemically reduced,[31] we suspect that reversible charge storage at the QD surface may be tied to luminescence blinking. We encourage others to consider this surface-mediated mechanism moving forward.

3.4 Explanation for Rejection of Other Charge Storage Mechanisms

We considered that charges might not be stored at the QD surface, but rather at some internal defect or at some site near the surface. We rejected this mechanism because it is inconsistent with our observation of ligand dissociation and subsurface stored charges are expected to be poor charge donors due to weak wavefunction overlap with molecular charge acceptors.

We considered that charges may localize to Cd that are on stoichiometric facets (Scheme 3.3b) based on computational results that when QD surfaces are perfectly passivated, adding extra electrons to the QD resulted in a Cd^0 atom being ejected from the (111) plane.[93] However, this mechanism does not explain our observation of ligand displacement. Furthermore, it does not explain that the number of stored charges is dependent on surface ligation.

We also considered that perhaps the storage of charges was not completely localized, but rather spread between a few surface atoms (Scheme 3.3c). In one computational investigation of PbS QDs, excess electrons caused reduction and dimerization of surface Pb that were on a stoichiometric facet.[94] If both Cd were not ligated, this would not explain our observations analogously to our rejection of Scheme 3.3b. Possibly one of the involved Cd might be ligated on an edge near a stoichiometric facet which could weaken Cd-ligand bonds, but we would not expect one surface ligand removed for every one electron stored, which was our experimental finding.

Lastly, computational results have suggested that surface chalcogen dimers may be reduced,[94,95] though one experimental investigation found that surface chalcogen dimers were hole traps, not electron traps.[96] The lack of dependence on ligation and no ligand desorption rules this out. Fur-

thermore, removing Z-type Cd should cause more of these dimers,[96] but fewer charges were stored in the samples where we removed Z-type Cd.

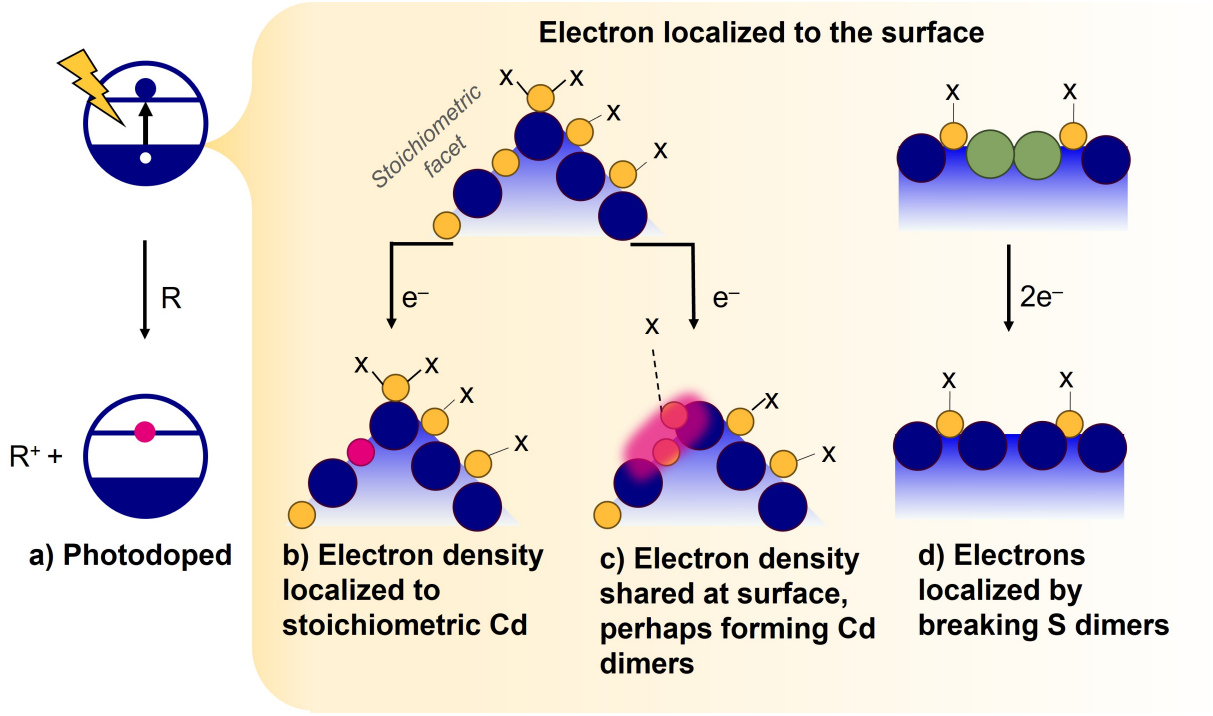

Scheme 3.3: Rejected mechanisms for charge storage. (a) n-type photodoping wherein a reducing agent (internal or external to the QD) quenches the photogenerated hole, leaving behind an electron in the conduction band. (b) Electron density localized to Cd on a stoichiometric surface. (c) Electron density shared between a few surface atoms. (d) Electrons localized to surface S dimers.

3.5 Materials and Methods

Unless otherwise noted, all manipulations were performed in an inert atmosphere glovebox.

3.5.1 Chemicals

Benzonitrile (>99.0%) was purchased from TCI and dried over phosphorous pentoxide then fractionally vacuum distilled (discarding the first and last 5%). The drying and distillation was re-

peated. Tetrabutylammonium hexafluorophosphate ([TBA][PF_6], 98%) was purchased from VWR Scientific and recrystallized twice from ethanol. Dimethyl sulfoxide-d6 (D, 99.9%) was purchased from Cambridge Isotope Laboratories and dried over CaH_2 then vacuum distilled. Acetonitrile-d3 (D, 99.8%) was purchased from Cambridge Isotope Laboratories and dried over 3angstrom sieves. Ferrocene was purchased from Sigma Aldrich and purified via vacuum sublimation. N,N,N',N'-Tetramethylethylenediamine (TMEDA, 99%) was purchased from Sigma Aldrich and dried over CaH2 then distilled. [2-(2-Methoxyethoxy)ethoxy]acetic acid (>95%) was purchased from TCI and dried over 3angstrom sieves, then distilled before storing over sieves in a nitrogen-filled glovebox. Ferrocenium hexafluorophosphate ($FcPF_6$, 97%) was purchased from Sigma Aldrich, dissolved in acetonitrile, then filtered. The filtrate was collected and dried. Triethyl phosphite (98%), methanol, cobaltocenium hexafluorophosphate (98%) and bromotrimethylsilane (97%) were purchased from Sigma-Aldrich and used as received. 2-[2-(2-methoxyethoxy)ethoxy]ethyl bromide was purchased from TCI and used as received.

3.5.2 Synthetic Procedures

Synthesis of (2-[2-(2-methoxyethoxy)ethoxy]ethyl)phosphonic acid (MEEEPA).

MEEEPA was prepared following literature procedure using the Michaelis-Arbuzov method.[97] 2-[2-(2-methoxyethoxy)
-ethoxy]ethyl bromide was converted to diethyl (2-[2-(2-methoxyethoxy)ethoxy]ethyl)phosphonate then to the phosphonic acid. After evacuating for several hours, the product was used without further purification and stored in the glovebox.

Oleic Acid-Capped CdS QD Synthesis.

The CdS QDs were prepared as described earlier[6] without modification and stored as a solution in toluene. Characterization can be found in Figure 3.13.

Preparation of MEEAA-capped CdS QDs.

The ligand exchange procedure was adapted from De Roo et al.[98] Briefly, oleic acid capped CdS QDs (456 nmol, 1 eq) were dried and resuspended in 5 mL chloroform. MEEAA (1.27 g, 7.11 mmol, 15600 eq) was added then stirred overnight to yield a clear suspension. Suspension and precipitation washes using chloroform and pentane were performed until a yellow solid was isolated, then after obtaining a yellow solid, two more washes were performed. The particles were stored as a suspension in chloroform. Characterization can be found in Figure 3.13.

TMEDA Etched, MEEAA-Capped CdS QDs.

To a solution of oleic acid capped CdS QDs (220 nmol, 1 eq) in 3.5 mL toluene, TMEDA (0.0272 g, 0.234 mmol, 1060 eq) was added. This solution was stirred for 3 hr then QDs were isolated with repeated precipitation and dissolution cycles with toluene and methanol then stored in 4 mL toluene. The TMEDA etching was repeated, this time with more TMEDA (0.140 g, 0.935 mmol, 4220 eq) and isolated with suspension and precipitation cycles using toluene and methanol. The resulting etched QDs were stored in toluene. The remaining oleic acid ligands were exchanged for MEEAA by stirring the toluene solution with MEEAA (0.711 g, 4.00 mmol, 10400 eq) and isolated with suspension and precipitation cycles using chloroform and pentane. Characterization can be found in Figure 3.12.

Preparation of MEEEPA-Capped CdS QDs.

The ligand exchange procedure follows the MEEAA exchange procedure closely, though with fewer equivalents and less time. Oleic acid capped CdS QDs (456 nmol, 1 eq) were dried and resuspended in 5 mL chloroform. MEEEPA (0.135 g, 0.592 mmol, 1300 eq) was added and stirred for 2 hours to yield a clear suspension. Four suspension and precipitation washes using chloroform and pentane were performed, then the isolated particles were stored in chloroform.

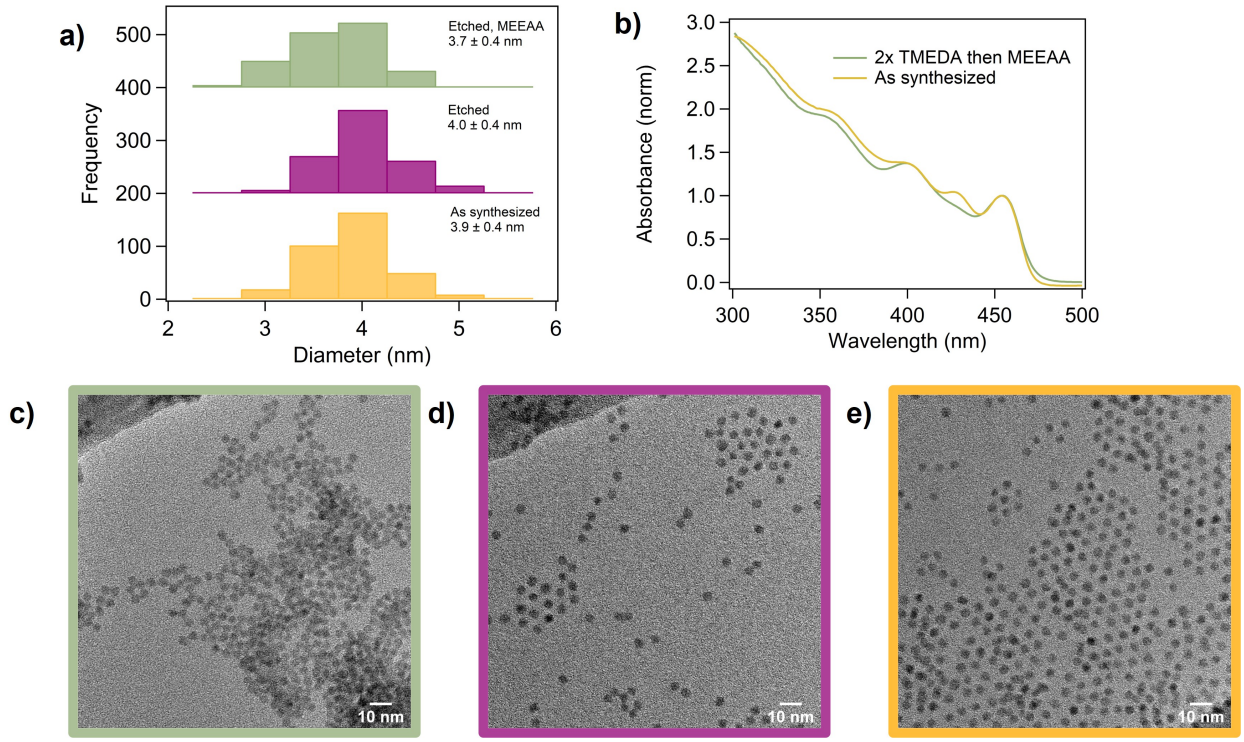

Figure 3.12: Characterization of a batch of CdS QDs as synthesized (oleate capped) and after TMEDA etching, then MEEAA ligand exchange. (a) Histograms of QD diameters measured by TEM. The etched MEEAA capped QDs are significantly different from the other two. (b) UV-vis absorbance of solutions of QDs. (c-e) Representative TEM images of the different QDs.

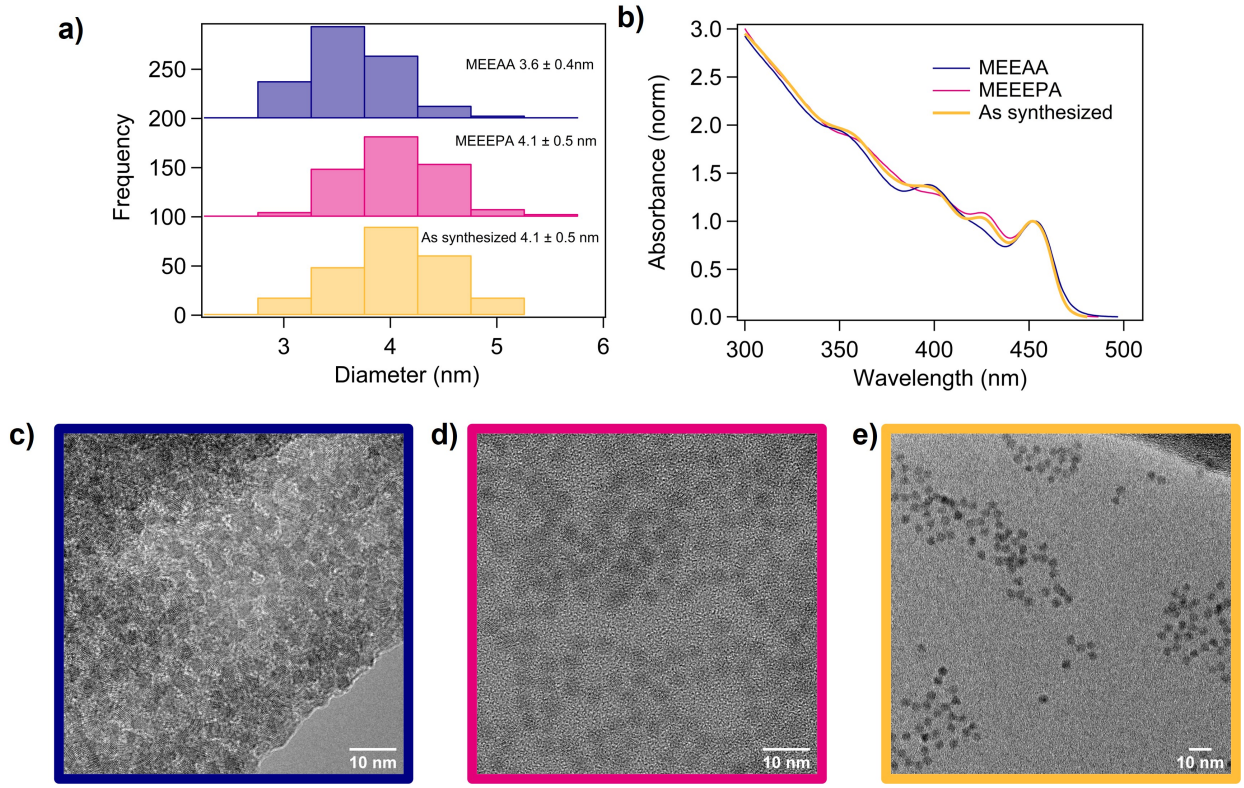

Figure 3.13: Characterization of a batch of CdS QDs as synthesized (oleate capped) and after ligand exchanges. (a) Histograms of QD diameters measured by TEM. The MEEAA capped QDs are significantly different from the other two. (b) UV-vis absorbance of solutions of QDs. (c-e) Representative TEM images of the different QDs.

Synthesis of Oleic Acid-Capped CdSe QDs.

Oleic acid capped CdSe QDs were prepared by modifying literature procedure[99] to exclude octadecylphosphonic acid allowing easier post synthetic ligand exchange. 120 mg CdO and 3.167 g oleic acid were combined in 12 mL hexadecane in a 50 mL three neck flask. This mixture was evacuated, heated to 90°C and held for 1hr. The flask was refilled with nitrogen then heated to 160°C until the solution was clear, then cooled to 100°C. The flask was evacuated again for 2hr. Then the flask was refilled with nitrogen then heated to 275°C. Separately, TOP-Se was prepared by combining 0.116 g elemental Se with 0.72g trioctylphosphine. The TOP-Se was swiftly injected into the cadmium oleate mixture. After 45 s, the flask was removed from heat and cooled with forced air. The hexadecane was removed from the flask with vacuum distillation. The CdSe QDs were isolated with repeated suspension and precipitation with toluene and methanol.

Preparation of MEEAA-Capped CdSe QDs.

Oleic acid capped CdSe QDs (1.8 µmol determined using optical absorbance,[100] 1 eq) were dried then resuspended in 5 mL chloroform. MEEAA (3.36 g, 18.9 mmol, 10400 eq.) was added to this solution and stirred overnight. The MEEAA-capped QDs were isolated with repeated suspension and precipitation with chloroform and pentane followed by size-selective precipitation. Characterization data can be found in Figure 3.14.

Synthesis of Myristic Acid-Capped InP QDs.

Myristic acid capped InP QDs were prepared from literature procedure using a hot injection of $In_{37}P_{20}(myristate)_{51}$ as a single source precursor.[101]

Preparation of MEEAA-capped InP QDs.

Myristic acid capped InP QDs (100 nmol, determined by optical absorption in a toluene solution)[102] were dried then resuspended in 1 mL chloroform. MEEAA (0.0967g, 0.542 mmol, 5430 eq) was added to this solution and stirred overnight. The QDs were then isolated with repeated suspension

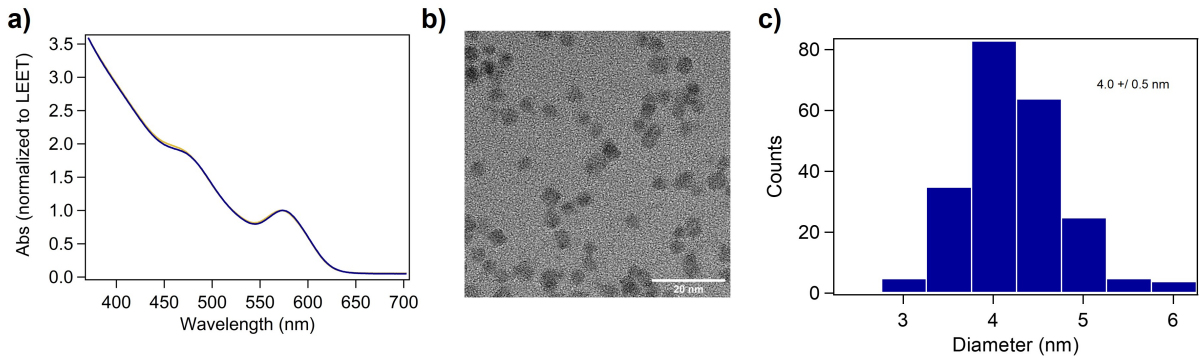

Figure 3.14: Characterization of CdSe QDs. (a) UV-vis absorbance of solutions of QDs with native oleate ligands (yellow) and with MEEAA ligands (blue). The traces nearly perfectly overlay. (b) Representative TEM of the CdSe QDs capped with MEEAA. (c) Histogram of QD diameters measured by TEM.

and precipitation with chloroform and pentane then stored in benzonitrile. Optical characterization found in Figure 3.15.

3.5.3 Data Acquisition

Absorbance Changes During Illumination.

QDs solutions in PhCN were loaded into a cuvette with a polished bottom. The cuvette was equipped with a high-vacuum PTFE valve to maintain air free conditions during the measurement. The solutions were illuminated from below using 448nm LEDs. Solutions of QDs were prepared such that the absorbance at the excitation wavelength was 0.45-0.5. After controlled time of illumination, the sample was moved into the spectrophotometer (Agilent Cary 5000) and an absorbance measurement was taken. The sample was quickly moved back to the LED illumination, and this process was repeated several times to track absorbance changes over extended illumination.

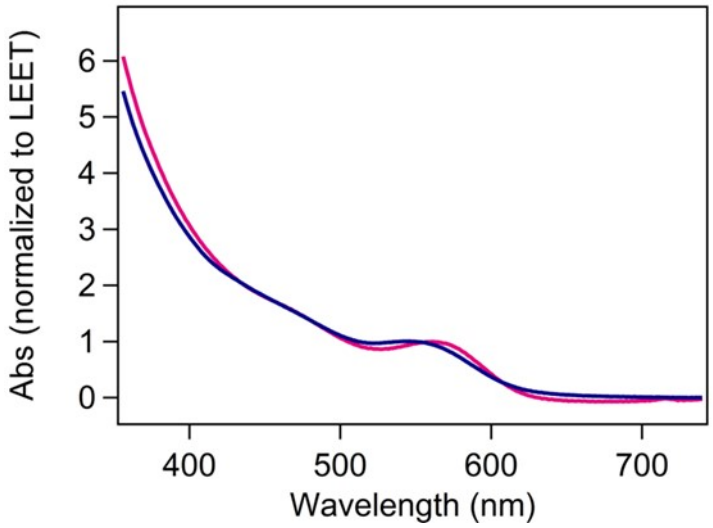

Figure 3.15: Uv-vis absorbance of solutions of InP with native myristate ligands (pink) and after MEEAA ligand exchange (blue).

Photoluminescence Changes During Illumination.

QDs solutions in PhCN were loaded into a fluorescence cuvette with a polished bottom. The absorbance at the excitation wavelength was about 0.1. The excitation wavelength was 420 nm. After taking the initial spectrum, the solution was brought into a nitrogen filled glovebox and irradiated for 30 min, then PL was measured again.

Transmission Electron Microscopy.

All imaging was done on an FEI Tecnai G2 F20 SuperTwin microscope operated at 200 kV using bright field imaging. Samples were prepared in a nitrogen glovebox by drop-casting 5 µL of dilute QD suspensions in chloroform onto a suspended ultrathin carbon film on a lacey carbon support film, 400 mesh, copper grids purchased from Ted Pella Inc., allowed to dry fully (10 min), then placed under vacuum overnight. TEM size analysis was performed using manual analysis in ImageJ based on images from at least two different grid locations and over 300 particle diameter measurements per sample.

Nuclear Magnetic Resonance spectroscopy.

NMR spectroscopy was performed on a Bruker Avance-I spectrometer operating at 300.13 MHz proton frequency. For DOSY, solutions were performed in nearly saturated solutions of QD in DMSO-d_6 spiked with 10 µL mesitylene. For quantification of stored charge by Fc^+ reavitvity, the solvent was 50:50 mixture of CD_3CN/benzonitrile. A 0.35 mL solution containing 10 nmol CdS QDs (concentration by optical spectroscopy) was illuminated for 45 minutes in a scintillation vial with magnetic stirring at 700 rpm. The illumination was stopped, then 60 seconds later 0.25 mL of solution containing 5 µmol $FcPF_6$ was added. This solution was transferred to an airfree NMR tube.

Cyclic Voltammetry.

All electrochemical experiments were performed in a nitrogen-filled glove box. The potentiostat used was an EC Epsilon from BASi. Glassy carbon disk electrodes with a diameter of 3.0 mm were polished using 5, 1, and 0.1 micron polishing powder with sonication in ultrapure water between steps. The counter electrode was a platinum wire, and the pseudoreference electrode was a silver wire in a ceramic-fritted glass tube (Pine) filled with 0.1 M [TBA][PF_6].

4 µmol of redox probe (Fc or cobaltocenium hexafluorophosphate) and either 30.8 nmol CdSe QD or 30.8 nmol InP QD or 9.5 nmol CdS QD were dispersed in 2.8 mL benzonitrile. The supporting electrolyte was 0.1M [TBA][PF_6]. The three electrode cell was assembled in a cuvette as we described earlier[6] and illuminated from the bottom using a 448 nm LED (from Luxeon Star, equipped with a 12° beam optic, FWHM 20 nm). The LED was driven at 0.5A, which corresponds to 0.77W. Cyclic voltammograms were taken at 10 mV/s with a potential range of 500 mV. Sequential cyclic voltammograms were taken 30 seconds apart during charging and discharging.

3.5.4 Data Processing

Determining k_{obs} from CV.

The observed rate of charge transfer (k_{obs} in units s^{-1}) were calculated using 3.3.

$$\frac{i_c}{i_p} = \frac{1}{0.446}\sqrt{\frac{RT}{nF\nu}k_{obs}} \tag{3.3}$$

Where i_c is the plateau current (the current measured at highest potential for electron transfer or lowest potential for hole transfer for each scan), i_p is the peak current for the cyclic voltammogram taken without any light, n is the number of electrons transferred at the electrode, and ν is the scan rate in V/s.

Determining Fraction of Ligands Bound with DOSY and Propagating Error.

The Bruker Avance-I spectrometer was equipped with a Bruker PABBI probe. The pulse program was stimulated echo and bipolar gradient pulses (stebpgp1s). The gradient strength was varied exponentially from 5-95% of the maximum gradient strength in 32 steps. A relaxation delay of 15s and a diffusion delay of $\Delta = 0.3$s were used. The gradient pulse duration was $\delta = 1500$ µs. The diffusion coefficients were extracted from the resulting DOSY data by fitting the decay the integration of the peak in question against the scaled gradient strength according to the Stejskal-Tanner equation (Q, defined in 3.4) to a two-component exponential decay (3.5).

$$Q = (\gamma\ \delta\ g)^2 \left(\Delta - \frac{\delta}{3}\right) \tag{3.4}$$

Where γ the gyromagnetic ratio of a proton and g is the gradient strength. The data to fit was obtained from integration in MestreNova v14 and then fit in Igor Pro v6.

$$I = A\exp\left(-D_1 Q\right) + Bexp\left(-D_2 Q\right) \tag{3.5}$$

Where I is the integration of the peak, D_1 and D_2 are the diffusion coefficients of the bound and free ligand in $cm^2\,s^{-1}$, and A and B reflect the relative molar content of the two components. Then, if $D_1 < D_2$, the fraction of ligands in solution bound to the QD are given by 3.6. The results of

this analysis are found in Table B.1.

$$\chi_{bound} = \frac{A}{A+B} \tag{3.6}$$

We can find that the error in the bound fraction, σ_χ by taking partial derivatives from 3.6.

$$\sigma_\chi = \sqrt{\left(\frac{\partial\chi}{\partial_A}\right)^2 * \sigma_A^2 + \left(\frac{\partial\chi}{\partial_B}\right)^2 * \sigma_B^2} \tag{3.7}$$

Where σ_A and σ_B are the uncertainty from fitting A and B in 3.5. The number of bound ligands per QD is the total number of ligands in solution per QD multiplied by χ. If we approximate that all uncertainty comes from the bound fraction extracted from DOSY, then the uncertainty in bound ligands per QD is just σ_χ multiplied by the total number of ligands in solution, obtained by quantitative 1D ^{1}H NMR with mesitylene internal standard. Values for each of these parameters discussed for each CdS surface can be found in Table B.2.

Quantification of Stored Charge by Fc^+ Reduction.

NMR was used to quantify the amount of Fc^+ that was reduced by the QDs. Because of the rapid electronic self-exchange between Fc (diamagnetic) and Fc^+ (paramagnetic), rather than observing two peaks, one for each species, we observe only one peak for both. This behavior is well-understood, and the mole fraction of Fc is related to position of the observed peak by 3.8.

$$\chi_d = \frac{\delta_{dp} - \delta_p}{\delta_d - \delta_p} \tag{3.8}$$

Where χ_{dp} is the observed peak, χ_d is the NMR shift for Fc only (4.12 in CD_3CN/PhCN) and χ_p is the NMR shift of pure Fc^+ (32.70). Then the number of electrons transferred per quantum dot, Fc/QD, was calculated using the moles of $FcPF_6$ added as well as the moles of QD using 3.9.

$$\frac{Fc}{QD} = \frac{mol\ added\ FcPF_6}{mol\ QD} \times \chi_d \tag{3.9}$$

Calculation of Change in Bound Ligands by Shifting of ^1H NMR Peak Position

As described in the main text, in a system in fast equilibrium on the NMR experiment timescale, the observed peak is related to the mole ratio and chemical shift of the two components:

$$\delta_{obs} = \chi_{bound}\delta_{bound} + \chi_{free}\delta_{free} \tag{3.10}$$

where δ are chemical shifts and χ are mole fractions. Since $\chi_{bound} + \chi_{free} = 1$, we can rearrange to get

$$\chi_{bound} = \frac{\delta_{obs} - \delta_{free}}{\delta_{bound} - \delta_{free}} \tag{3.11}$$

We cannot directly measure χ_{bound} because it was not possible to completely remove free ligand even after multiple runs through a size-selective column. However, we can manipulate the equation to eliminate this term. Dividing before and after illumination, we get

$$\frac{\chi_{bound,after}}{\chi_{bound,before}} = \frac{\delta_{obs,after} - \delta_{free}}{\delta_{obs,before} - \delta_{free}} \tag{3.12}$$

We substitute the experimentally determined chemical shifts for variables:

$$\frac{\chi_{bound,after}}{\chi_{bound,before}} = 0.889 \tag{3.13}$$

So there are approximately 11% fewer ligands on MEEAA capped CdS QDs after one hour of illumination, which at 430 ligands/QD represents a loss of 48 ligands.

3.5.5 X-ray Photoelectron Spectroscopy

Preparation of Thin Films for Photoemission Spectroscopy

The substrate was gold coated glass, which was cleaned before deposition by rinsing in ethyl acetate, 1M nitric acid, then ultrapure water. The substrate was then dried *in vacuo* for several hours, then brought into a nitrogen-filled glovebox where all subsequent manipulations were performed. Concentrated (*ca.* 0.1 mM) QD solutions were prepared in chloroform, then 20 µL × 2 layers were spin coated at 1800 rpm. Once the films had been created, they were loaded into sealed containers (under nitrogen) and shipped to the analysis site (University of Arizona) where they were opened in a glove box (less than ppm O_2 and H_2O) connected to the Kratos surface analysis system so that it was possible to position them on the sample stub and introduce them into the analysis chamber without exposure to air.

Photoemission Spectroscopy Data Acquisition

XPS data for conformal thin films of MEEAA and MEEEPA modified QDs, and for thin films of the neat ligand (2-[2-(2-methoxyethoxy)ethoxy]acetic acid) were acquired using a Kratos Axis Ultra PES system with a measurement pressure of ca. 2×10^{-9} Torr. For XPS measurements a monochromatic Al Kα excitation source was used (1486.6 eV, 300 W, pass energy of 20 eV). The core level binding energies (BE) for each QD are referenced to the Au $4\,f_{7/2}$ when the from the buried substrate could be detected (BE = 84.00 eV) and to the C 1s level for adventitious carbon (CHx, BE = 285 eV).

Each sample was first analyzed using XPS to examine relevant core level spectra, including Cd 3d, S 2p, C 1s and O 1s bands (see below) and then the samples were subjected to UPS characterization. After this first round of analysis the QD samples on Au were withdrawn from the analysis chamber to an Argon-filled antechamber where they could be illuminated with the same blue LED UV lights used throughout this work (448 nm LED from Luxeon Star, equipped with a 12° beam optic, FWHM 20 nm). The LED was driven at 0.5A, which corresponds to 0.77W. The LED optic was placed against the transparent window to the antechamber and light was aimed directly at the sample.

After 1 hr of illumination, the QD samples were returned to vacuum in the analysis chamber and the same XPS/UPS characterization was carried out, with the sample at the same position, so that difference spectra (after illumination versus before) could be reliably obtained. For purposes of characterization of the spectral changes in the C 1s envelopes, especially for the MEEAA-QDs, we also characterized thin films of just the carboxylate ligand itself on Au substrates, using the same experimental conditions.

Relative Atomic Ratios from XPS

for both the MEEAA- and MEEEPA-QDs the relative atomic ratios for S/Cd (corrected for relative sensitivity factors) are 1:1 within experimental error, consistent with a CdS QD that is close to stoichiometric in the near surface region (sampling depth for these XPS experiments is *ca.* 3 nm,

but these spectra are especially sensitive to the outermost atomic components of the QD). The S/Cd ratios were unchanged after illumination.

Cd 3d and S 2p Spectral Envelopes are Unchanged After Illumination of QD Thin Films

We carefully analyzed both the Cd 3d and S 2p spectra of MEEAA-QDs and MEEEPA-QDs to ascertain whether there were significant spectral changes (e.g. evidence for fully or partially reduced Cd sites) that occurred after 60 minutes of illumination. For both MEEAA and MEEEPA capped CdS, high resolution Cd 3d spectra show peaks that are somewhat asymmetric, suggesting more than one form of coordination environment in the near surface region, which others have also found in CdS[52] and CdSe.[52,103] For both QD types the Cd 3d and S 2p spectra were, within experimental error, unchanged because of the prolonged illumination process (SI Figure 9). The fact that there were no new peaks or shoulders on the main peaks is not surprising, since the number of stored charges per QD, revealed by the Fc^+ titration, is of the order 50 steady state, which means that those near surface states are below detection limits for a technique such as XPS with a detection limit of *ca.* 1-5 relative atomic percent.

REFERENCES

(1) Kamat, P. V. *The Journal of Physical Chemistry Letters* **2013**, *4*, 908–918.

(2) Livache, C.; Martinez, B.; Goubet, N.; Gréboval, C.; Qu, J.; Chu, A.; Royer, S.; Ithurria, S.; Silly, M. G.; Dubertret, B.; Lhuillier, E. *Nature Communications* **2019**, *10*, 2125.

(3) Shirasaki, Y.; Supran, G. J.; Bawendi, M. G.; Bulović, V. *Nature Photonics* **2013**, *7*, 13–23.

(4) Wilker, M. B.; Schnitzenbaumer, K. J.; Dukovic, G. *Israel Journal of Chemistry* **2012**, *52*, 1002–1015.

(5) Ye, C.; Zhang, D.-S.; Chen, B.; Tung, C.-H.; Wu, L.-Z. *ACS Central Science* **2024**, *10*, 529–542.

(6) Homer, M. K.; Kuo, D.-Y.; Dou, F. Y.; Cossairt, B. M. *Journal of the American Chemical Society* **2022**, *144*, 14226–14234.

(7) Cai, T.; Liu, Y.; Wang, L.; Dong, W.; Zeng, G. *Journal of Photochemistry and Photobiology C: Photochemistry Reviews* **2019**, *39*, 58–75.

(8) Savateev, O. *Advanced Energy Materials* **2022**, *12*, 2200352.

(9) Hirakawa, T.; Kamat, P. V. *Journal of the American Chemical Society* **2005**, *127*, 3928–3934.

(10) Hirakawa, T.; Kamat, P. V. *Langmuir* **2004**, *20*, 5645–5647.

(11) Takai, A.; Kamat, P. V. *ACS Nano* **2011**, *5*, 7369–7376.

(12) Liu, L.; Yang, W.; Li, Q.; Gao, S.; Shang, J. K. *ACS Applied Materials & Interfaces* **2014**, *6*, 5629–5639.

(13) Ravikumar, M. P.; Bharathkumar, S.; Urupalli, B.; Murikinati, M. K.; Muthukonda Venkatakrishnan, S.; Mohan, S. *Energy & Fuels* **2022**, *36*, 11503–11514.

(14) EL-Sheshtawy, H. S.; El-Hosainy, H. M.; Shoeir, K. R.; El-Mehasseb, I. M.; El-Kemary, M. *Applied Surface Science* **2019**, *467-468*, 268–276.

(15) Chiu, Y.-H.; Hsu, Y.-J. *Nano Energy* **2017**, *31*, 286–295.

(16) Liu, L.; Sun, W.; Yang, W.; Li, Q.; Shang, J. K. *Scientific Reports* **2016**, *6*, 20878.

(17) Li, Q.; Wai Li, Y.; Liu, Z.; Xie, R.; Ku Shang, J. *Journal of Materials Chemistry* **2010**, *20*, 1068–1072.

(18) Zhao, D.; Chen, C.; Yu, C.; Ma, W.; Zhao, J. *The Journal of Physical Chemistry C* **2009**, *113*, 13160–13165.

(19) Dong, F.; Xiong, T.; Sun, Y.; Zhao, Z.; Zhou, Y.; Feng, X.; Wu, Z. *Chemical Communications* **2014**, *50*, 10386–10389.

(20) Chiou, Y.-D.; Hsu, Y.-J. *Applied Catalysis B: Environmental* **2011**, *105*, 211–219.

(21) J. Peterson, J.; D. Krauss, T. *Physical Chemistry Chemical Physics* **2006**, *8*, 3851–3856.

(22) Chon, J. W. M.; Zijlstra, P.; Gu, M.; van Embden, J.; Mulvaney, P. *Applied Physics Letters* **2004**, *85*, 5514–5516.

(23) Bao, H.; Gong, Y.; Li, Z.; Gao, M. *Chemistry of Materials* **2004**, *16*, 3853–3859.

(24) Jones, M.; Nedeljkovic, J.; Ellingson, R. J.; Nozik, A. J.; Rumbles, G. *The Journal of Physical Chemistry B* **2003**, *107*, 11346–11352.

(25) Asami, H.; Abe, Y.; Ohtsu, T.; Kamiya, I.; Hara, M. *The Journal of Physical Chemistry B* **2003**, *107*, 12566–12568.

(26) Hess, B. C.; Okhrimenko, I. G.; Davis, R. C.; Stevens, B. C.; Schulzke, Q. A.; Wright, K. C.; Bass, C. D.; Evans, C. D.; Summers, S. L. *Physical Review Letters* **2001**, *86*, 3132–3135.

(27) Cordero, S. R.; Carson, P. J.; Estabrook, R. A.; Strouse, G. F.; Buratto, S. K. *The Journal of Physical Chemistry B* **2000**, *104*, 12137–12142.

(28) Carrillo-Carrión, C.; Cárdenas, S.; M. Simonet, B.; Valcárcel, M. *Chemical Communications* **2009**, *0*, 5214–5226.

(29) Krivenkov, V.; Samokhvalov, P.; Zvaigzne, M.; Martynov, I.; Chistyakov, A.; Nabiev, I. *The Journal of Physical Chemistry C* **2018**, *122*, 15761–15771.

(30) Efros, A. L.; Rosen, M. *Physical Review Letters* **1997**, *78*, 1110–1113.

(31) Galland, C.; Ghosh, Y.; Steinbrück, A.; Sykora, M.; Hollingsworth, J. A.; Klimov, V. I.; Htoon, H. *Nature* **2011**, *479*, 203–207.

(32) Tsui, E. Y.; Carroll, G. M.; Miller, B.; Marchioro, A.; Gamelin, D. R. *Chemistry of Materials* **2017**, *29*, 3754–3762.

(33) Hartley, C. L.; Kessler, M. L.; Dones Lassalle, C. Y.; Camp, A. M.; Dempsey, J. L. *Chemistry of Materials* **2021**, *33*, 8612–8622.

(34) Hartley, C. L.; Kessler, M. L.; Dempsey, J. L. *Journal of the American Chemical Society* **2021**, *143*, 1251–1266.

(35) Hartley, C. L.; Dempsey, J. L. *Nano Letters* **2019**, *19*, 1151–1157.

(36) Wu, K.; Du, Y.; Tang, H.; Chen, Z.; Lian, T. *Journal of the American Chemical Society* **2015**, *137*, 10224–10230.

(37) Ye, Y.; Wang, X.; Ye, S.; Xu, Y.; Feng, Z.; Li, C. *The Journal of Physical Chemistry C* **2017**, *121*, 17112–17120.

(38) Rowland, C. E.; Schaller, R. D. *The Journal of Physical Chemistry C* **2013**, *117*, 17337–17343.

(39) Widness, J.; Enny, D.; McFarlane-Connelly, K.; Miedenbauer, M.; Krauss, T.; Weix, D. **2022**, DOI: 10.26434/chemrxiv-2022-3x02c.

(40) Araujo, J. J.; Brozek, C. K.; Kroupa, D. M.; Gamelin, D. R. *Nano Letters* **2018**, *18*, 3893–3900.

(41) Araujo, J. J.; Brozek, C. K.; Liu, H.; Merkulova, A.; Li, X.; Gamelin, D. R. *ACS Nano* **2021**, *15*, 14116–14124.

(42) Hughes, K. E.; Hartstein, K. H.; Gamelin, D. R. *ACS Nano* **2018**, *12*, 718–728.

(43) Shulenberger, K. E.; Keller, H. R.; Pellows, L. M.; Brown, N. L.; Dukovic, G. *The Journal of Physical Chemistry C* **2021**, *125*, 22650–22659.

(44) Rinehart, J. D.; Schimpf, A. M.; Weaver, A. L.; Cohn, A. W.; Gamelin, D. R. *Journal of the American Chemical Society* **2013**, *135*, 18782–18785.

(45) Colvin, V. L.; Alivisatos, A. P. *The Journal of Chemical Physics* **1992**, *97*, 730–733.

(46) Norris, D. J.; Sacra, A.; Murray, C. B.; Bawendi, M. G. *Physical Review Letters* **1994**, *72*, 2612–2615.

(47) He, S.; Li, Q.; Jin, T.; Lian, T. *The Journal of Chemical Physics* **2022**, *156*, 054704.

(48) Kobosko, S. M.; DuBose, J. T.; Kamat, P. V. *ACS Energy Letters* **2020**, *5*, 221–223.

(49) Anderson, N. C.; Hendricks, M. P.; Choi, J. J.; Owen, J. S. *Journal of the American Chemical Society* **2013**, *135*, 18536–18548.

(50) Boles, M. A.; Ling, D.; Hyeon, T.; Talapin, D. V. *Nature Materials* **2016**, *15*, 141–153.

(51) Prather, K. V.; Stoffel, J. T.; Tsui, E. Y. *Chemistry of Materials* **2023**, acs.chemmater.3c00481.

(52) Singh, S.; Leemans, J.; Zaccaria, F.; Infante, I.; Hens, Z. *Chemistry of Materials* **2021**, *33*, 2796–2803.

(53) Hartley, C. L.; Dempsey, J. L. *Chemistry of Materials* **2021**, DOI: 10.1021/acs.chemmater.1c00520.

(54) Hiller, W. *Macromolecular Chemistry and Physics* **2019**, *220*, 1900255.

(55) Calvin, J. J.; Ben-Moshe, A.; Curling, E. B.; Brewer, A. S.; Sedlak, A. B.; Kaufman, T. M.; Alivisatos, A. P. *The Journal of Physical Chemistry C* **2022**, *126*, 12958–12971.

(56) Harris, R. D.; Amin, V. A.; Lau, B.; Weiss, E. A. *ACS Nano* **2016**, *10*, 1395–1403.

(57) Ritchhart, A.; Cossairt, B. M. *Inorganic Chemistry* **2019**, *58*, 2840–2847.

(58) Heiba, Z. K.; Mohamed, M. B.; Imam, N. G. *Journal of Alloys and Compounds* **2015**, *618*, 280–286.

(59) Ahmed, S.; Wunder, S. L. *Langmuir* **2009**, *25*, 3682–3691.

(60) Fan, H.; Leve, E. W.; Scullin, C.; Gabaldon, J.; Tallant, D.; Bunge, S.; Boyle, T.; Wilson, M. C.; Brinker, C. J. *Nano Letters* **2005**, *5*, 645–648.

(61) Rubio, J.; Izquierdo, M. A.; Burguete, M. I.; Galindo, F.; Luis, S. V. *Nanoscale* **2011**, *3*, 3613–3615.

(62) Harvey, S. M.; Olshansky, J. H.; Li, A.; Panuganti, S.; Kanatzidis, M. G.; Hupp, J. T.; Wasielewski, M. R.; Schaller, R. D. *Journal of the American Chemical Society* **2024**, *146*, 3732–3741.

(63) Fritzinger, B.; Capek, R. K.; Lambert, K.; Martins, J. C.; Hens, Z. *Journal of the American Chemical Society* **2010**, *132*, 10195–10201.

(64) Kelm, J. E.; Dempsey, J. L. *Journal of the American Chemical Society* **2024**, DOI: 10.1021/jacs.3c11811.

(65) Kessler, M. L.; Kelm, J. E.; Starr, H. E.; Cook, E. N.; Miller, J. D.; Rivera, N. A.; Hsu-Kim, H.; Dempsey, J. L. *Chemistry of Materials* **2022**, *34*, 1710–1721.

(66) Gomes, R.; Hassinen, A.; Szczygiel, A.; Zhao, Q.; Vantomme, A.; Martins, J. C.; Hens, Z. *The Journal of Physical Chemistry Letters* **2011**, *2*, 145–152.

(67) Boehme, S. C.; Wang, H.; Siebbeles, L. D.; Vanmaekelbergh, D.; Houtepen, A. J. *ACS Nano* **2013**, *7*, 2500–2508.

(68) Chang, W. J.; Park, K.-Y.; Zhu, Y.; Wolverton, C.; Hersam, M. C.; Weiss, E. A. *ACS Applied Materials & Interfaces* **2020**, *12*, 36523–36529.

(69) Sun, W.; Olikagu, C.; Carothers, K. J.; Pattadar, D.; Pyun, J.; Saavedra, S. S.; Armstrong, N. R. *The Journal of Physical Chemistry C* **2022**, DOI: 10.1021/acs.jpcc.2c05692.

(70) Puntambekar, A.; Wang, Q.; Miller, L.; Smieszek, N.; Chakrapani, V. *ACS Nano* **2016**, *10*, 10988–10999.

(71) Dou, F; Nishiwaki, E; Larson, H; Zion, T; Nguyen, H; Cossairt, B *ChemRxiv* **2024**, DOI: 10.26434/chemrxiv-2024-ds99w.

(72) Shubert-Zuleta, S. A.; Tandon, B.; Roman, B. J.; Gan, X. Y.; Milliron, D. J. *Chemistry of Materials* **2023**, *35*, 3880–3891.

(73) Cohn, A. W.; Rinehart, J. D.; Schimpf, A. M.; Weaver, A. L.; Gamelin, D. R. *Nano Letters* **2014**, *14*, 353–358.

(74) NIST X-ray Photoelectron Spectroscopy Database, Gaithersburg MD.

(75) Aschendorf, C. J.; Degbevi, M.; Prather, K. V.; Tsui, E. Y. *Chemical Science* **2023**, *14*, 13080–13089.

(76) Keeble, D. J.; Thomsen, E. A.; Stavrinadis, A.; Samuel, I. D.; Smith, J. M.; Watt, A. A. *The Journal of Physical Chemistry C* **2009**, *113*, 17306–17312.

(77) Morris-Cohen, A. J.; Peterson, M. D.; Frederick, M. T.; Kamm, J. M.; Weiss, E. A. *The Journal of Physical Chemistry Letters* **2012**, *3*, 2840–2844.

(78) Morris-Cohen, A. J.; Frederick, M. T.; Cass, L. C.; Weiss, E. A. *Journal of the American Chemical Society* **2011**, *133*, 10146–10154.

(79) DuBose, J. T.; Kamat, P. V. *The Journal of Physical Chemistry C* **2020**, *124*, 12990–12998.

(80) Zhao, F.; Li, Q.; Han, K.; Lian, T. *The Journal of Physical Chemistry C* **2018**, *122*, 17136–17142.

(81) Scholz, F.; Dworak, L.; Matylitsky, V. V.; Wachtveitl, J. *ChemPhysChem* **2011**, *12*, 2255–2259.

(82) Gutiérrez, M.; Henglein, A. *Berichte der Bunsengesellschaft für physikalische Chemie* **1983**, *87*, 474–478.

(83) Reber, J. F.; Meier, K. *The Journal of Physical Chemistry* **1984**, *88*, 5903–5913.

(84) Nedoluzhko, A. I.; Shumilin, I. A.; Nikandrov, V. V. *The Journal of Physical Chemistry* **1996**, *100*, 17544–17550.

(85) Venturi, M.; Mulazzani, Q. G.; Hoffman, M. Z. *Radiation Physics and Chemistry (1977)* **1984**, *23*, 229–236.

(86) Bauer, R.; Werner, H. A. F. *Journal of Molecular Catalysis* **1992**, *72*, 67–74.

(87) Ebbesen, T. W.; Ferraudi, G. *The Journal of Physical Chemistry* **1983**, *87*, 3717–3721.

(88) Mohammad, M.; Iqbal, R.; Khan, A. Y.; Bhatti, M.; Zahir, K.; Jahan, R. *The Journal of Physical Chemistry* **1981**, *85*, 2816–2820.

(89) Aruda, K. O.; Bohlmann Kunz, M.; Tagliazucchi, M.; Weiss, E. A. *The Journal of Physical Chemistry Letters* **2015**, *6*, 2841–2846.

(90) Knowles, K. E.; Tagliazucchi, M.; Malicki, M.; Swenson, N. K.; Weiss, E. A. *The Journal of Physical Chemistry C* **2013**, *117*, 15849–15857.

(91) Hughes, K. E.; Stein, J. L.; Friedfeld, M. R.; Cossairt, B. M.; Gamelin, D. R. *ACS Nano* **2019**, *13*, 14198–14207.

(92) Heath, J. R. *Chemical Society Reviews* **1998**, *27*, 65–71.

(93) Du Fossé, I.; ten Brinck, S.; Infante, I.; Houtepen, A. J. *Chemistry of Materials* **2019**, *31*, 4575–4583.

(94) Voznyy, O.; Thon, S. M.; Ip, A. H.; Sargent, E. H. *The Journal of Physical Chemistry Letters* **2013**, *4*, 987–992.

(95) Giansante, C.; Infante, I. *The Journal of Physical Chemistry Letters* **2017**, *8*, 5209–5215.

(96) Houtepen, A. J.; Hens, Z.; Owen, J. S.; Infante, I. *Chemistry of Materials* **2017**, *29*, 752–761.

(97) De Roo, J.; Zhou, Z.; Wang, J.; Deblock, L.; Crosby, A. J.; Owen, J. S.; Nonnenmann, S. S. *Chemistry of Materials* **2018**, *30*, 8034–8039.

(98) De Roo, J.; Yazdani, N.; Drijvers, E.; Lauria, A.; Maes, J.; Owen, J. S.; Van Driessche, I.; Niederberger, M.; Wood, V.; Martins, J. C.; Infante, I.; Hens, Z. *Chemistry of Materials* **2018**, *30*, 5485–5492.

(99) Hanifi, D. A.; Bronstein, N. D.; Koscher, B. A.; Nett, Z.; Swabeck, J. K.; Takano, K.; Schwartzberg, A. M.; Maserati, L.; Vandewal, K.; van de Burgt, Y.; Salleo, A.; Alivisatos, A. P. *Science* **2019**, *363*, 1199–1202.

(100) Jasieniak, J.; Smith, L.; van Embden, J.; Mulvaney, P.; Califano, M. *The Journal of Physical Chemistry C* **2009**, *113*, 19468–19474.

(101) Nayon Park; Madison Monahan; Andrew Ritchhart; Max R. Friedfeld; Brandi M. Cossairt *Journal of Visualized Experiments* **2019**, DOI: 10.3791/59425.

(102) Achorn, O. B.; Franke, D.; Bawendi, M. G. *Chemistry of Materials* **2020**, *32*, 6532–6539.

(103) Shallcross, R. C.; Graham, A. L.; Karayilan, M.; Pavlopoulous, N. G.; Meise, J.; Pyun, J.; Armstrong, N. R. *The Journal of Physical Chemistry C* **2020**, *124*, 21305–21318.

Appendix A

SUPPORTING INFORMATION FOR CHAPTER 2

A.1 Electrochemistry Modeling Details

Electrochemical modeling was performed in DigiElch v8. This powerful technique allows the fitting of many parameters relevant to the electrochemical experiment, so care must be taken to avoid overfitting the system. With each additional reaction added to the model there are more unknown variables to be fit, so we only allow three reactions in the model. These processes are the two reactions in the E_rC_i' reaction mechanism with a possible third reaction to regenerate QD* in the models with low values of γ. While these three reactions are a simplification of the many photophysical and chemical processes in the system, this generalization allows us to probe the effective rate of charge extraction.

We determined some parameters independently of photoelectrochemical experiments to minimize the number of values that are allowed to float during the general fitting. The reduction potential (E^0) and the heterogeneous electron transfer rate constant (k_s), and either concentration or diffusion coefficient for each probe are first obtained by fitting CVs without illumination. These values are assumed to be unchanged during experiments under illumination. The analytical concentration of M must be known to obtain the other parameters to be fit but can be complicated because of the sublimation of some metallocenes during sample preparation. For Fc, we assume that the analytical concentration is exactly the targeted concentration (4 µmol in 2.8 mL). Then, the diffusion coefficient of Fc, E^0 and k_s, are fit to the data for a series of CVs with varying scan rate. We then assume that the substituted ferrocenes have approximately the same diffusion coefficient as Fc ($4.67 \times 10^{-6}\,\mathrm{cm^2\,s^{-1}}$). Then, we determine the analytical concentration, along with E^0 and k_s by fitting the dark scans for $FcNH_2$, FcCOOH, and $FcCOCH_3$. For Co(Cp)(dppe), we assumed

that the concentration was equal to the targeted concentration and fit the data to determine E^0, k_s, and the diffusion coefficient. These values can be found and summarized in Table A.1

When γ is small (low [QD*]), a third reaction to regenerate QD* after electron transfer must be included in the model. To maintain thermodynamic consistency, the regeneration of QD* requires the photon to be explicitly written as a reagent, or "hν" in the electrochemical model. The diffusion coefficient of hν and the concentration of hν are set to extreme values to force the photocharging step to be fast compared to photoinduced charge transfer and to force [QD*] to be equal to the analytical concentration of the QDs, allowing zones KD and KS to be reached despite a low value of γ. The diffusion coefficient of hν is set to three orders of magnitude larger than that of M (0.01 $cm^2\,s^{-1}$), the concentration is set to five orders of magnitude larger than [QD] (0.75M). Then, when the data set for Fc is modeled, the forward rate constant (k_f) and equilibrium constant (K_{eq}) for the regeneration step are allowed to float. These values do not have any physical meaning, because buried in them are the assumptions for parameters of hν. Once the rate and equilibrium constants for photocharging are fit for the Fc data, they are assumed to be equal for all experiments with the same [QD] and the same light intensity.

By forcing the regeneration reaction to be fast and using the dark traces to model Er, only the photoinduced charge transfer reaction of interest remains to be fit. No simulation runs converged well for the value of the equilibrium constant for the photoinduced charge transfer reaction. This observation makes reasonable chemical sense, as the reaction is expected to be irreversible. The backward reaction would require injecting an electron from M to QD, which was not observed via open circuit potential measurement when QD and M are combined. With so much uncertainty in the very slow rate of the backward reaction, this equilibrium constant was set to a very large value (10^9), forcing the backward rate to be small and not influential in the model. In sum, if the backward charge transfer reaction is forced to be slow then the forward photoinduced charge transfer reaction is the rate limiting chemical reaction in the model and k_{PCT} is fit.

Using this modeling procedures described above, both with and without regeneration of QD*, we fit a series of CVs with varying scan rate. These can be found in Table A.3 and Table A.2

The area of the electrode was set to 0.0707 cm^2 and no uncompensated resistance was added to the model. For all probes, the charge transfer coefficient α was set to 0.5. The diffusion coefficient of CdS was set to $3.12 \times 10^{-6}\,cm^2\,s^{-1}$ based on analogous determination as Henckel *et. al* using 6-(Ferrocenyl)hexanethiol,[1] but if QD* is large or quickly regenerated, the diffusion coefficient doesn't greatly impact the model. The diffusion coefficient of hν was set to 0.01 $cm^2\,s^{-1}$. In all experiments, the nominal concentration of CdS was 1.1×10^{-5} M. All simulations converged well when k_{PCT} was fit and the goodness of fit showed a clear dependence on the value of k_{PCT} (Figure A.1). Reported standard error of fitted values from the software was $< 1\%$ of the fit value.

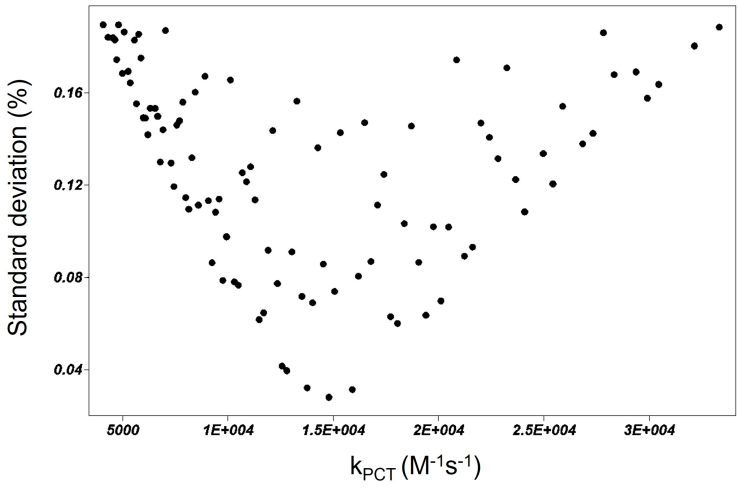

Figure A.1: A plot of best sets of modeled parameters, plotted with the standard deviation against the value of k_{PCT} used in each set. The global minimum shows that when k_{PCT} is $1.49 \times 10^4\,M^{-1}\,s^{-1}$, the error between model and experiment is minimized and the goodness of fit depends strongly on k_{PCT}.

A.2 Parameters Used for Electrochemical Modeling

Table A.1: Model parameters for all cyclic voltammogram models.

Probe	Diffusion coefficient probe ($cm^2\,s^{-1}$)	Concentration M	E^0 (V vs Fc)	k_s $cm\,s^{-1}$
$FcNH_2$	4.67E-06	0.00139	-0.3875	0.0012
Fc (average)	4.67E-06	0.00143	0	0.0014
FcCOOH	4.67E-06	0.00191	0.245	0.0011
$FcCOCH_3$	4.67E-06	0.00171	0.262	0.0012

Table A.2: Model parameters low γ, including regenration of QD*.

Probe	[QD*] (M)	Diffusion coefficient hν (cm2/s)	[hν] (M)	k_f (regeneration, $M^{-1}\,s^{-1}$)	Keq (regeneration)	k_{PCT} ($M^{-1}\,s^{-1}$)	k_{obs} (s^{-1})
$FcNH_2$	1.1E-05	0.01	0.744	450	4.10	2.57E+04	2.82E-01
Fc (average)	1.1E-05	0.01	0.744	450	4.10	4.10E+04	4.50E-01
FcCOOH	1.1E-05	0.01	0.744	450	4.10	5.00E+04	5.48E-01
$FcCOCH_3$	1.1E-05	0.01	0.744	450	4.10	5.10E+04	5.59E-01
Co(Cp)(dppe)	1.1E-05	0.01	0.744	450	4.10	1.49E+04	1.63E-01

Table A.3: Model parameters for high γ, no regeneration of QD*.

Probe	[QD*] (M)	k_{PCT} ($M^{-1}\,s^{-1}$)	k_{obs} (s^{-1})
$FcNH_2$	0.11	1.89E+00	2.08E-01
Fc (average)	0.11	2.99E+00	3.29E-01
FcCOOH	0.11	3.76E+00	4.14E-01
$FcCOCH_3$	0.11	3.58E+00	3.93E-01
Co(Cp)(dppe)	0.11	1.10E+00	1.21E-01

REFERENCES

(1) Henckel, D. A.; Enright, M. J.; Panahpour Eslami, N.; Kroupa, D. M.; Gamelin, D. R.; Cossairt, B. M. *Nano Letters* **2020**, *20*, 2620–2624.

Appendix B

SUPPORTING INFORMATION FOR CHAPTER 3

B.1 DOSY Fitting Results and Fitting Error

Table B.1: Results of fitting DOSY integrations for different CdS QDs solutions.

Sample	A	B	χ_{bound}
Oleic acid	1.90E+02	2.11E+02	4.74E-01
MEEAA	4.84E+02	2.17E+02	6.91E-01
MEEEPA	5.46E+03	1.11E+04	3.29E-01
Etched MEEAA	1.61E+02	3.96E+02	2.89E-01

Table B.2: Propogation of error from DOSY fitting to calculate an uncertainty in the number of ligands per QD.

Sample	σ_A	σ_B	σ_χ	Total ligand/QD	Bound ligand/QD	Unc. ligand/QD
Oleic acid	2.80E+01	2.77E+01	4.92E-02	5.18E+02	2.46E+02	2.55E+01
MEEAA	8.96E+01	8.72E+01	9.46E-02	6.26E+02	4.32E+02	5.92E+01
MEEEPA	1.05E+03	1.03E+03	4.71E-02	1.19E+03	3.90E+02	5.59E+01
Etched MEEAA	7.97E+01	7.90E+01	1.10E-01	1.35E+02	3.91E+01	1.48E+01

B.2 Raw Cyclic Voltammograms Used to Plot k_{obs} Over Time

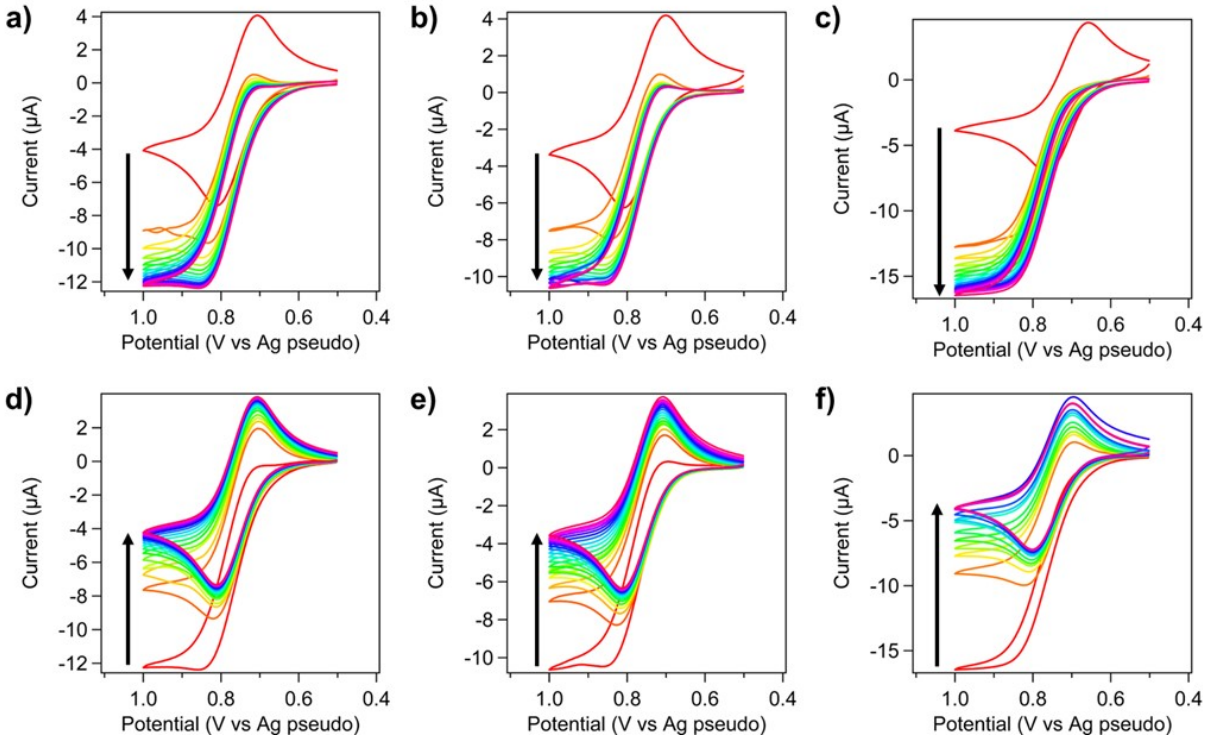

Figure B.1: Raw CV data used to acquire k_{obs} in Figure 3.10 Data was taken at a scan rate of 10 mV/s with a potential window of 500 mV. 30 seconds between scans. (a-c) Charging data over the course of 25 minutes of illumination for MEEAA (a), MEEEPA (b), and etched MEEAA (c). (d-f) Decay data of the course of 25 minutes after illumination ended for MEEAA (d), MEEEPA (e), and etched MEEAA (f).

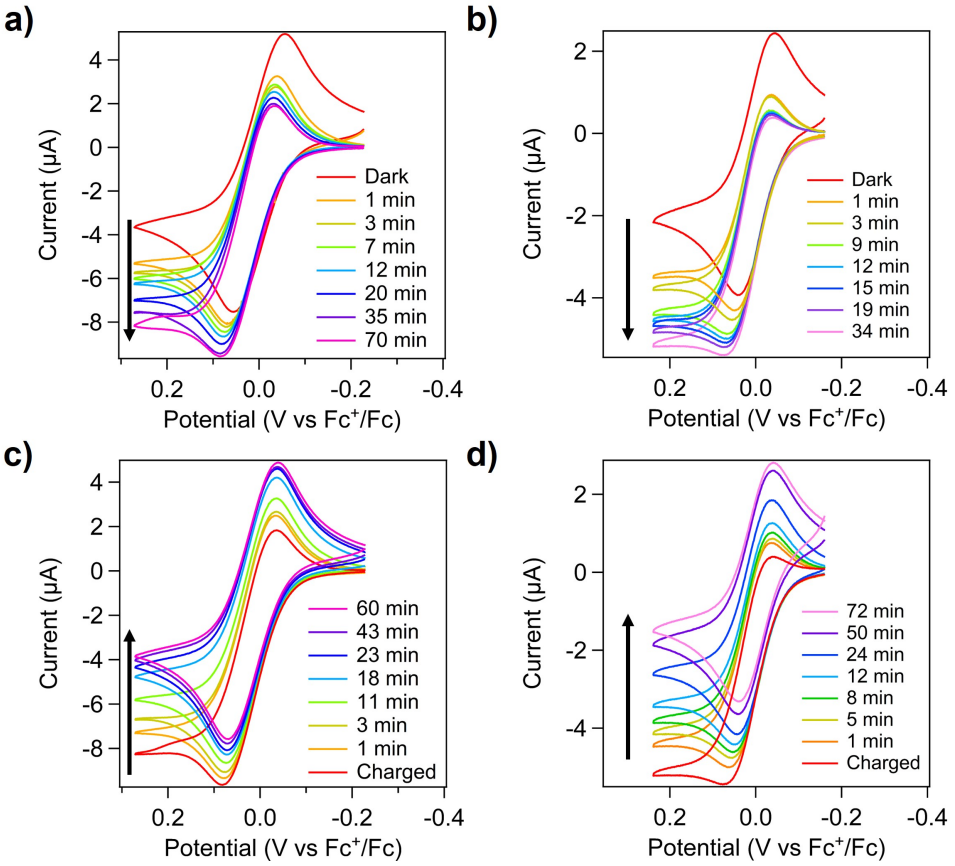

Figure B.2: Raw CV data used to acquire Figure 3.10 in Figure 3.10 Data was taken at a scan rate of 10 mV/s with a potential window of 500 mV. (a, b) Charging data for MEEAA capped CdSe (a) and MEEAA capped InP (b). (c, d) Decay data after illumination ended for MEEAA capped CdSe (c) and MEEAA capped InP (d).

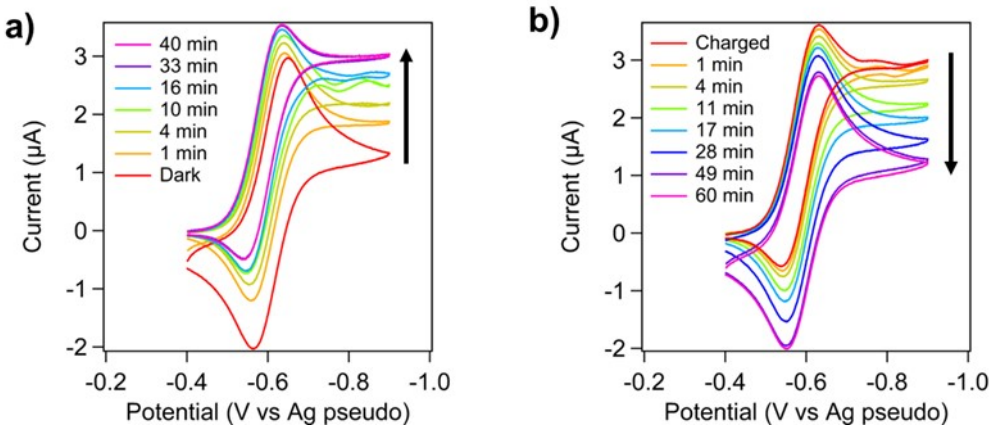

Figure B.3: CV data showing hole transfer from InP QDs to cobaltocene. (a) Charging data over the course of 40 minutes of illumination. (b) Discharging data showing long-lived hole transfer for 60 minutes after illumination ended.

B.3 Parameters Used to Fit k_{obs} Over Time

k_{obs} against the time (t) since illumination started (charging curves) or since illumination ended (discharging curves) was fit to the exponential function

$$k_{obs} = k_{obs,0} + Ae^{\frac{-(t-t_0)}{\tau}} \tag{B.1}$$

Where t_0 is set to the time at which the first data point was acquired. Values for fitting data are found in Table B.3 and Table B.4

Table B.3: Fitting parameters (± fitting uncertainty) from fitting k_{obs} against time during illumination.

Sample	t_0 (min)	$k_{obs,0}$ (s^{-1})	A (s^{-1})	τ (min)
CdS MEEAA	0.833	0.264 ± 0.004	-0.116 ± 0.004	10.0 ± 0.9
CdS MEEEPA	0.833	0.279 ± 0.005	-0.132 ± 0.006	7 ± 1
CdS etched MEEAA	0.833	0.684 ± 0.005	-0.276 ± 0.005	8.4 ± 0.6
InP MEEAA	0.833	0.205 ± 0.001	-0.112 ± 0.002	17.7 ± 0.7
CdSe MEEAA	0.833	0.112 ± 0.002	-0.065 ± 0.002	24 ± 2

Table B.4: Fitting parameters (± fitting uncertainty) from fitting k_{obs} against time after illumination ends.

Sample	t_0 (min)	$k_{obs,0}$ (s^{-1})	A (s^{-1})	τ (min)
CdS MEEAA	0.833	0.0312 ± 0.0009	0.0723 ± 0.001	5.9 ± 0.3
CdS MEEEPA	0.833	0.033 ± 0.006	0.086 ± 0.006	10 ± 2
CdS etched MEEAA	0.833	0.031 ± 0.004	0.169 ± 0.005	7.3 ± 0.6
InP MEEAA	0.833	0.0077 ± 0.0008	0.1379 ± 0.0007	25.5 ± 0.4
CdSe MEEAA	0.833	0.0246 ± 0.0006	0.063 ± 0.001	11.1 ± 0.5